UNIVERSITY OF Southampton

University of Southampton Research Repository
ePrints Soton

Copyright © and Moral Rights for this thesis are retained by the author and/or other copyright owners. A copy can be downloaded for personal non-commercial research or study, without prior permission or charge. This thesis cannot be reproduced or quoted extensively from without first obtaining permission in writing from the copyright holder/s. The content must not be changed in any way or sold commercially in any format or medium without the formal permission of the copyright holders.

When referring to this work, full bibliographic details including the author, title, awarding institution and date of the thesis must be given e.g.

AUTHOR (year of submission) "Full thesis title", University of Southampton, name of the University School or Department, PhD Thesis, pagination

http://eprints.soton.ac.uk

UNIVERSITY OF SOUTHAMPTON
FACULTY OF SCIENCE
DEPARTMENT OF PHYSICS

ION IMPLANTED AND EPITAXIALLY GROWN CRYSTAL WAVEGUIDE LASERS

by Alan Clifford Large

Thesis submitted for the degree of Doctor of Philosophy
September 1994

UNIVERSITY OF SOUTHAMPTON

ABSTRACT

FACULTY OF SCIENCE

PHYSICS

Doctor of Philosophy

ION IMPLANTED AND EPITAXIALLY GROWN CRYSTAL WAVEGUIDE LASERS

by Alan Clifford Large

This thesis reports the results of investigations into laser action in optical waveguides formed by the methods of helium ion implantation and liquid phase epitaxial growth.

Helium ion implantation has been used to produce waveguides in a range of dielectric materials. Of these Nd:GGG and Yb:YAG have been operated as planar waveguide lasers. The most important part of the work on ion implantation has been the fabrication of channel waveguides using a gold stopping mask to prevent ion damage in certain regions. Using this method channel waveguide lasers have been produced in Nd:YAG, Nd:GGG and Nd:MgO:$LiNbO_3$. These have all shown low threshold operation with the Nd:YAG channels lasing with an absorbed power threshold of 540μW when diode pumped.

The second method used to fabricate waveguides was that of liquid phase epitaxial growth. This has produced doped YAG waveguides of extremely high optical quality and with very low propagation losses (typically 0.1dB/cm). End pumped experiments on planar Nd:YAG waveguides have produced lasers with absorbed power thresholds as low as 670μW. As well as the 1.06μm transition laser action in Nd:YAG guides has also been obtained at 1.32μm and 946nm. Laser action has been demonstrated in a diode-array side-pumped configuration where the pump and signal light propagate perpendicular to each other. Yb:YAG waveguides have lased on the quasi-three-level transitions at 1.03 and 1.05μm. Because of the strong reabsorption losses present in this laser system the effect of any waveguide propagation loss becomes negligible and the resulting laser performance is excellent. When diode pumped at 968nm the laser threshold was 43mW and the slope efficiency 77%.

Contents

Acknowledgements

Firstly I would like to thank my supervisor, Anne Tropper, for her help and guidance over the past few years. I would also like to thank Dave Shepherd, Dave Hanna, Simon Field, Julian Jones and Toby Warburton - the other Southampton people involved in the waveguide work. A big thanks has to go to our collaborators at LETI and at the University of Sussex for making all the waveguides and therefore making my life much easier. I would like to thank SERC and the ORC for their financial support.

Thanks go to my parents for their support, for telling me to hurry up and for reminding me what good food tastes like.

Finally I would like to thank all my friends in the laser group, the ORC, Not Lasers FC, the Pub Quiz Team and all the staff at Southampton Golf Course. Oh, and before I go I'd like to say that the reason I took so long to submit was simply that I was waiting for Albion Rovers to win a match.

Chapter 1 - Introduction

1.1. Introduction.

This thesis describes the results of a three year investigation into the lasing behaviour of optical waveguides fabricated in oxide crystals by ion-implantation and liquid phase epitaxy. It contains an account of the first demonstration of lasing in channel waveguides formed by ion-implantation. These channels have lased with submilliwatt thresholds. It also describes the results of the first laser experiments in epitaxially grown garnet layers. These layer have proven to be of excellent optical quality and have produced planar waveguides with very low propagation losses. This has made possible submilliwatt thresholds in a planar waveguide geometry, laser operation in a transverse pumping scheme and high slope efficiency operation of quasi-three-level transitions. The ability to dope these guides with many different ions offers a wide range of possible laser transitions.

Most of the lasers discussed in this thesis are based on a doped garnet structure; the most common laser of this type being the Nd:YAG laser. The garnet structure offers the advantages of robustness and high thermal conductivity which allows for the production of high power lasers. A further advantages is the range of dopants which can be substituted into the garnet lattice. Epitaxially grown YAG layers have been doped with a range of lanthanide ions (neodymium, ytterbium, erbium and thulium) as well as the transition metal ion, chromium (in the form of Cr^{3+} and Cr^{4+}). Materials such as ytterbium and neodymium doped YAG have of strong diode pumpable absorptions which gives the potential of miniature devices.

The main advantage that waveguides offer over bulk systems is the ability to maintain small spot sizes over long distances. Because of this low pump powers can lead to high optical intensities inside the waveguide. These high pump intensities lead to high gains in laser materials and can therefore produce lasers with very low power thresholds - making them very suitable for diode pumping where high powers are not always

available. As well as being favourable to laser systems, the high intensities obtained in the waveguides lead to efficient non-linear processes such as second harmonic generation and parametric amplification. In these situations a further advantage of the waveguide geometry is that it prevents any walk-off between the pump and signal light. The disadvantage of a waveguide geometry is that it introduces extra propagation loss into the system. Only in situations where this loss is more than compensated for by the optical confinement will the waveguide show a real advantage over bulk.

The best known type of optical waveguide is that of an optical fibre where a circular glass core is surrounded by a cladding of lower refractive index. The advantages of guided wave devices have been seen in the production of efficient lasers, amplifiers and upconversion lasers [1-3] in fibres. Although a few crystal fibres have been produced in materials such as Nd:YAG [4] most fibres are fabricated in glasses. Crystals offer several advantages over glasses, one of which is the extremely large range of linewidths available in the laser transitions. These can range from the high gain 1.06μm transition in Nd:YAG to materials such as Ti:Al_2O_3 in which the laser output can be tuned over several hundred nanometres. The high gain transitions also have strong absorptions which allow for the fabrication of very small devices and gives the possibility of efficient side pumping. A further advantage of crystals is that they can offer far higher non-linear, electro-optic and acousto-optic properties than glasses. A disadvantage of fibres is their circular geometry. This is only really suited to single laser cavities whereas in a waveguide more complicated structures such as y branch cavities can be produced by photolithographic processes. This ability to pattern the surface of the material with the desired waveguide structure is the motivation behind current research into fabricating a lossless splitter using planar waveguide technology.

The bulk of research at the moment into crystal waveguides centres on $LiNbO_3$ because of its large non-linear and electro-optic coefficients. The two main techniques for forming waveguides in $LiNbO_3$ are proton exchange and Ti indiffusion [5,6]. By using the electro-optic properties of $LiNbO_3$ mode-locked lasers have been made in both Nd^{3+} and Er^{3+} doped $LiNbO_3$ [7,8].

Both proton exchange and Ti indiffusion are fabrication techniques which are specific to $LiNbO_3$ and $LiTaO_3$. The motivation for working with ion-implantation is its versatility. To form waveguides by ion-implantation the sample has to be bombarded with high energy ions (usually helium or hydrogen) to modify its refractive index near the surface. This can be tried on any material and has been found to work on a wide range of materials with waveguide lasers being fabricated in seven of these. The work on ion-implantation is done in collaboration with Professor Townsend's group at the University of Sussex where the accelerator for the ion-implantation is housed. The basic process of ion-implantation leads to the formation of planar waveguides [9]. With the propagation losses in these waveguides generally being about 1dB/cm there is little advantage gained from having a planar guide. The formation of channel waveguides is therefore very important and is one of the main parts of the work in this thesis. Channel waveguides fabricated in Nd:YAG have shown no increase in loss over planar guides and when diode pumped have lased with thresholds less than 1mW. However, for ion-implantation to become a realistic method of waveguide fabrication the losses would have to be reduced to about 0.2dB/cm. This is possible in some materials such as lead germanate glass and yttrium orthosilicate and it is materials such as these which will ultimately produce results which show a significant advantage over bulk lasers.

The other method of waveguide fabrication covered by the work in this thesis is that of liquid phase epitaxial growth [10]. At the moment these layers are limited to planar guides in doped YAG but even this has shown the potential of epitaxial growth as a fabrication method for low loss guides. The work on epitaxially grown waveguides is done in collaboration with Bernard Ferrand's group at LETI (Laboratoire d'Electronique, de Technologie et d'Instrumentation), part of CENG (Centre d'Etudes Nucléaires de Grenoble) in Grenoble. They have been working on the epitaxial growth of garnet films for many years and have great expertise in the field. Waveguides have been fabricated with Nd^{3+} and Yb^{3+} doped layers and have successfully operated as waveguide lasers. The diode pumped Yb:YAG guide has shown a threshold of 43mW with a slope efficiency of 77% - far better than has been achieved in similar bulk systems. If the current effort to produce channels in epitaxially grown layers without significantly

increasing the propagation loss succeeds then threshold reductions of a further order of magnitude should be possible.

The work on epitaxially grown waveguides is contained in chapter 6 of this thesis. Chapter 2 describes the theory of a simple asymmetric slab waveguide and also outlines some alternative waveguide fabrication methods. The experimental techniques used to characterise the guides are described in chapter 3. Work on ion-implanted planar and channel guides is covered in chapters 4 and 5 respectively.

1.2. References.

1. R.Allen and L.Esterowitz, Applied Physics Letters, **55**, pp.721-722, 1989.
2. R.J. Mears, L. Reekie, I.M. Jauncey and D.N. Payne, Electronics Letters, **23**, pp.1026-1027, 1987.
3. I.Y.Allain, M.Monerie and H.Poignant, Electronics Letters, **26**, pp.261-263, 1990.
4. M.F.Digonnet, C.J.Gaeta, D.O'Meara and H.J.Shaw, Journal of Lightwave Technology, **5**, pp.642-646, 1987.
5. E.Lallier, J.P.Pocholle, M.Papuchon, M.P.De Micheli, M.J.Li, Q.He, D.B.Ostrowsky, C.Grezes-Besset and E.Pelletier, IEEE Journal of Quantum Electronics, **27**, pp.618-625, 1991.
6. R.Brinkman, W.Sohler, H.Suche and C.Wersig, IEEE Journal of Quantum Electronics, **28**, pp.466-470, 1992.
7. E.Lallier, J.P.Pocholle, M.Papuchon, Q.He, M.De Micheli, D.B.Ostrowsky, C.Grezes-Besset and E.Pelletier, Electronics Letters, **27**, pp.936-937, 1991.
8. H.Suche, L.Baumann, D.Hiller and W.Sohler, Electronics Letters, **29**, pp.1111-1112, 1993.
9. P.D.Townsend, Reports on Progress in Physics, **50**, pp.501-588, 1987.
10. B.Ferrand, D.Pelenc, I.Chartier and C.Wyon, Journal of Crystal Growth, **128**, pp.966-969, 1993.

Chapter 2 - Waveguide Laser Theory

2.1. Introduction

The simple theory of a slab dielectric waveguide gives a good insight into the workings of all waveguide systems. In this chapter I will start by outlining various different waveguide fabrication methods. The solution to the problem of the asymmetric slab waveguide will then be described and the points arising from the solution discussed. Finally I will discuss the parameters which govern the threshold and slope efficiencies of longitudinally pumped lasers and show that in most cases these are particularly suited to a waveguide geometry. General theory about waveguides and their fabrication is covered in several textbooks [1,2].

2.2. Waveguide Fabrication Techniques

A waveguide consists of a central core surrounded by regions of lower refractive index. This allows light to be reflected at the boundaries by the process of total internal reflection and the light is therefore guided down the core. There are many different methods for creating the refractive index changes required to produce a waveguide. In this section I will give a brief outline of the most common of these.

Sputtered films [3] - In this process a target of suitable source material is bombarded with either atoms or ions. These free atoms or molecules from the surface of the target which then form a thin film layer on a nearby substrate. If the refractive index of the sputtered film is higher than that of the substrate then a waveguide is produced. The initial bombardment can be done in either an electric discharge or by accelerating ions and firing them at the target. A modification of this technique is laser ablation [4] where a laser beam is used to free the atoms from the target.

Ion Exchange [5-8] - Replacing light ions, such as sodium and lithium, in a glass with heavier ones like silver, thallium or potassium can increase the refractive index in a glass. For example, if soda-lime glass is placed in a molten solution of $AgNO_3$ then some

of the Ag^+ ions will replace Na^+ ions. This process can be speeded up by applying an electric field across the crystal. A second, shorter ion exchange which replaces some of the heavier ions at the surface by lighter ones can be done to produce buried guides. This method has been extremely successful, producing waveguides with losses as low as 0.1dB/cm. Unfortunately, this method is only applicable to certain types of glasses.

Proton exchange [9-13] - This is a technique which is specific to $LiNbO_3$ and $LiTaO_3$. Here the lithium in the crystal is replaced with hydrogen to produce an area of increased index at the crystal surface. This is done by soaking the substrate in heated ($\sim$200°C) benzoic acid for several hours. Only the extra-ordinary refractive index is increased by this method and it is therefore unsuitable for laser systems where the laser emission is not polarised along z. For systems such as Nd:MgO:$LiNbO_3$ where the emission is correctly polarised results using this process have been very successful. A feature of this technique is that it reduces the photorefractive effects in the material but unfortunately also reduces the non-linear and electro-optic coefficients.

Metal Indiffusion [14-17] - This is another technique which is specific to $LiNbO_3$ and $LiTaO_3$ although in this case it produces a refractive index increase for both polarisations. Laser systems such as Er:MgO:$LiNbO_3$ as well as Nd:MgO:$LiNbO_3$ can and have worked in this type of waveguide. In this type of fabrication a metal layer of either Ti or Nb (for $LiNbO_3$ or $LiTaO_3$ respectively) is evaporated onto the crystal surface and is then diffused in at a temperature of about 1000°C in an argon/oxygen atmosphere for several hours.

Etching [18,19] - If a stripe on the surface of a material is masked off and the material is then etched away a raised channel will be formed. This provides confinement on three sides and if a planar guide already existed a completely confined channel will be produced. Methods for etching are either wet, where the material is dissolved in a solvent, or dry, where the techniques used to make sputtered guides can be used to remove the material.

Ion-implantation - This uses ion bombardment to change the refractive index of the

material. Usually a low refractive index barrier is formed several microns into the material. The main advantage of this technique is its versatility. Only one set of apparatus is needed and any material can be tested. Guides formed by this method usually have propagation losses in the region of 1dB/cm which means that methods which are more specific to certain materials (eg. Ti indiffusion for $LiNbO_3$) usually produce better guides. There are however many materials with no existing alternative method of fabrication.

Epitaxial Growth - This is a technique where the waveguide is formed by a thin layer grown on a substrate. This growth can be done from a solution (liquid phase epitaxy), from a chemical vapour or from a molecular beam. Given the right condition waveguides grown by this technique can have very good crystal quality.

Crystal Fibres [20-22] - This is another method where a crystal is grown to form a waveguide. The most successful method for crystal fibre growth is that of laser heated pedestal growth where the fibre is pulled from the end of a feed crystal which is melted by a carbon dioxide laser. If a thin cladding layer is deposited on top of the fibre the losses can be reduced to values as low as 0.014dB/cm for Nd:YAG. Nd:YAG crystal fibres have produced lasers with submilliwatt thresholds.

The processes of ion-implantation and epitaxial growth were the ones on which the experimental work described in this thesis were based. They will be discussed in more detail in chapters 3 and 5 respectively.

2.3. The Asymmetric Slab Waveguide

The asymmetric slab waveguide consists of three layers of dielectric material, each layer of which has a different refractive index. The middle one of these layers has the highest index and light is confined within this region by total internal reflection at the top and bottom surfaces. Such a system is shown in figure 2.1 where a guide region of refractive index n_2 is surrounded by regions of index n_1 and n_3. The boundaries of the waveguide are at $x = \pm d/2$ and the light is assumed to propagate in the z direction. Maxwell's equations govern the transmission of light and these are the starting place for

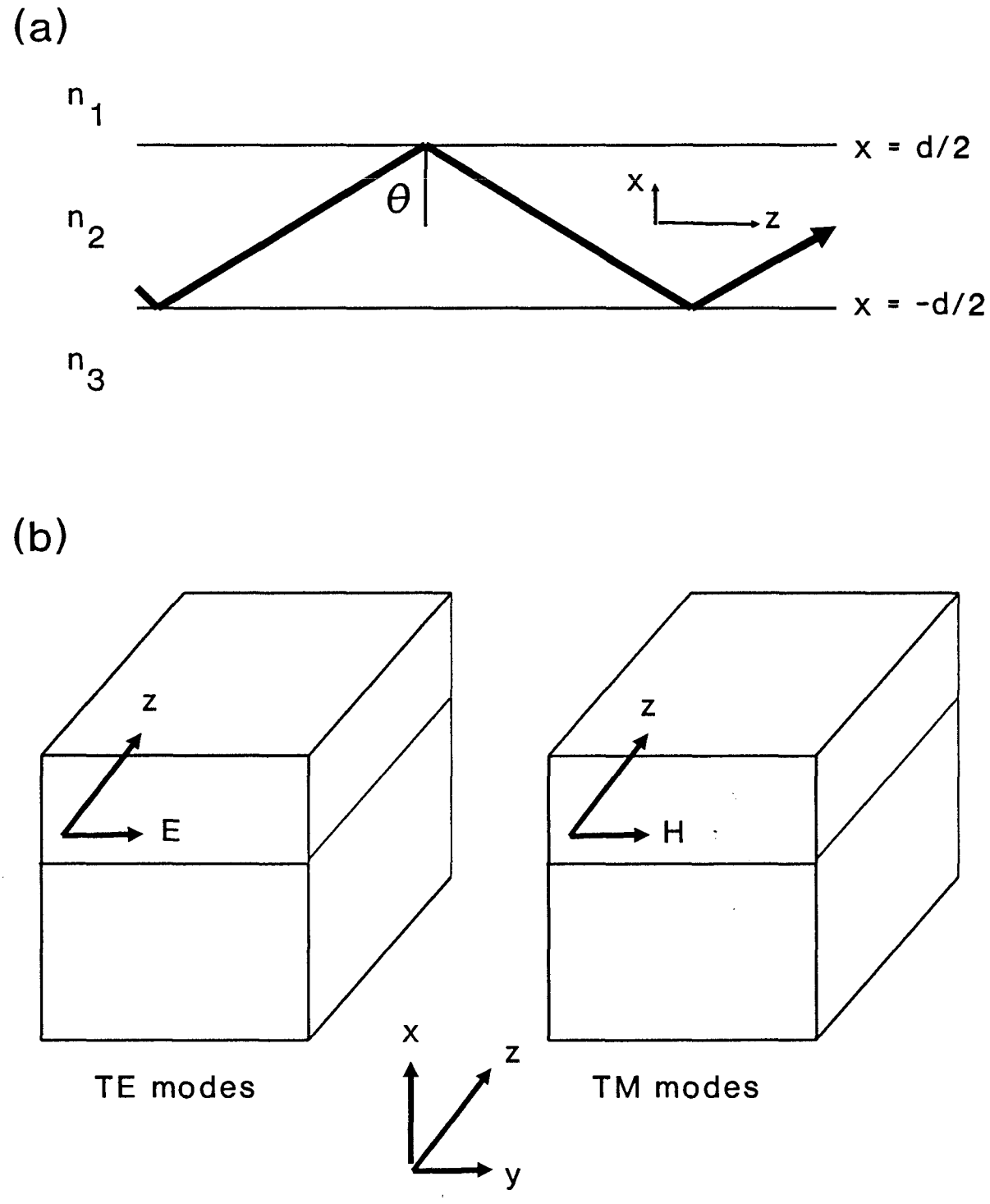

Figure 2.1 - Diagram of a planar waveguide showing (a). the three regions of refractive index and the angle of propagation in the guide and (b). the orientation of TE and TM modes.

the analysis. Maxwell's equations can be written as follows.

$$\underline{\nabla} \times \underline{E}(\underline{r},t) = -\frac{\partial}{\partial t} \underline{B}(\underline{r},t) \tag{2.1}$$

$$\underline{\nabla} \times \underline{H}(\underline{r},t) = \frac{\partial}{\partial t} \underline{D}(\underline{r},t) + \underline{J}(\underline{r},t) \tag{2.2}$$

$$\underline{\nabla}.\underline{D}(\underline{r},t) = \rho(\underline{r},t) \tag{2.3}$$

$$\underline{\nabla}.\underline{B}(\underline{r},t) = 0 \tag{2.4}$$

where $\underline{E}$ and $\underline{H}$ are the electric and magnetic fields, $\underline{D}$ and $\underline{B}$ are the electric and magnetic displacements, $\underline{J}$ is the current density, ρ is the charge density, $\underline{r}$ defines the position in space and t is time. These quantities are related by the expressions $\underline{B} = \mu\underline{H}$ and $\underline{D} = \epsilon\underline{E}$, where μ is the magnetic permeability and ϵ is the electric permittivity of the material. These are defined by $\mu = \mu_r\mu_0$ and $\epsilon = \epsilon_r\epsilon_0$ where μ_r is the relative permeability of the medium, μ_0 is the permeability of free space, ϵ_r is the relative permittivity of the medium and ϵ_0 is the permittivity of free space. Substituting these into (2.1) and (2.2) and assuming $\underline{J} = 0$ (ie. no current flow) we get

$$\underline{\nabla} \times \underline{E}(\underline{r},t) = -\frac{\partial}{\partial t} \mu\underline{H}(\underline{r},t) \tag{2.5}$$

$$\underline{\nabla} \times \underline{H}(\underline{r},t) = \frac{\partial}{\partial t} \epsilon\underline{E}(\underline{r},t) \tag{2.6}$$

In the case of the asymmetric slab waveguide we are looking for solutions to these equations which are sinusoidal in shape across region **2** but which decay evanescently into regions **1** and **3**. For a wave which has its electric field polarised along the y axis (transverse electric or TE) the function for the electric field will be of the form

$$\underline{E}(\underline{r},t) = E_y(x,z)e^{i\omega t} \tag{2.7}$$

which may be written in terms of three amplitude coefficients, A_1-A_3, and a phase

constant, Ψ.

$$E_y(x,z) = \begin{bmatrix} A_1 e^{-\alpha_{1x}x} & x>d/2 \\ A_2 \cos(k_{2x}x+\psi) & |x| \le d/2 \\ A_3 e^{+\alpha_{3x}x} & x<-d/2 \end{bmatrix} e^{ik_z z} \qquad (2.8)$$

The transverse wavenumbers in each region (α_{1x},k_{2x} and α_{3x}) are given by the dispersion relation for that region. ie.

$$\alpha_{1x} = \sqrt{k_z^2 - \omega^2\mu_1\epsilon_1}$$

$$k_{2x} = \sqrt{\omega^2\mu_2\epsilon_2 - k_z^2} \qquad (2.9)$$

$$\alpha_{3x} = \sqrt{k_z^2 - \omega^2\mu_3\epsilon_3}$$

Equation (2.8) can be solved for k_{2x} by noting that the tangential components of both the electric and magnetic fields are continuous at the boundaries between the layers. As $\underline{E}$ and $\underline{H}$ are perpendicular the components that are continuous are E_y and H_z. H_z can be obtained by taking the z component of equation (2.5).

$$\frac{\partial}{\partial x} E_y - \frac{\partial}{\partial y} E_x = -\frac{\partial}{\partial t}\mu H_z$$

This gives the z component of the magnetic field to be

$$H_z = -\frac{i}{\omega\mu}\frac{\partial}{\partial x} E_y \qquad (2.10)$$

Substituting (2.8) into (2.10) gives the equation for H_z as

$$H_z = \begin{bmatrix} -\frac{i\alpha_{1x}}{\omega\mu_1}A_1 e^{-\alpha_{1x}x} & x>d/2 \\ -\frac{ik_{2x}}{\omega\mu_2}A_2\sin(k_{2x}x + \psi) & |x|\le d/2 \\ +\frac{i\alpha_{3x}}{\omega\mu_3}A_3 e^{+\alpha_{3x}x} & x<d/2 \end{bmatrix} e^{ik_z z} \qquad (2.11)$$

Applying the boundary conditions of continuity at x=d/2 to (2.8) and (2.11) and eliminating A_1 and A_2 gives

$$\tan(k_{2x}d/2 + \psi) = \frac{\mu_2\alpha_{1x}}{\mu_1 k_{2x}}$$

which using the relation $\tan(x)=\tan(x\pm n\pi)$ can be rewritten as

$$k_{2x}\frac{d}{2} + \psi = \tan^{-1}\left(\frac{\mu_2\alpha_{1x}}{\mu_1 k_{2x}}\right) \pm n\pi \qquad (2.12)$$

similarly applying the boundary conditions at x=-d/2 gives the relation

$$k_{2x}\frac{d}{2} - \psi = \tan^{-1}\left(\frac{\mu_2\alpha_{3x}}{\mu_3 k_{2x}}\right) \pm m\pi \qquad (2.13)$$

Combining (2.12) and (2.13) to eliminate Ψ produces an equation which can be solved using equation (2.9) to obtain k_z. This equation is

$$k_{2x} - \tan^{-1}\left(\frac{\mu_2\alpha_{1x}}{\mu_1 k_{2x}}\right) - \tan^{-1}\left(\frac{\mu_2\alpha_{3x}}{\mu_3 k_{2x}}\right) = p\pi \qquad (2.13)$$

This analysis can be extended to transverse magnetic (TM) modes which have their magnetic fields polarised along the y axis. Equation (2.6) can be used to obtain the E_z component and the equation can then be solved by applying the boundary conditions at $x=\pm d/2$. The resulting equation giving the conditions for guidance of TM modes is

UNIVERSITY OF SOUTHAMPTON LIBRARY

$$k_{2x} - \tan^{-1}\left(\frac{\epsilon_2 \alpha_{1x}}{\epsilon_1 k_{2x}}\right) - \tan^{-1}\left(\frac{\epsilon_2 \alpha_{3x}}{\epsilon_3 k_{2x}}\right) = p\pi \qquad (2.14)$$

These equations can be solved either numerically or graphically. A numerical solution is given in appendix A. This solves for an effective refractive index, n_e, which is related to k_z by the relation

$$n_e = \frac{k_z}{k_o}$$

where k_o is the wavenumber in free space. The value of n_e can vary from n_2 to the highest of the substrate refractive indices. This is also related to the variation in the angle of propagation of the light in the guide as shown in figure 2.1. As n_e varies from n_3 to n_2 (if we assume that $n_1 \leq n_3 < n_2$) then the angle θ varies from 90°, as the light travels straight along the guide, to $\sin^{-1}(n_3/n_2)$ the critical angle for total internal reflection within the guide. Some of the special cases arising from this solution deserve attention.

Modes near cut off ($n_e \rightarrow n_3$) - The angle of light in the guide is close to the critical angle the evanescent field extends well into region **3**. If the waveguide is symmetrical (ie. $n_1 = n_3$) then there is no cut off for the zero order mode although it may extend far into the substrates. Figure 2.2a shows the intensity profile of modes near cut off.

Modes far from cut off ($n_e \rightarrow n_2$) - Light is well confined within the waveguide with very little in the substrate regions. An example of the intensity profile of such a mode is shown in figure 2.2b.

Modes past cut off ($\theta < \theta_c$) - If the angle of the light in the guide is just past cut off then the light will leak out of the guide. This will happen first at the boundary with the higher refractive index substrate. Although some light could be transmitted through such a system the losses would be extremely high.

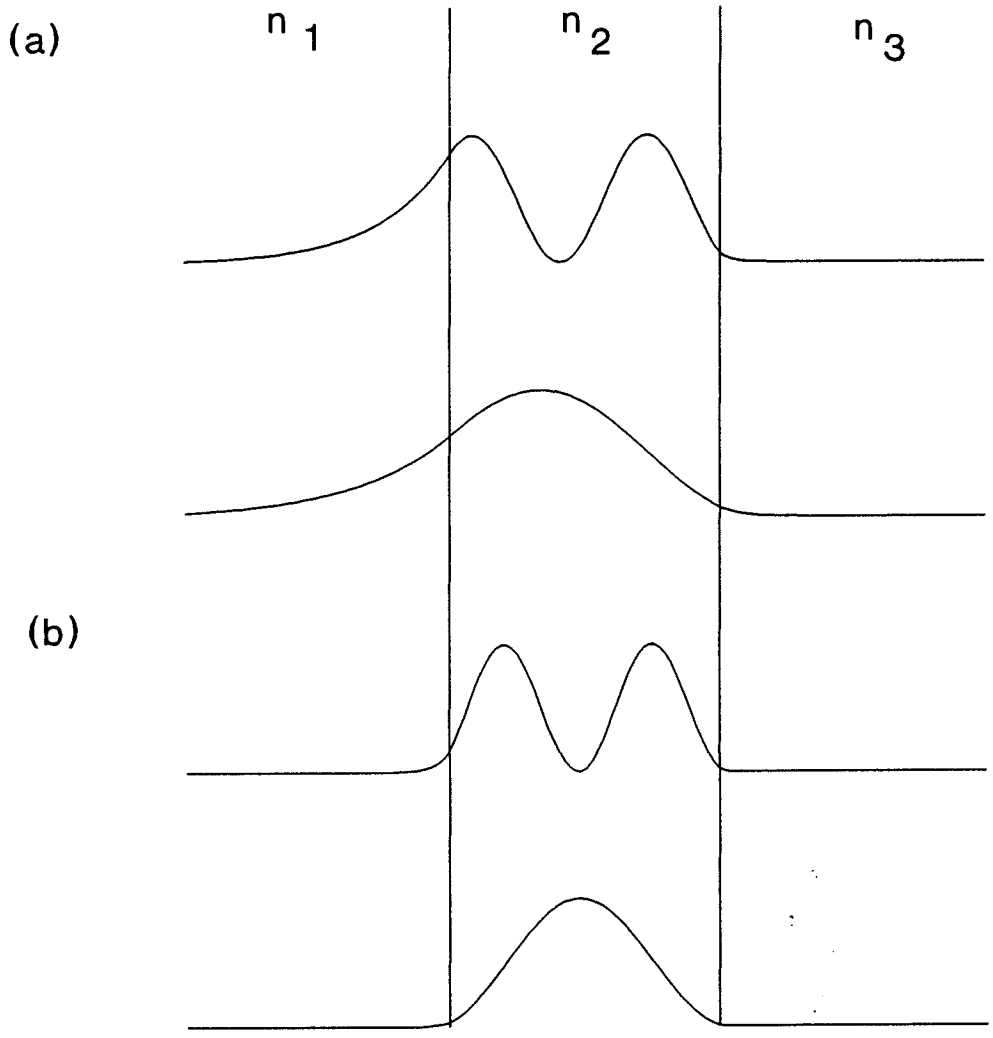

Figure 2.2 - Intensity profiles of modes
(a). Near cut off and
(b). Far from cut off

The theory discussed here is valid for step index planar guides such as ones made by sputtering or the epitaxially grown ones which will be discussed in chapter 5. This type of analysis, though, can be used to estimate the number and sizes of the modes in most types of waveguide. More complicated theories such as the WKB approximation for graded index guides [23,24] and the effective index method for channel guides [25] where the waveguide is considered as two planar guides can be used to get exact solutions to the guidance conditions.

2.4. Laser Theory Applied to Waveguides

The performance of a bulk dielectric laser system can in principle be greatly enhanced if a low-loss waveguide can be fabricated in the gain medium to confine the laser mode within a small volume. Here I will look at some of the theory governing laser action in both bulk systems and in channel waveguides. An intermediate case is that of planar waveguides which I will mention later in this section.

In general the threshold of a longitudinally pumped laser system is given by [26]

$$P_{th}=\frac{\pi h\nu}{4\sigma_e\tau_f}(\overline{w_p^2}+\overline{w_l^2}).L \qquad (2.15)$$

where ν is the pump frequency, σ_e is the emission cross section, τ_f is the fluorescence lifetime, $\bar{w}_p$ and $\bar{w}_l$ are the average pump and laser spot sizes in the gain medium and L is the overall round trip loss in the system. This assumes that the pump and signal are both fundamental Gaussian modes and that the pump quantum efficiency is unity (ie. one laser photon for every pump photon). The optimum setup for laser operation in bulk systems is approximately that of confocal focusing through the gain medium. In this case the average spot sizes are given by [26]

$$\bar{w}=\sqrt{\frac{\lambda l}{\sqrt{3}\pi n}}$$

where λ is the wavelength, l is the length of the laser medium and n is the refractive index of the laser material. Substituting into the equation (2.15) gives an expression for

the threshold of a bulk laser.

$$P_{th}=\frac{h\nu l}{4\sqrt{3}\sigma_e\tau_f n}(\lambda_p+\lambda_l).L \tag{2.16}$$

For a channel waveguide laser the pump and signal spot sizes do not vary over the length of the laser and the threshold is given by

$$P_{th}=\frac{\pi h\nu}{4\sigma_e\tau_f}(w_{px}^2+w_{lx}^2)^{1/2}(w_{py}^2+w_{ly}^2)^{1/2}.L \tag{2.17}$$

where w_p etc. are the x and y components of the pump and laser signals. For waveguide lasers to give us the benefits we want we need the laser threshold to be low compared to that of bulk system. The ratio of the channel threshold ($P_{th,ch}$) to bulk threshold ($P_{th,b}$) is

$$\frac{P_{th,ch}}{P_{th,b}} = \frac{\sqrt{3}\pi n(w_{px}^2+w_{lx}^2)^{1/2}(w_{py}^2+w_{ly}^2)^{1/2}}{l(\lambda_p+\lambda_l)}.\frac{L_{ch}}{L_b} \tag{2.18}$$

When this number is at its lowest waveguides then have the greatest advantage over bulk, that is for long crystal lengths and small waveguide spot sizes. As an example, if a channel waveguide supports a mode which propagates with a radius of 3μm at $\lambda_p \simeq \lambda_l = 1\mu$m and the bulk and guide losses are assumed to be 0.03dB/cm (as in bulk Nd:YAG) and 0.3dB/cm respectively then the threshold for the waveguide will be 10 times smaller than that of the bulk laser for a 1cm length of material. This assumes that highly reflecting mirrors are used at either end of the laser and therefore the total loss is entirely due to propagation losses. An obvious disadvantage of waveguide systems is that they introduce higher than normal propagation losses and this is what has to be overcome by the advantage of having small spot sizes.

The slope efficiency, η, of such a system is given by [27]

$$\eta=\frac{T\nu_l}{L\nu_p}(1-e^{-\alpha_p l})\eta_q\eta_{pl} \tag{2.19}$$

where T is the transmission of the output coupler, η_q is the fraction of absorbed pump

photons that lead to subsequent population of the upper laser level and η_{pl} is a factor which takes into account the overlap between the pump and signal modes. At threshold the value of η_{pl} is given by the expression

$$\eta_{pl} = \frac{w_{lx}w_{ly}(2w_{px}^2+w_{lx}^2)^{1/2}(2w_{py}^2+w_{ly}^2)^{1/2}}{(w_{px}^2+w_{lx}^2)(w_{py}^2+w_{ly}^2)}$$

As the laser is operated further above threshold the value of η_{pl} tend towards 1.

The main difference between bulk and waveguide in the expression for slope efficiency is the higher amount of propagation loss present in the waveguide. This has to be compensated for by using a higher value of output coupling, T. In the example given above if an T=1% output coupler was used in the bulk system this would have to be replaced by a T=13% output coupler in the waveguide case to obtain the same slope efficiency. This produces a total round trip loss which is twelve times greater in the waveguide system than in the bulk one. However despite the increase in output coupling there is little change in the ratio of thresholds as this already accounts for a ten times higher loss in the waveguide. Therefore the waveguide laser operating with the same slope efficiency as a bulk device would have a threshold which is ten times lower than in the bulk laser case despite the higher value of output coupling needed to achieve this slope efficiency.

The case of channel waveguides is one that is ideal for low threshold lasers. Often, though, it is easier to form planar guides where the light is confined in only one direction. This gives only part of the advantage of a channel but still brings added loss into the system. For planar waveguides to give an advantage over bulk waveguide losses would have to be of the order of 0.1dB/cm. This can be seen in the case of epitaxially grown planar guides, where waveguides with losses of 0.1dB/cm or less can be seen to rival bulk laser devices.

2.5. Three-Level and Quasi-Three-Level Lasers

In a three-level laser the lower laser level is the ground state of the laser ion. Most so-called three-level systems are actually quasi-three-level, meaning that the lower laser level is populated by thermal excitation from the ground state. Thus any laser photons that are emitted have a chance of being reabsorbed, exciting the ion up to the upper laser level. An extra loss is therefore introduced into the cavity which increases laser thresholds. The laser threshold is now given by [28,29]

$$P_{th}=\frac{\pi h\nu}{4\sigma_e\tau_f}(\overline{w_p^2}+\overline{w_l^2}).(L+T+2\sigma_a N_1^0 l) \qquad (2.20)$$

where N_1^0 is the thermal population in the lower laser level and σ_a is the absorption cross section of the laser transition. This last term in the equation acts as an extra propagation loss and in transitions of a relatively strong three level nature can dominate. For example for the 946nm transition in 1% doped Nd:YAG this is equivalent to a loss of 0.17dB/cm but for the 1.03μm transition in 6.5% doped Yb:YAG this is equivalent to 2.6dB/cm. For materials such as Yb:YAG this can become dominant term in the loss part of the threshold calculation. For such transitions even low loss planar guides can show a great advantage over bulk systems as is seen in chapter 6.5 for a planar epitaxially grown Yb:YAG waveguide.

2.6. References

1. D.L.Lee, Electromagnetic Principles of Integrated Optics, published by Wiley, 1986.
2. A.Yariv, Optical Electronics, published by Holt-Saunders, 1985.
3. S.Takada, M.Ohnishi, H.Hayakawa and N.Mikoshiba, Applied Physics Letters, **24**, pp.490-492, 1975.
4. J.A.Agnostelli, G.H.Braunstein and T.N.Blanton, Applied Physics Letters, **63**, pp.123-125, 1993.
5. N.A.Sanford, K.J.Malone and D.R.Larson, Optics Letters, **15**, pp.366-368, 1990.
6. G.H.Chartier, P.Jaussaud, A.D.de Oliveira and O.Parriaux, Electronics Letters, **14**, pp.132-134, 1978.

7. H.Aoki, O.Maruyama and Y.Asahara, IEEE Photonics Technology Letters, **2**, pp.459-460, 1990.
8. A.N.Miliou, X.F.Cao, R.Srivastava and R.V.Ramaswamy, IEEE Photonics Technology Letters, **4**, pp.416-418, 1993.
9. E.Lallier, J.P.Pocholle, M.Papuchon, M.P.De Micheli, M.J.Li, Q.He, D.B.Ostrowsky, C.Grezes-Besset and E.Pelletier, IEEE Journal of Quantum Electronics, **27**, pp.618-625, 1991.
10. S.Nouh, P.Baldi, M.De Micheli, G.Monnom, D.B.Ostrowsky, E.Lallier and M.Papuchon, Electronics Letters, **28**, pp.2337-2338, 1992.
11. M.Goodwin and C.Stewart, Electronics Letters, **19**, pp.223-225, 1983.
12. E.Lallier, J.P.Pocholle, M.Papuchon, Q.He, M.De Micheli, D.B.Ostrowsky, C.Grezes-Besset and E.Pelletier, Electronics Letters, **27**, pp.936-937, 1991.
13. E.Lallier, D.Papillon, J.P.Pocholle, M.Papuchon, M.De Micheli, D.B.Ostrowsky, Electronics Letters, **29**, pp.175-176, 1993.
14. R.Brinkman, W.Sohler, H.Suche and C.Wersig, IEEE Journal of Quantum Electronics, **28**, pp.466-470, 1992.
15. M.Hempstead, J.S.Wilkinson and L.Reekie, IEEE Photonics Technology Letters, **8**, pp.852-855, 1992.
16. P.Becker, R.Brinkman, M.Dinand, W.Sohler and H.Suche, Applied Physics Letters, **61**, pp1257-1259, 1992.
17. H.Suche, L.Baumann, D.Hiller and W.Sohler, Electronics Letters, **29**, pp.1111-1112, 1993.
18. J.L.Jackel, R.E.Howard, E.L.Hu and S.P.Lyman, Applied Physics Letters, **38**, pp.907-909, 1981.
19. M.Nakazawa and Y.Kimura, Electronics Letters, **28**, pp2054-2056, 1992.
20. C.A.Burrus and J.Stone, Applied Physics Letters, **26**, pp.318-320, 1975.
21. J.Stone, C.A.Burrus, A.G.Dentai and B.I.Miller, Applied Physics Letters, **29**, pp.37-39, 1976.
22. M.F.Digonnet, C.J.Gaeta, D.O'Meara and H.J.Shaw, Journal of Lightwave Technology, **5**, pp.642-646, 1987.
23. D.Marcuse, IEEE Journal of Quantum Electronics, **9**, pp.1000-1006, 1973.

24. J.Janta and J.Ctyroky, Optics Communications, **25**, pp.49-52, 1978.

25. K.S.Chiang, Optics Letters, **16**, pp.714-716, 1991.

26. M.J.F.Digonnet and C.J.Gaeta, Applied Optics, **24**, pp.333-342, 1985.

27. W.A.Clarkson and D.C.Hanna, Journal of Modern Optics, **36**, pp.483-498, 1989.

28. W.P.Risk, Journal of the Optical Society of America B, **5**, pp.1412-1423, 1988.

29. T.Y.Fan and R.L.Byer, IEEE Journal of Quantum Electronics, **23**, pp.605-612, 1987.

Chapter 3 - Experimental Techniques

3.1. Introduction.

In this chapter I will describe the experimental techniques used to assess waveguides. These vary from simple experimental arrangements such as that used to measure waveguide transmission, to more complicated layouts for measuring the refractive indices of waveguide modes, or for characterising waveguide laser performance. In most of these arrangements the incident light is coupled into and out of the waveguide using microscope objectives as shown in figure 3.1. The objectives are mounted on three axis (xyz) positioners so that they can be adjusted to find the optimum launch. The waveguide itself is mounted on a three axis (xyz) positioner with two additional rotational movements so that the end faces of the crystal can be aligned perpendicular to the incoming light.

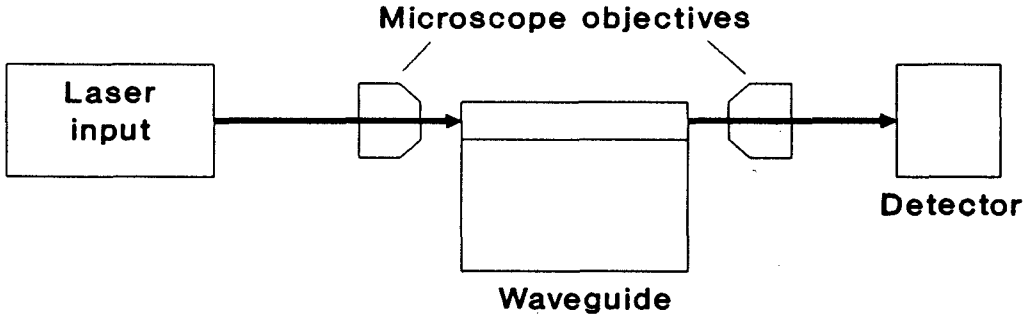

Figure 3.1 - Simple arrangement for launching light into and coupling light out of waveguides.

Various laser sources are used to assess the waveguides and these are summarised in the following table.

Laser	Make	Maximum Power	Wavelength Range	Notes
Argon ion laser	Coherent Innova 70	6W	450-515nm	Used as pump for dye laser and Ti:sapphire
R6G Dye Laser	Coherent 599-OEM	500mW	550-630nm	Pumped by 6W argon ion laser
Ti:sapphire	Spectra Physics Model 3900	500mW	700-1000nm	Pumped by 6W argon ion laser
Single stripe laser diode	SDL 5402	50mW	780-860nm	
Single stripe laser diode	SDL 5412	100mW	780-860nm	
Laser diode array	SDL 2432	500mW	785-835nm	10 stripe array
Laser diode array	SDL 6362	1W	920-970nm	

Table 3.1 - List of pump lasers giving output powers and operating wavelengths.

These sources can be used to pump the absorption bands of the waveguide material to obtain fluorescence or laser measurements, or can be used off absorption to measure waveguide transmissions.

Another important feature of the experimental arrangements is the choice of detector. A large area ($25mm^2$) silicon photodiode is very good for wavelengths up to $1\mu m$. For longer wavelengths the detectors used were germanium for wavelengths up to $1.6\mu m$ and an electrically cooled indium gallium arsenide (InGaAs) detector for wavelengths up to $2.2\mu m$.

In the remaining sections of this chapter I will describe more specific experimental arrangements for measuring waveguide transmissions, fluorescence lifetimes, fluorescence spectra, refractive index profiles and laser performance.

3.2. Waveguide Transmission Measurements.

One of the simplest waveguide measurements that can be made is that of transmission. This involves measuring the power before the launch objective (P_{in}) and the power in the focused output from the waveguide (P_{out}). The transmission (including launch and propagation loss) is given by the equation.

$$T_{p,l} = \frac{P_{out}}{P_{in}} \cdot \frac{1}{T_{obj,in} T_{obj,out}} \cdot \frac{1}{(1-R_{in})(1-R_{out})} \qquad (3.1)$$

where $T_{p,l}$ is the combined propagation and launch loss, $T_{obj,in}$ and $T_{obj,out}$ are the transmissions of the input and output objectives and R_{in} and R_{out} are the Fresnel reflection coefficients of the crystal end faces. Although the launch and propagation losses cannot be separated, this measurement gives some insight into the quality of the waveguides. From measurements made on short lengths of waveguide, where the propagation loss is almost negligible, launch efficiencies are known to be typically about 60-80%. Using these typical values an estimate can be made for the propagation loss. Alternatively, by assuming an 100% launch efficiency, the measurement gives an upper limit for propagation loss.

3.3. Fluorescence Lifetime Measurement.

The best waveguide fabrication process is one which will not only produce low loss waveguides but which will also not change the spectroscopic properties of the material. One of the key characteristics of a laser transition is the fluorescence lifetime. To measure a fluorescence lifetime the waveguide is pumped by light which is tuned to one of the absorption bands of the material. The pump is chopped at a speed such that the rise and fall times of the chopped pump radiation are much less than the fluorescence lifetime to be measured. The output from the waveguide is filtered to cut out any transmitted pump and the remaining fluorescence is detected on a photodiode and displayed on an oscilloscope. Providing that the response time of the photodiode is quick enough the fluorescence lifetime can be measured directly from the fluorescence signal on the oscilloscope. This is not a very accurate method of measuring the lifetime but is

sufficient to compare the signals in both waveguide and bulk samples. If the fluorescence lifetime is the same in both bulk and waveguide samples then no extra non-radiative decay paths are being introduced by the waveguide fabrication method.

3.4. Fluorescence Spectroscopy.

The experimental arrangement used to obtain fluorescence spectra is shown in figure 3.2. The chopped fluorescence light is passed through a motorised monochromator and detected on a photodiode. This signal is then amplified by a lock-in amplifier and displayed on a chart recorder. The plot obtained is that of fluorescence intensity against wavelength. A variety of monochromators were used, with gratings blazed for detection centred around 500nm, 1μm and 2μm. The wavelength resolution of the spectra was determined by noting the width of the pump laser spectrum. In all cases reported in this thesis this was much narrower than any of the features in the fluorescence spectra meaning that width of any spectral features were not limited by the equipment but were in fact accurate. In no case has the spectral response of the detector been corrected for but in most situations (except for Cr^{3+}-doped guides) the wavelength range of the fluorescence spectrum is so small that the detector response is virtually constant.

For laser experiments it is useful to know whether any change in the emission cross section of the laser transition occurs due to the waveguide fabrication process. Comparisons of the fluorescence signals from both waveguide and bulk samples were therefore routinely made. The emission cross section (σ_e) is related to the fluorescence intensity (I) by the equation [1]

$$\sigma_e(\lambda) = \frac{\eta \lambda^5}{\tau_f \left(\int \lambda I(\lambda) d\lambda\right) f 8\pi n^2 c} I(\lambda) \qquad (3.2)$$

where η is the radiative quantum efficiency of the upper laser level, λ is the wavelength, f is the fraction of the excited population in the upper state of the considered transition, n is the refractive index and τ_f is the fluorescence lifetime of the upper level. The amount

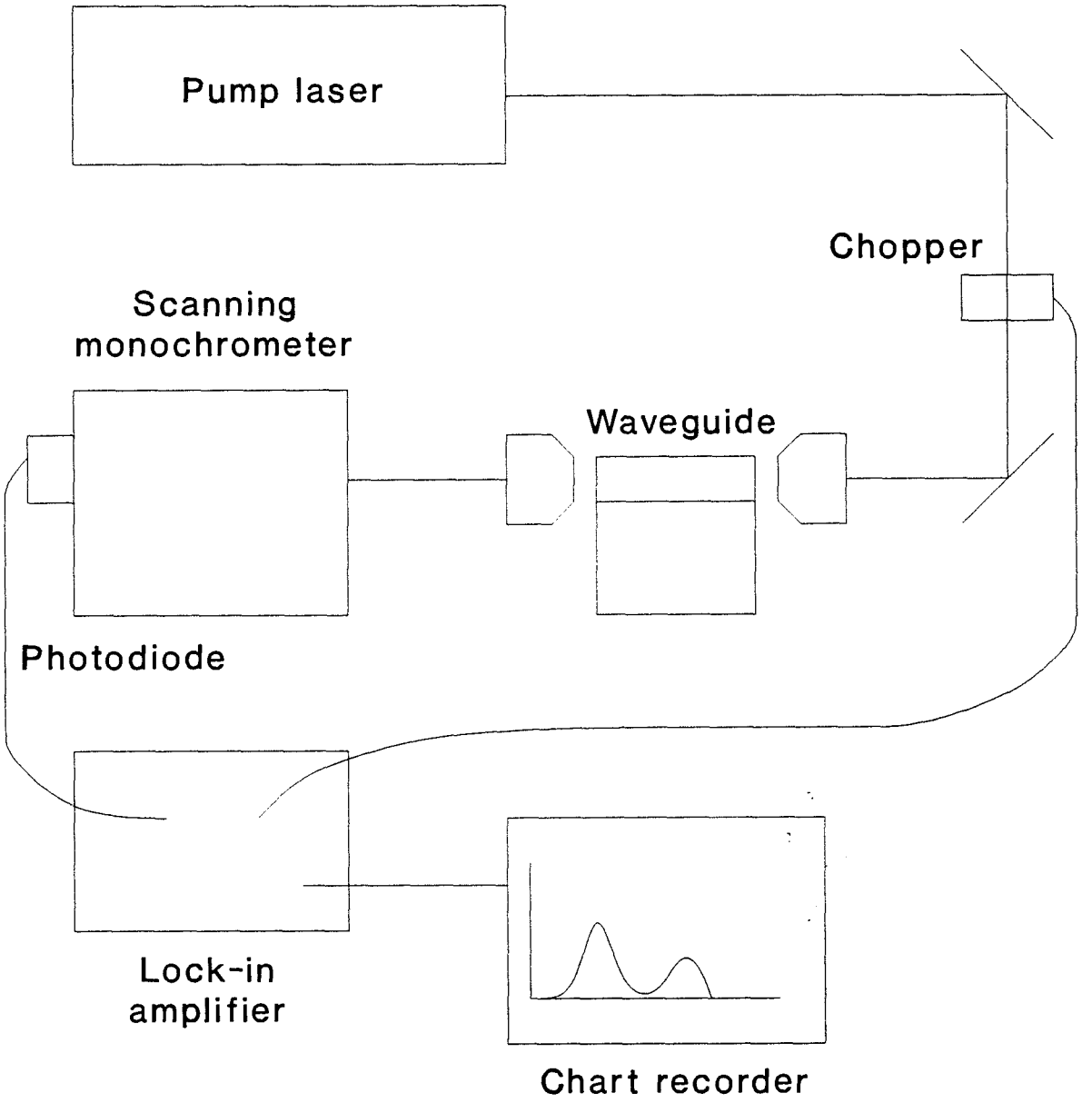

Figure 3.2 - Experimental arrangement for measuring the fluorescence spectrum of a waveguide.

of fluorescence from the upper level is assumed to be the same for both waveguide and bulk. This is true as long as the pumping efficiency to the upper level remains unchanged and no extra non-radiative transitions appear (ie. no change in the fluorescence lifetime). The areas under the bulk and waveguide spectra can then be normalised and the relative heights of the fluorescence peaks calculated. If the values of n, η, f and τ_f in equation (3.2) are the same for waveguide and bulk, and the wavelength range of the emission band is small enough for the approximation

$$\int \lambda I(\lambda) d\lambda = \lambda \int I(\lambda) d\lambda \qquad (3.3)$$

to be made, then the relative change in emission cross section is equal to the relative change in fluorescence intensity. This type of analysis is very useful for ion-implanted waveguides where the fluorescence spectra for narrow transitions (eg. 1.06μm transition in YAG) are usually broadened in the waveguide region.

3.5. Prism Coupled Loss Measurements.

The method used to couple light into the waveguide in the experiments described up to this point is that of direct end coupling using a lens to focus the light into the waveguide. An alternative method is that of prism coupling where a high refractive index prism is used to couple the light into and out of the guide.

The process by which the light is coupled in and out can be described in terms of frustrated total internal reflection. The prism is physically clamped to the surface of the waveguide and therefore a thin air gap exists between the prism and guide. When light is reflected off the surface of the prism parallel to the waveguide then normally it would be totally internally reflected but if the air gap is small enough then the evanescent field will extend into the waveguide. If the component of the wavenumber parallel to the interface is the same as that corresponding to one of the waveguide modes then light will be coupled into the waveguide. Therefore only at certain angles of incidence will light be coupled into the waveguide. The angles of incidence for which light is coupled into

the waveguide can be analysed to give the effective refractive indices of the existing waveguide modes.

One of the advantages of this is that the distance between the input and output prisms can be varied along the length of the waveguide. Provided that a sample can be found which is long enough to obtain sufficient data then an accurate measure of the waveguide propagation loss. This measurement of loss combined with simple transmission measurements of the waveguide enables the launch efficiency to be calculated. The main disadvantage of this technique is that light cannot be launched into waveguides with cladding layers. This makes the technique unsuitable for epitaxially grown waveguide most of which have a cladding grown on top of the waveguide layer.

3.6. Measurement of Refractive Index Profiles.

One experimental technique which is particularly relevant to the characterisation of ion-implanted waveguides is that of using measurements of mode refractive index to calculate the waveguide refractive-index profile. These measurements of mode refractive index are done by prism coupling a diverging beam of light into a waveguide in a process known as "dark mode" prism coupling.

If a single isosceles prism is used to couple the light into the waveguide, as shown in figure 3.3, then light which is not coupled into the waveguide will be reflected out of the prism. At angles where light is coupled into the waveguide modes there will be a reduction in the reflected intensity. By measuring the angles at which these so called dark modes occur a set of values for mode refractive indices can be built up. Included in this information are the refractive indices for highly lossy modes which leak out of the waveguide. This means that even for guides which have only one well confined mode many points are still available for analysis.

The information obtained from the dark mode prism coupling can be used to fit a refractive index profile [2]. This method was used for all the ion-implanted guides described in this thesis. For ion-implanted guides the refractive index profile is assumed

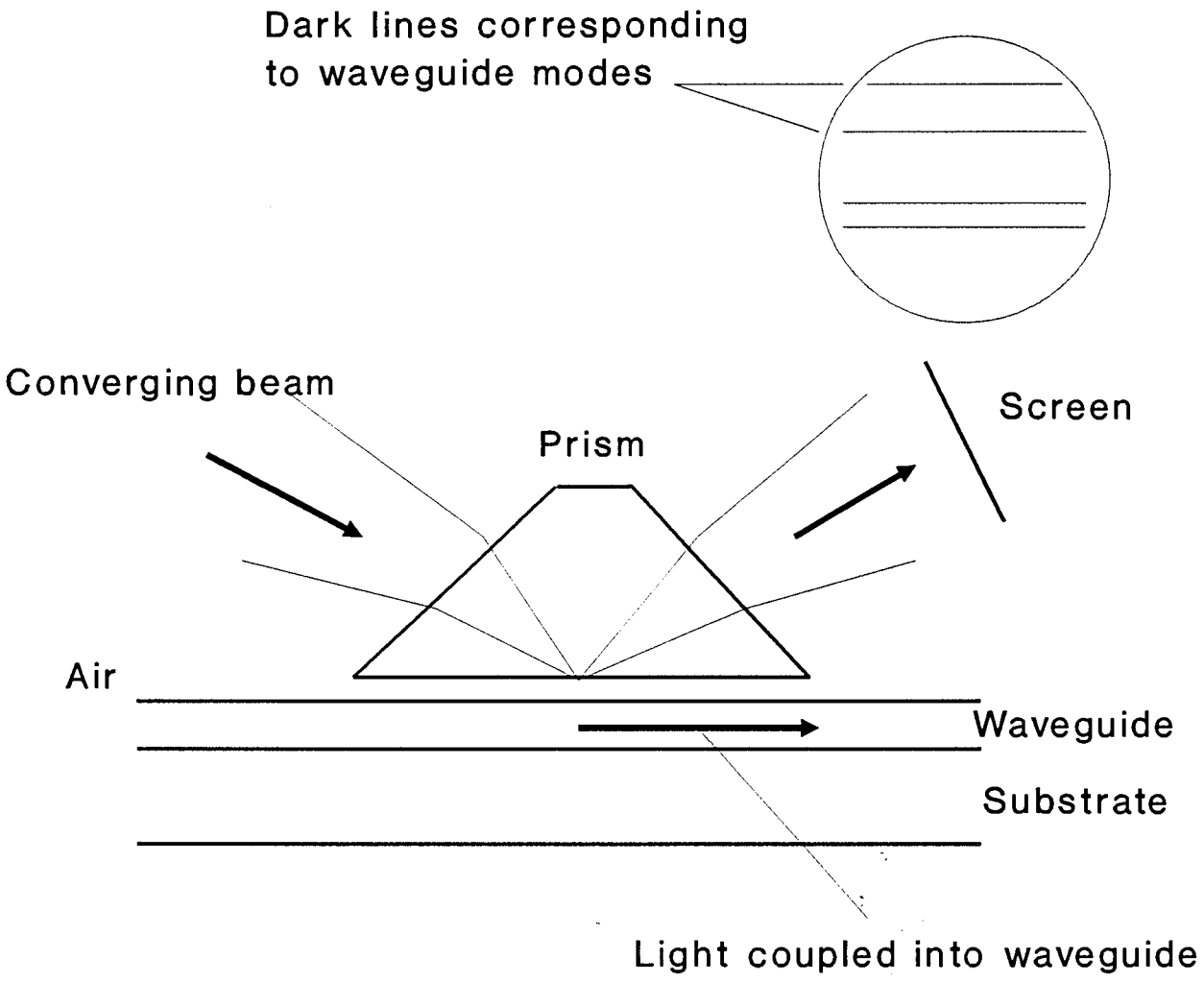

Figure 3.3 - Diagram of "dark mode" prism coupling into a waveguide.

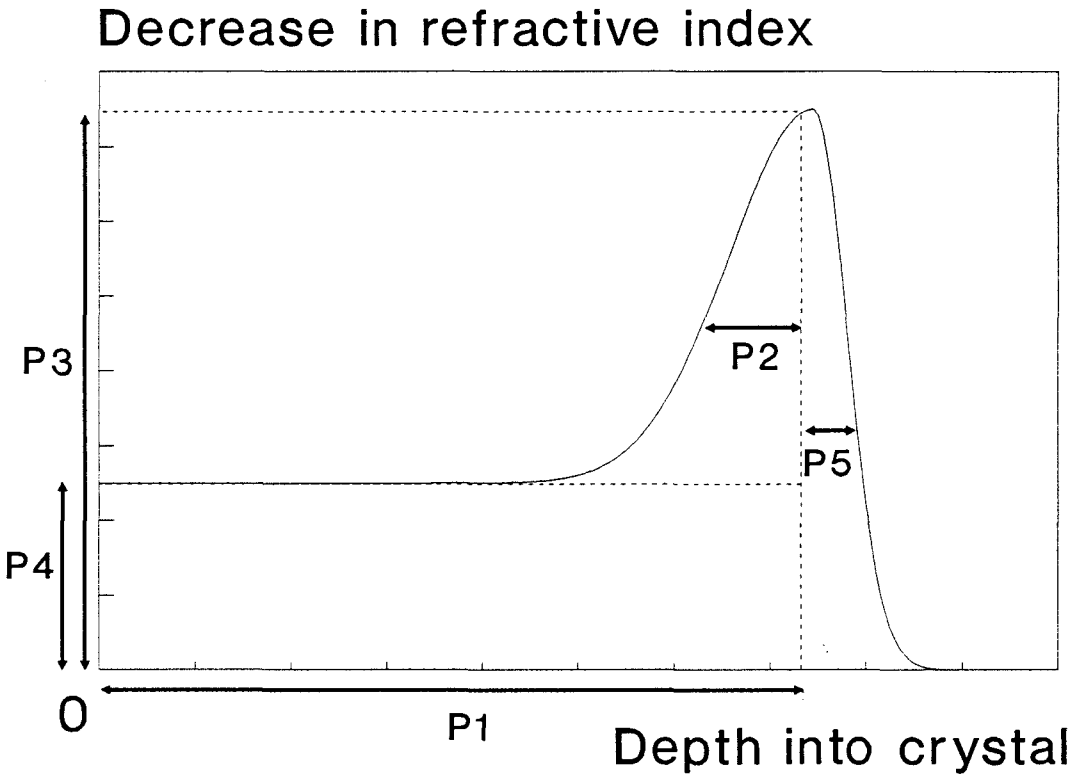

Figure 3.4 - Plot of refractive index against depth into crystal showing the five parameters used to fit a refractive index profile to experimentally taken mode measurements.

to be represented by a constant offset to the bulk value in the electronic stopping region with a damage barrier made up of two half Gaussians. The fitted curve has five adjustable parameters which are shown in figure 3.4. P1 is the ion range in the material, P2 and P5 are widths of the two half gaussian sections which make up the damage barrier, P3 is the height of the damage barrier and P4 is the change in refractive index in the electronic slowing region. The analysis is done by splitting the waveguide region into about 50-100 separate parts and then accounting for the reflections at the boundaries between these regions.

3.7. Waveguide Laser Experiments.

The experimental arrangement used for laser experiments is the same as that used for fluorescence lifetime measurements and is shown in figure 3.5. The main addition to the fluorescence experiment is that of two mirrors attached to both ends of the crystal. These are held in place using the surface tension of a drop of fluorinated liquid. The liquid was chosen for its high thermal conductivity so that any heat generated in the waveguide would not cause the liquid to evaporate. Another addition to the layout is a variable attenuator which can be used adjust the power of the pump laser. For threshold measurements the fluorescence output is detected with a photodiode and viewed on an oscilloscope. The launch into the waveguide can then be tweaked so that lasing occurs at the lowest possible input power. After this the slope efficiency can be measured by stepping up the power at the input and measuring both the power incident on the launch objective and the power after the colour filter.

3.8. References.

1. B.F.Aull and H.P.Jenssen, IEEE Journal of Quantum Electronics, **18**, pp.925-930, 1982.
2. P.J.Chandler and F.L.Lama, Optica Acta, **25**, pp.127-143, 1986.

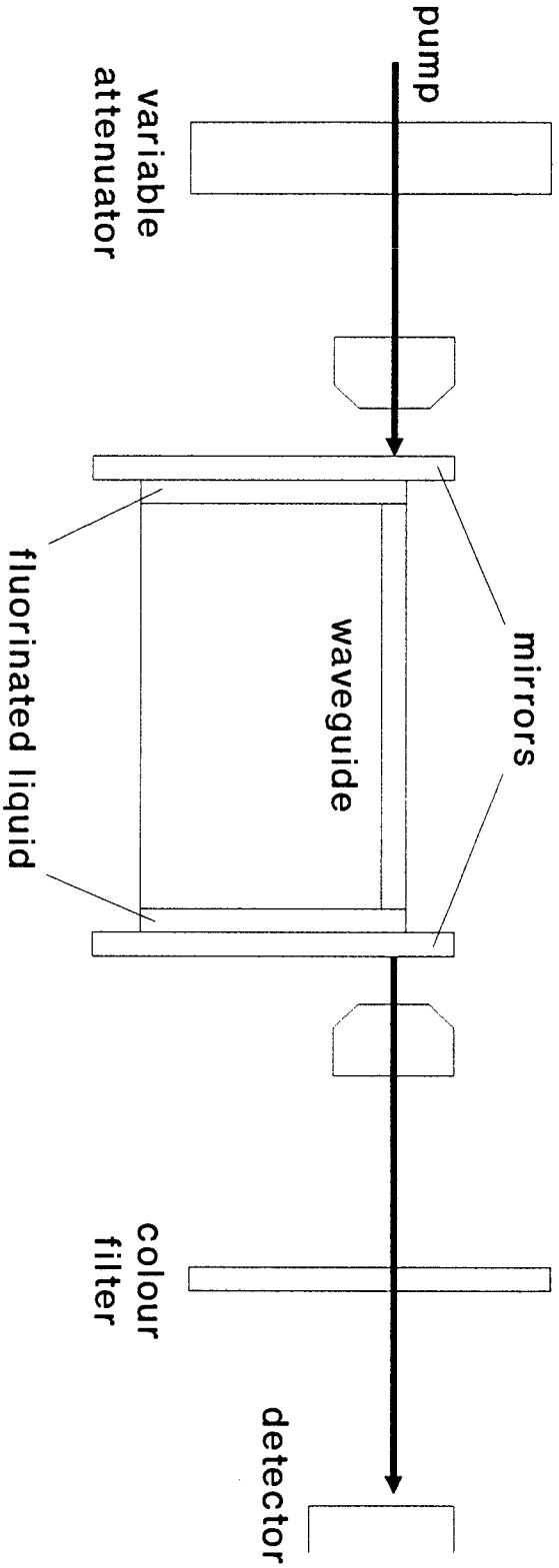

Figure 3.5 - Experimental arrangement for waveguide laser experiments.

Chapter 4 - Ion-Implanted Planar Waveguides

4.1. Introduction

Ion-implantation is a way of modifying the surface properties of a material. These properties could be the hardness, wear or friction of the material or one of its optical properties such as absorption, reflectivity or refractive index [1]. Here it is the change in optical properties which are used to create waveguides. By changing the refractive index of a material ion-implantation can be used to form optical waveguides in a wide range of materials. This can be done by implanting either light ions, such as hydrogen and helium, to form a low refractive index barrier a few microns under the surface of the material [2-6] or by implanting heavier ions a few 100 nanometres into the surface and then thermally diffusing them deeper into the crystal [7]. Ion-implantation can also be used to implant dopant ions into an existing waveguide [8]. In this chapter I will firstly describe the formation of waveguides by the implantation of light ions. Then I will describe the waveguide characteristics, spectroscopic changes and laser performance of planar waveguides formed by He^+ ion implantation into in Nd^{3+}-doped $Gd_3Ga_5O_{12}$ (GGG) and Yb^{3+}-doped $Y_3Al_5O_{12}$ (YAG) crystals. The actual ion-implantation for these samples and the refractive index profile measurements were carried out at the University of Sussex by Peter Chandler and co-workers whereas the laser and spectroscopic measurements were obtained at Southampton.

4.2. Theory of Ion-Implantation

When light ions at energies of several MeV are implanted into a material they are slowed down by electronic and nuclear collisions. The rate at which nuclear collisions slow the ions is very low for ion energies above about 100keV, so for ions of energies about 3MeV, like the ones used to form ion-implanted waveguides, electronic collisions dominate until the ions have lost sufficient energy to interact with the nuclei in the material. These nuclear collisions produce damage and amorphise the material, usually decreasing its refractive index. For ions implanted along the x axis into a material whose surface is given by the $x=0$ plane the final distribution of the ions is given by the

equation [9]

$$R(x,y,z) = \frac{1}{\sqrt{8\pi^3\sigma_{\parallel}^2\sigma_{\perp}^4}}\exp\left(-\frac{(x-R_p)^2}{2\sigma_{\parallel}^2}\right)\exp\left(-\frac{(y^2+z^2)}{2\sigma_{\perp}^2}\right) \qquad (4.1)$$

This is a Gaussian distribution and is shown in figure 4.1a. R_p is the range of the ions, $\sigma_{\parallel}$ is the standard deviation of the spread parallel to the direction of implantation and $\sigma_{\perp}$ is the standard deviation of the spread perpendicular to this. The values of these quantities for different ions in different elements are tabulated [9] and can be used to obtain estimates of ion ranges for compounds by taking a weighted average. A theoretical plot of the variation of refractive index with depth into the crystal is shown in figure 4.1b. This index shape confines light between the surface and the low refractive index barrier.

As well as refractive index changes in the nuclear damage region, defects are also produced in the electronic stopping region. Because of this, the waveguides often have to be annealed to remove defects and reduce waveguide losses. For example, $LiNbO_3$ waveguides have to be annealed at 200°C for 40 minutes to reduce the losses from 30dB/cm to 1dB/cm.

In practice the refractive index profile produced by ion-implantation is almost impossible to predict. This can be seen by looking at three of the materials investigated before the start of the work covered by this thesis. Figure 4.2 shows the refractive index profiles produced when three different materials (lithium niobate, yttrium aluminium perovskite and yttrium aluminium garnet) are implanted with high energy He^+ ions. Each material shows a different response.

Lithium Niobate, $LiNbO_3$ - The ordinary and extraordinary refractive indices react differently to ion-implantation. The ordinary index is decreased throughout the ion range with the maximum decrease occurring in the nuclear damage region. The extraordinary index, however, is actually increased in the region of electronic collisions. Although the

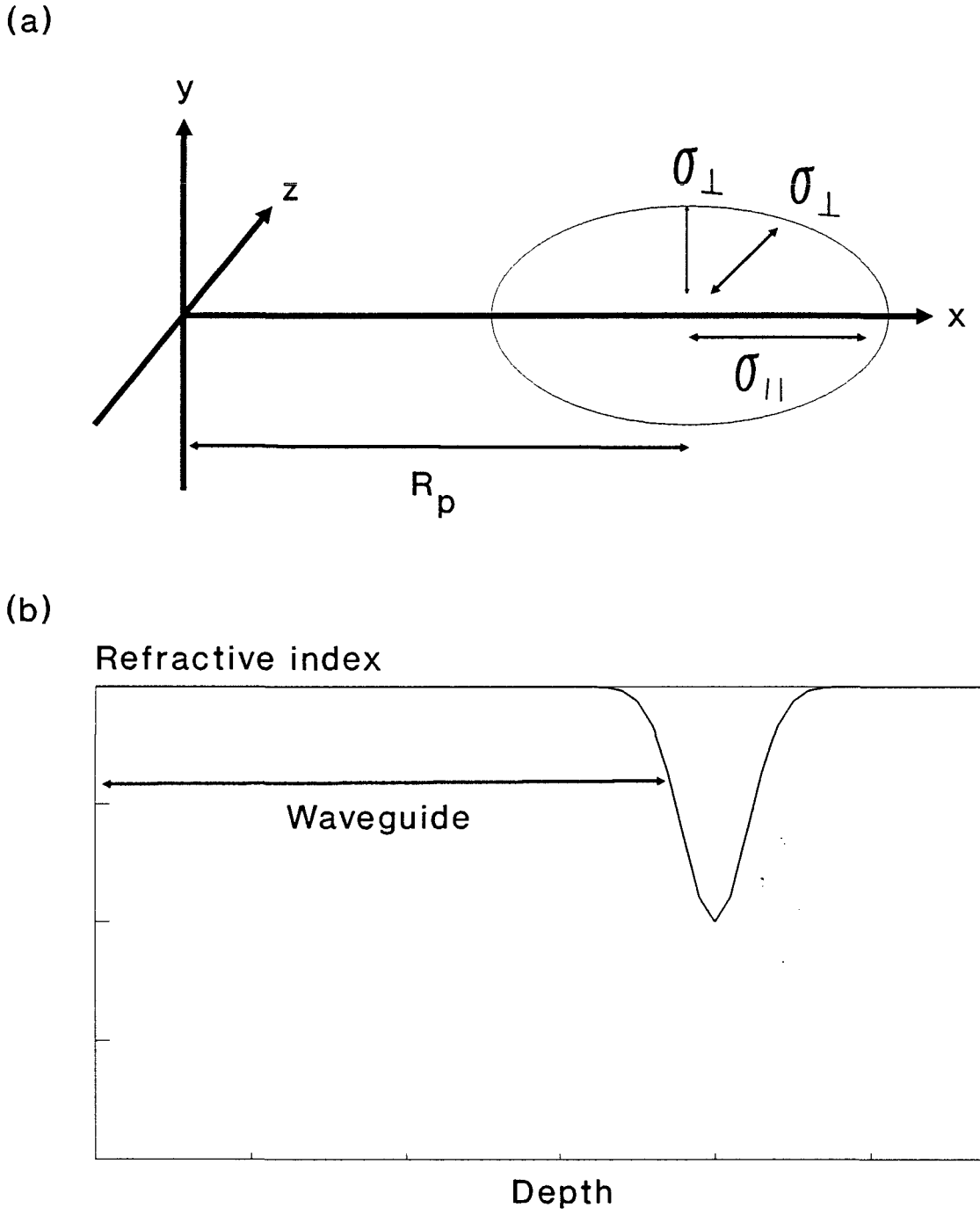

Figure 4.1 - a. Distribution of ions implanted along the x axis into a material. b. Theoretical plot of refractive index against depth for an ion implanted material.

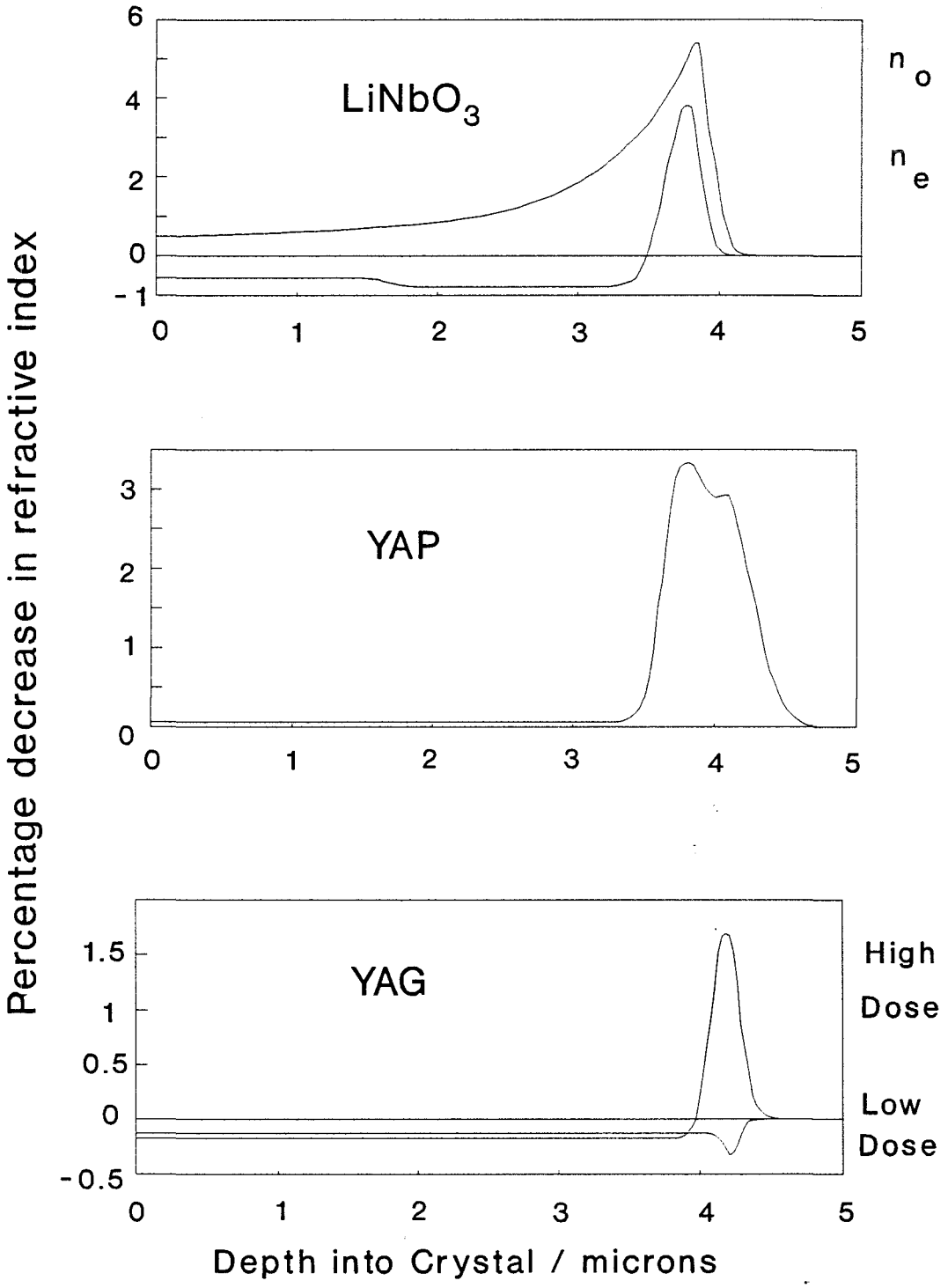

Figure 4.2 - Variation of refractive index with depth into crystal for $LiNbO_3$, YAP and YAG.

reason for this is not fully understood, it has been suggested that the crystal is restructuring under electronic bombardment [3]. This increase in refractive index proves very useful as it means that the lower order waveguide modes can be confined without the help of the damage barrier.

Yttrium Aluminium Perovskite, ($YAlO_3$) YAP - There is almost no change in the refractive index in the electronic collision region so the waveguide modes have to be entirely confined using the damage barrier. For best results the width of the barrier is increased using three implants at energies of 2.0, 2.15 and 2.3MeV [10]. Even with this optimisation the waveguide propagation losses are about 15dB/cm.

Yttrium Aluminium Garnet, ($Y_3Al_5O_{12}$) YAG - The refractive index changes produced by implanting He^+ ions into YAG were found to be highly dose dependent. For low doses (less than $1.5x10^{16}$ ions/cm^2) the index is increased throughout the ion range, reaching a peak of 0.3% in the nuclear damage region and remaining constant at 0.1% in the electronic slowing area. An index decrease of about 2.0% occurs in the nuclear damage region for higher ion doses [11]. The index rise in the electronic slowing region is still present. Because of these different reactions at different ion doses the final waveguide is usually made up of several implants. Several low dose implants at different energies are used to produce an index rise in the electronic slowing region and one high dose, high energy implant is used to produces a damage barrier at the bottom of the guide. Another observation is that the increases in refractive index in the electronic slowing region (described above for TM modes) are smaller for TE modes. The YAG crystal is therefore changing from its original isotropic state to a anisotropic one in the implanted region. The result of this is that the laser output from Nd:YAG waveguides is TM polarised because at the laser wavelength of 1.06μm one TM mode but no TE mode exists [12].

The index changes discussed here are examples of some of the effects that can be produced by ion-implantation. In the next two sections I will describe the properties and laser results obtained for planar He^+ implanted waveguides formed in Nd^{3+}-doped GGG

and Yb^{3+}-doped YAG.

4.3. Nd:GGG Planar Waveguide Laser [13]

The crystal gadolinium gallium garnet ($Gd_3Ga_5O_{12}$ or GGG) is a isotropic, cubic crystal. The interest in this crystal host lies in the fact that it can be Cr^{3+}-doped to produce a widely-tunable, vibronic laser material [14]. To test the response of GGG to ion-implantation a Nd^{3+}-doped crystal was used. This is a high gain material and should give a good insight into the suitability of GGG as a host for ion-implanted waveguide lasers. Nd:GGG was first operated as a laser in a flashlamp pumped configuration in 1964 by Geusic et. al. [15].

In the first experiment a 2.7 atomic percent (at.%) doped sample was implanted with a dose of $4x10^{16}$ ions/cm^2 at an energy of 2.5MeV. The original refractive index of the crystal was 1.95. Analysis of the waveguide dark modes indicated that there was an index rise of 0.25% in the electronic slowing region and a index decrease of 2% in the damage barrier for TM modes. A smaller index rise was observed for TE modes and as a consequence of this they did not support a mode at the laser wavelength of 1.06μm. When a sample with a higher doping level of 3.35 at.% was implanted with the same implant no mode was observed at 1.06μm. Analysis of the guide showed that this was because the size of damage barrier was dependent on dopant concentration. The refractive index profiles for waveguide formed in both 2.7 and 3.35 at.% doped material using ion doses of $2x10^{16}$ ions/cm^2 at an energy of 2.9MeV are shown in figure 4.3. These values of ion dose and energy were used in the final waveguide laser experiments. A transmission measurement was made in order to determine the propagation loss in the waveguide. For a 2.5mm length of crystal a transmission of 78% (including launch efficiency) was measured. With launch efficiencies typically about 80% the propagation loss was estimated to be at most 1dB/cm.

The spectroscopy of the waveguide was also investigated to see if any changes occurred in the fluorescence spectrum or lifetime of the laser transition. No change was detected between the bulk and waveguide fluorescence lifetimes with $\tau_{fl}=180\mu s$ in both

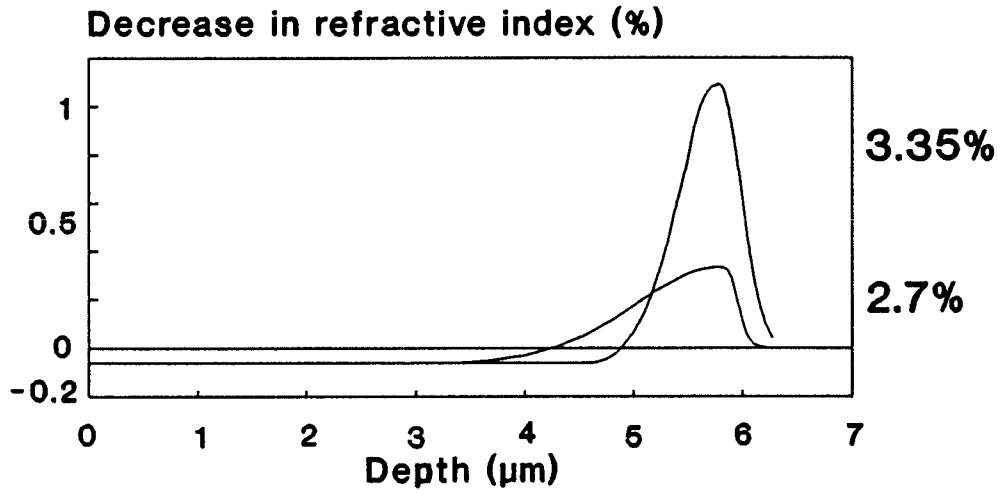

Figure 4.3 - Decrease in refractive index plotted as a function of depth below the implanted surface for samples of 2.7at.% and 3.35at.% doped Nd:GGG.

cases. However the fluorescence spectrum for the $^4F_{3/2} \rightarrow {}^4I_{11/2}$ transition (centred round a wavelength of 1.06μm) was altered by ion-implantation and this is shown in figure 4.4. The waveguide fluorescence was significantly broadened compared to that from the bulk crystal and the height at the peak of the fluorescence was reduced by a factor of 0.58. Taking this into account gives a value for emission cross section of 1.7×10^{-23} m^2.

The fluorescence spectrum was also measured for the $^4F_{3/2} \rightarrow {}^4I_{9/2}$ transition at 940nm in the guide implanted with 2.5MeV He^+ ions. This waveguide did not support a mode at 1.06μm and this could be used as a method of suppressing the 1.06μm transition in favour of the 940nm one. It can be seen from the spectra shown in figure 4.5 that there is no difference between the bulk and waveguide, a feature which has been observed in other relatively broad transitions such as $^3H_4$ to $^3H_6$ in Tm:$LiNbO_3$ and $^4S_{3/2}$ to $^4I_{9/2}$ in Er:YAP.

At first an R6G dye laser at 588nm was used to pump the crystal. With mirrors which were highly reflecting at 1.06μm attached to the crystal an incident power threshold of 20mW was measured. Allowing for the mirror and launch objective transmissions as well as an 80% launch efficiency this becomes 12.5mW of absorbed

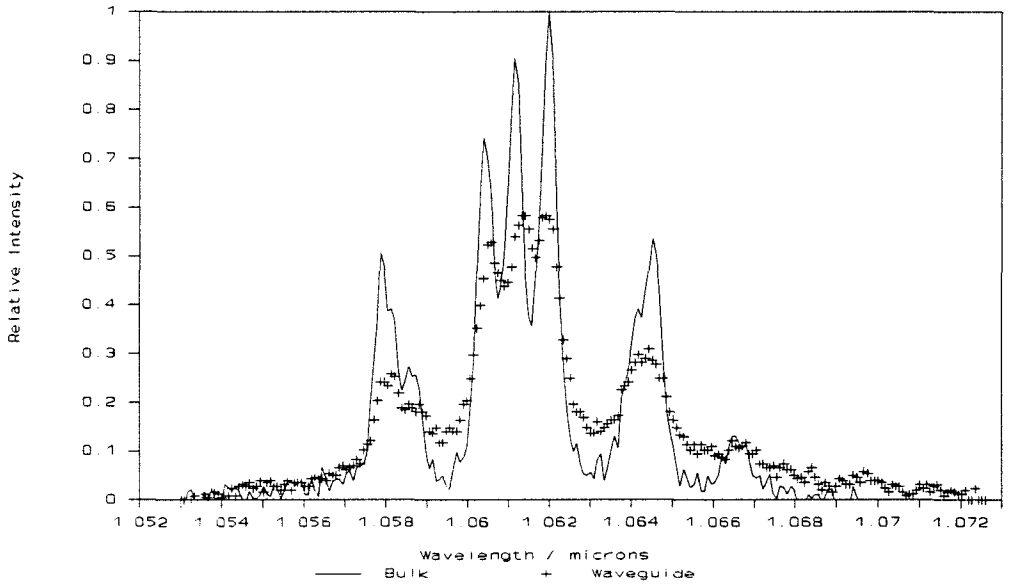

Figure 4.4 - Waveguide and bulk fluorescence spectra in Nd:GGG at wavelengths around 1.06μm.

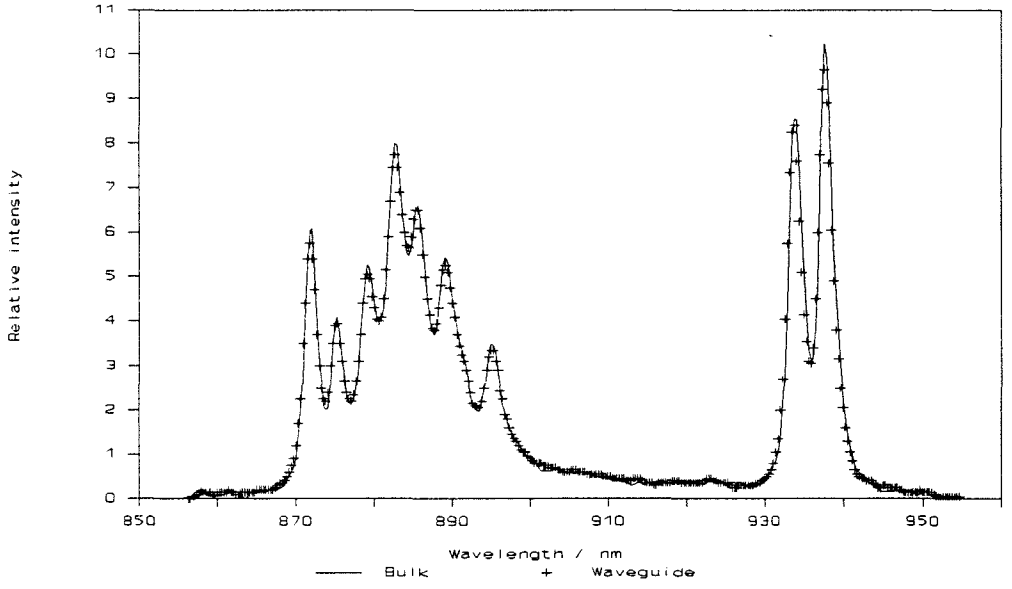

Figure 4.5 - Waveguide and bulk fluorescence spectra in Nd:GGG at wavelengths around 900nm.

pump power.

A 500mW, ten-stripe laser diode array (SDL 2432) was also used to check the properties of the waveguide laser. This was temperature-tuned to the Nd:GGG absorption at 805nm. Because of the closeness of the pump and laser wavelengths this should give better performance than the 588nm pump. With highly reflecting mirrors at each end of the waveguide the lowest absorbed power threshold obtained was 8mW. With an 83% reflecting output coupler the threshold became 60mW of absorbed power and the slope efficiency was 30%. The plot of absorbed pump power against output power is shown in figure 4.5.

The waveguide laser mode had spot sizes of 4.6μm in the guided plane and 72μm in the unguided. If channel waveguides could be fabricated in this material then the spot size in the unguided plane and therefore the laser thresholds could be reduced by a factor of ten. This is what is in fact observed in the channel Nd:GGG waveguides which are described in chapter 5.4.

The fabrication of waveguides in both Nd^{3+}-doped and undoped GGG show the suitability of the material as a host for ion-implanted waveguides. However the first trials on Cr^{3+}:GGG showed that waveguides fabricated in a similar manner had extremely high propagation losses. This seems to be a feature of Cr^{3+}-doped materials in general which, when ion-implanted, tend to have higher losses than their undoped relatives.

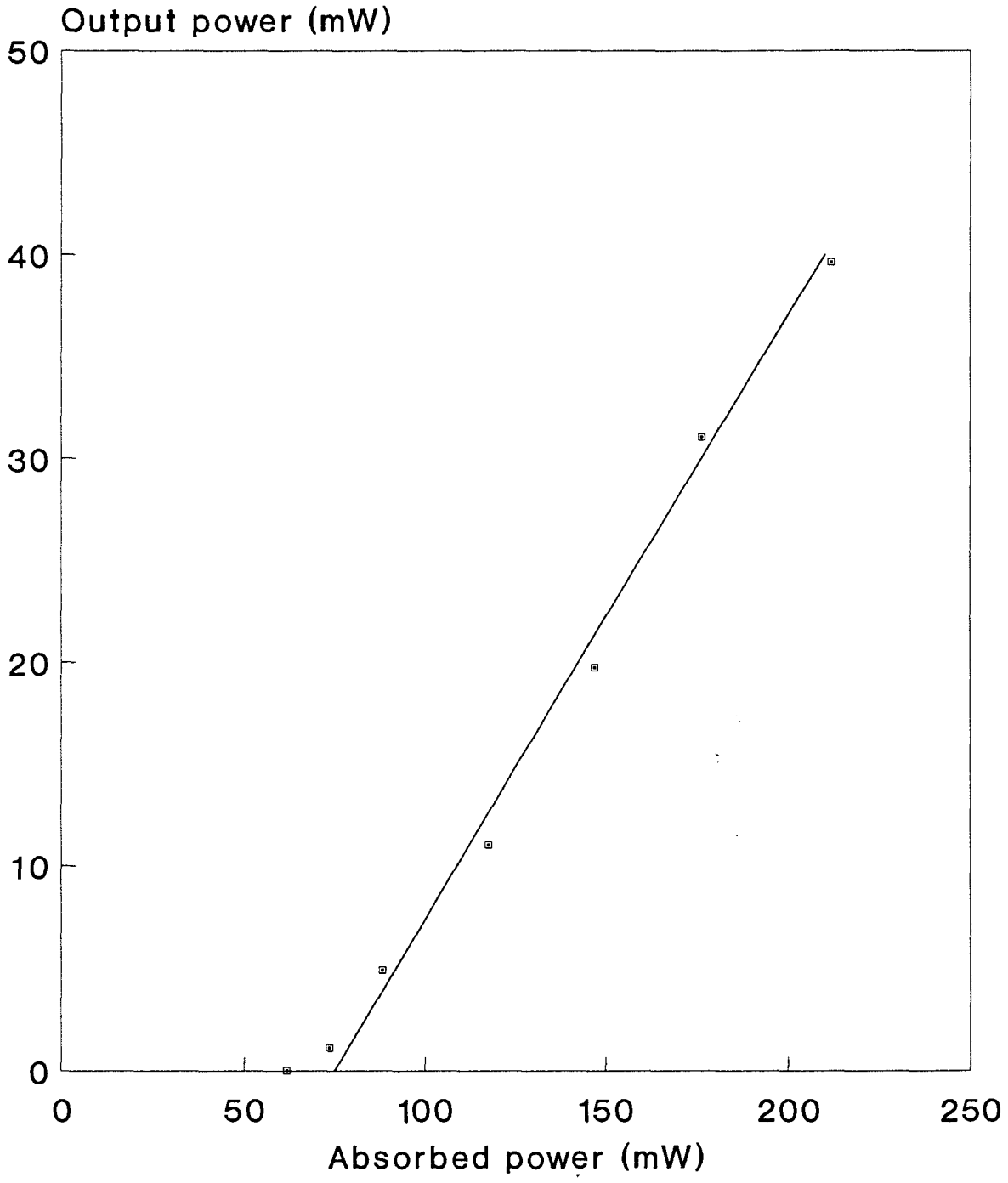

Figure 4.6 - Output power vs. input power for a diode laser pumped (805nm) Nd:GGG planar waveguide laser.

4.4. Yb:YAG Planar Waveguide Laser [16]

A material which has been successfully operated as a ion-implanted waveguide laser is Yb^{3+}-doped yttrium aluminium garnet ($Y_3Al_5O_{12}$, YAG). This is similar to GGG in that it is a cubic isotropic crystal. Figure 4.7 shows the energy levels of Yb:YAG with the three possible pump wavelengths of 920nm, 941nm and 968nm marked as well as the laser transition at 1.03μm. Above the $^2F_{5/2}$ manifold at an energy of $\sim 10000cm^{-1}$ there is a large gap to the manifolds of the next electronic state at $\sim 75000cm^{-1}$. Because of this gap there is no excited state absorption present in the crystal. Another feature of this energy gap is that there is no concentration quenching of the upper laser level and therefore the material can be highly doped (at least 20 at.% [17]) without reduction in the fluorescence lifetime. A further advantage of Yb:YAG is that the pump and laser wavelengths are closer than in Nd:YAG, making the pumping more efficient and causing less heat generation. Unfortunately, the lower laser level is thermally populated at room temperature and a reabsorption loss is therefore introduced into the crystal. At room temperature 4% of the ground state population is in the lower laser level, introducing a loss of about 2.5dB/cm. With this added loss term present in the laser cavity the relative importance of the waveguide propagation loss to the overall loss is reduced. However, all the advantages of the waveguide geometry still exist.

To fabricate a waveguide in Yb:YAG a standard implant for Nd:YAG was used. This is $3x10^{16}$ ions/cm^2 of He^+ at 2.65MeV to form a damage barrier together with doses of $0.75x10^{16}$ ions/cm^2 at 1.7, 1.9 ,2.1 and 2.3MeV to give the maximum index rise in the guiding region. The measured refractive index profile is shown in figure 4.8. As in Nd:YAG there was greater confinement for TM modes than TE modes and the output of the laser was therefore TM polarised. The mode spot size in the guided plane was measured to be 2.5μm at a wavelength of 1μm.

Spectroscopic measurement indicated that the fluorescence lifetimes were the same in both waveguide and bulk crystal with τ_{fl} = 1.16ms in both cases. The fluorescence spectrum was, however broadened with the emission cross section reduced by a factor of 0.67 at the fluorescence peak of 1.03μm.

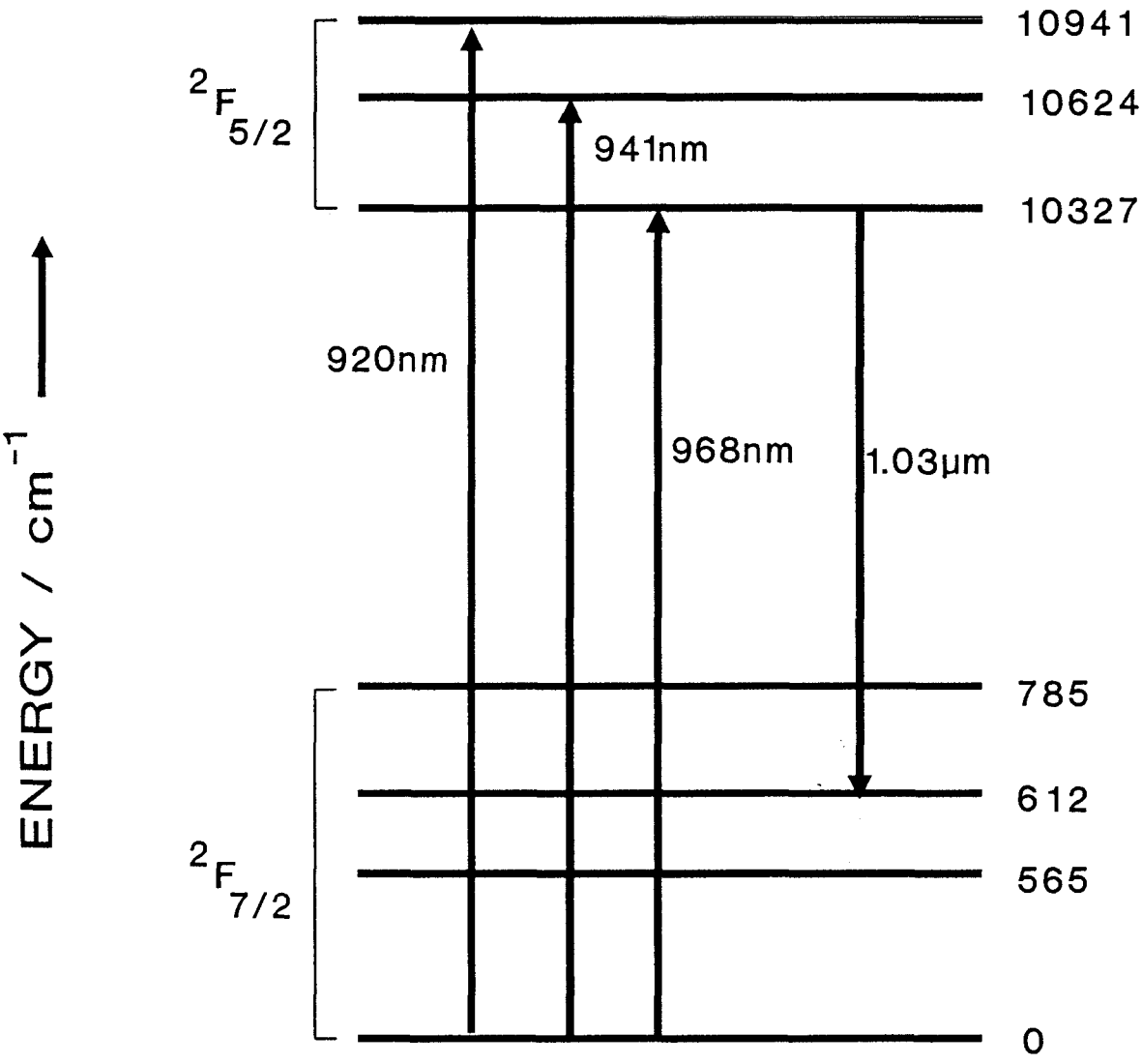

Figure 4.7 - Energy level diagram of Yb:YAG showing the pump wavelengths at 920, 941 and 968nm and the laser transition at 1.03μm.

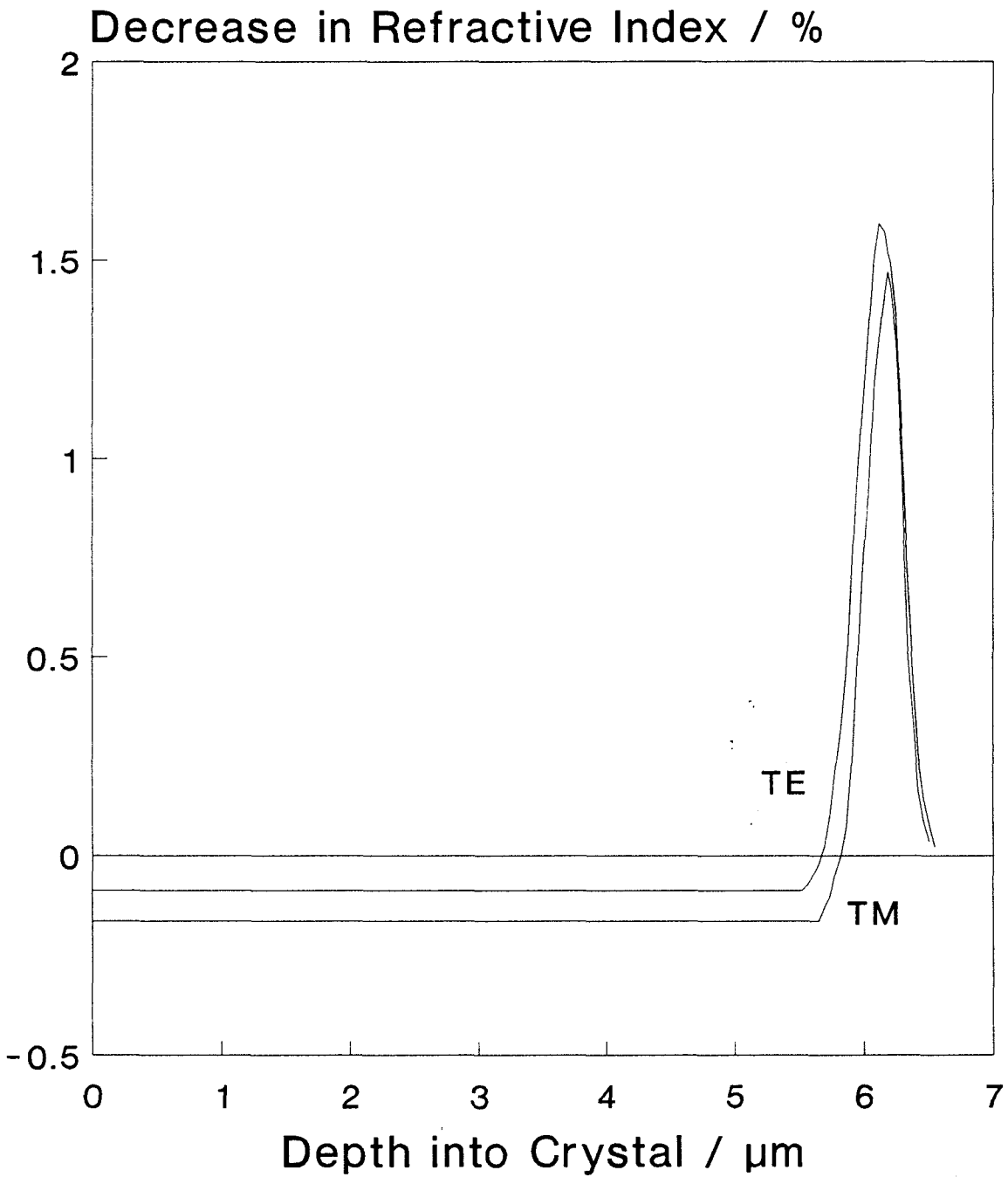

Figure 4.8 - Refractive index profile of an ion-implanted Yb:YAG waveguide

To test the waveguide as a laser a 1.65mm length of crystal was pumped by a Ti:Sapphire laser operating at 941nm. With HR mirrors attached to both ends of the guide the threshold power was 56mW incident on the launch objective. This corresponded to 30mW of absorbed pump power. The actual threshold is higher than the theoretical one of 9mW. This is probably due to imperfect mirror contact at the ends of the crystal. When one of the HR mirrors was replaced with a 83% reflectivity output coupler the threshold increased to 74mW of absorbed power and the slope efficiency was 19%. The plot of output power against absorbed pump power is shown in figure 4.9.

The waveguide used in these experiments was rather lossy at ~2dB/cm. For Yb:YAG planar waveguides to outperform bulk lasers then a method of fabricating lower loss waveguides has to be found. This is the case for the epitaxially grown Yb:YAG waveguides discussed in chapter 6.8. Another way to improve the performance of the waveguide laser would be to fabricate channel waveguides in Yb:YAG.

4.5. Conclusions

The fabrication of planar waveguides by ion-implantation is a useful step towards the production of channel waveguides by the same method. Virtually all of the information (spectroscopy, ideal implant conditions, vertical spot sizes) applying to the channels is can be measured in the planar guides. Planar waveguide lasers formed by ion-implantation will rarely be able to rival bulk lasers due to the levels of propagation loss (~ 1dB/cm) generally present in the guides and the limitations of the planar geometry. Some materials do however react well to ion implantation and have produce waveguides with losses as low as 0.1dB/cm. One such material is yttrium ortho-silicate (Y_2SiO_5) which has recently produced guides with losses of 0.2dB/cm. This material can be doped with Nd^{3+}, Yb^{3+}, Er^{3+} or Cr^{4+} and is a very encouraging prospect for the future of ion-implanted waveguide lasers. The formation of planar waveguides should however always be a step towards producing channel waveguides will perform better as long as the propagation losses are not increased. The fabrication of channel waveguides by ion-implantation is discussed in the next chapter.

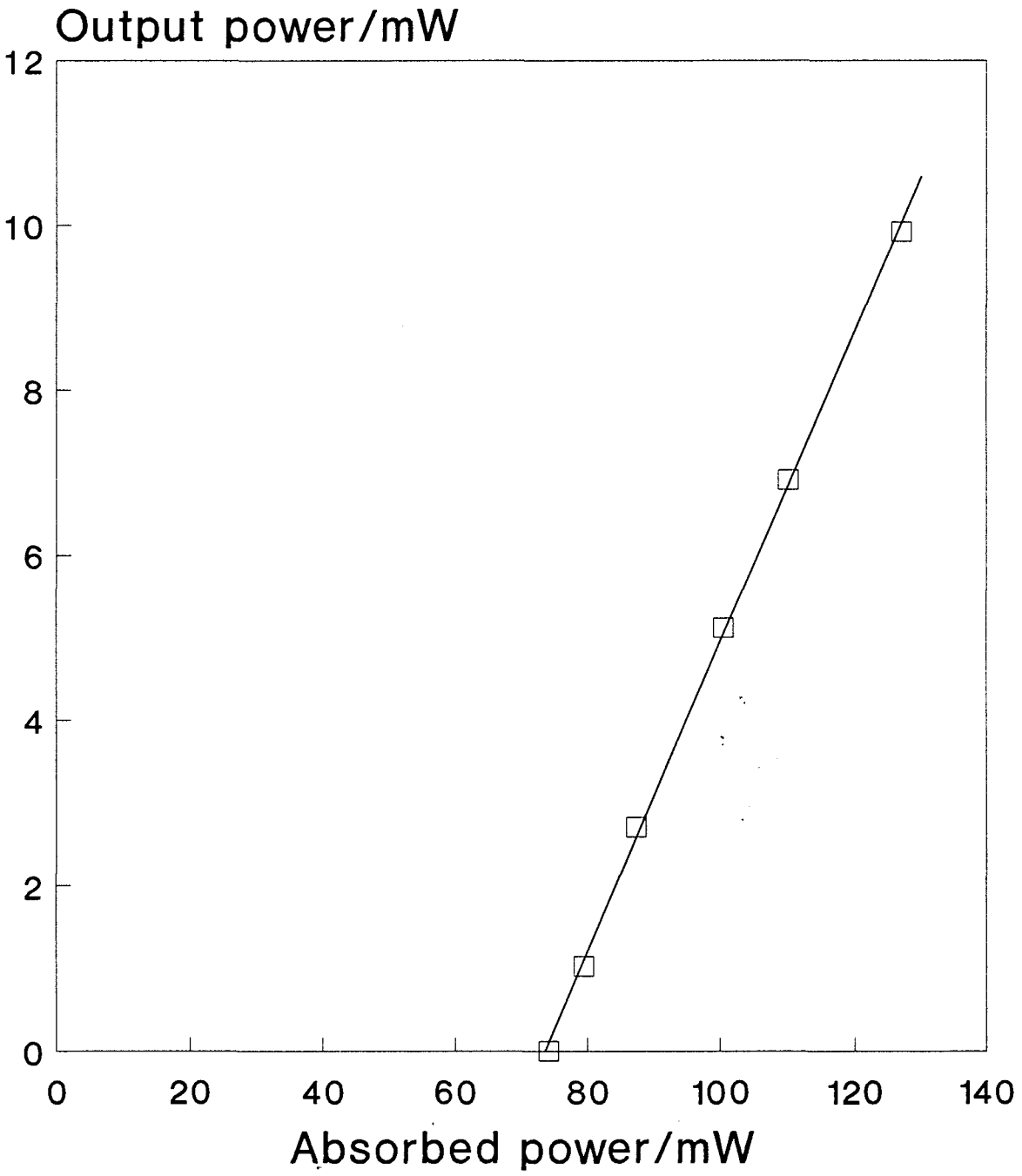

Figure 4.9 - Plot of output laser power against absorbed pump power for an ion-implanted, Yb:YAG, planar waveguide laser.

4.6. References

1. P.D.Townsend, Reports on Progress in Physics, **50**, pp.501-558, 1987.
2. P.J.Chandler and P.D.Townsend, Nuclear Instruments and Methods in Physics Research, **B19/20**, pp.921-926, 1987.
3. P.D.Townsend, Nuclear Instruments and Methods in Physics Research, **B46**, pp.18-25, 1990.
4. G.Götz and H.Karge, Nuclear Instruments and Methods, **209/210**, pp.1079-1088, 1983.
5. J.R.Kulish, H.Franke, A.Singh, R.A.Lessard and E.J.Knystautas, Journal of Applied Physics, **63**, pp.2517-2521, 1988.
6. I.K.Naik, Applied Physics Letters, **43**, pp.519-520, 1983.
7. T.Bremer, W.Heiland, C.Buchal, R.Irmscher and B.Stritzker, Journal of Applied Physics, **67**, pp.1183-1187, 1990.
8. A.Polman, D.C.Jacobson, D.J.Eaglesham, R.C.Kistlern and J.M.Poate, Journal of Applied Physics, **70**, pp.3778-3784, 1991.
9. U.Littmark and J.F.Ziegler, The Stopping Ranges of Ions in Matter, vol.6, published by Pergamon Press, 1980.
10. S.J.Field, D.C.Hanna, D.P.Shepherd, A.C.Tropper, P.J.Chandler, P.D.Townsend and L.Zhang, Electronics Letters, **26**, pp.1826-1827, 1990.
11. L.Zhang, P.J.Chandler, P.D.Townsend, S.J.Field, D.C.Hanna, D.P.Shepherd and A.C.Tropper, Journal of Applied Physics, **69**, pp.3440-3446, 1991.
12. S.J.Field, D.C.Hanna, D.P.Shepherd, A.C.Tropper, P.J.Chandler, P.D.Townsend and L.Zhang, IEEE Journal of Quantum Electronics, **27**, pp.428-433, 1991.
13. S.J.Field, D.C.Hanna, A.C.Large, D.P.Shepherd, A.C.Tropper, P.J.Chandler, P.D.Townsend and L.Zhang, Optics Communications, **86**, pp.161-166, 1991.
14. B.Struve and G.Huber, Journal of Applied Physics, **57**, pp.45-48, 1985.
15. J.E.Geusic, H.M.Marcos and L.G.Van Uitert, Applied Physics Letters, **4**, pp.182-184, 1964.
16. D.C.Hanna, J.K.Jones, A.C.Large, D.P.Shepherd, A.C.Tropper, P.J.Chandler, M.J.Rodman, P.D.Townsend and L.Zhang, Optics Communications, **99**, pp.211-

215, 1993.

17. T.Y.Fan, Proceedings of Solid State Lasers : New Developments and Applications, NATO ASI Series, Elba, 1992.

Chapter 5 - Ion-Implanted Channel Waveguides

5.1. Introduction.

To improve the performance of ion-implanted planar waveguides, a method of fabricating channel guides had to be found. If this could be done without increasing the waveguide propagation loss then the further confinement would reduce waveguide laser thresholds by about a factor of 10. To fabricate channels the surface of the sample must be masked to prevent the ions from penetrating certain regions of the crystal surface. This can be done by using photolithographic techniques to form the desired mask on the surface of the sample [1]. An alternative approach is to simply use a mechanical mask to cover the surface. This has been successfully done [2] by using a grid of forty 8μm wide SiO_2 fibres or 13μm tungsten wires to produce channel waveguides with losses of 1dB/cm in $KNbO_3$.

The method chosen here was that of electroplating gold into gaps in a photoresist mask. This allows the side of the sample to be precisely aligned with the stripes so that the end faces of the waveguides can be polished accurately perpendicular to the channels. Many steps are involved and these are described briefly in the next section and in more detail in appendix B. Although the actual process of ion-implantation was done by our collaborators at the University of Sussex all the extra work associated with channel fabrication and all the laser experiments were done at Southampton. Channel waveguides have been fabricated in many materials and have produced lasers in Nd:YAG, Nd:GGG, and Nd:MgO:$LiNbO_3$.

5.2. Fabrication of Ion-Implanted Channel Waveguides.

When planar guides are formed by ion-implantation the reaction of the material to the ion is different for different materials. From the point of view of fabricating channel waveguides these two types of response require slightly different fabrication procedures. In one the refractive index increases in the guide region (index enhancement guides) and in the other it is unaffected or decreased (barrier guides). In the former case

the rise in refractive index can be used to form the channel and in the latter a low refractive index barrier has to be produced all around the desired waveguiding region. These two processes are illustrated in figure 5.1.

In both cases a gold mask has to be made on top of the crystal, and the method for doing this is always the same. The fabrication process for producing channels is long and involved. This is therefore discussed in detail in appendix B and only a brief outline is given here.

To electroplate the gold mask onto the crystal surface a electrical contact has to be made. This is done by evaporating a 100nm layer of 80% Nickel, 20% Chromium onto the polished crystal surface. On top of this a 4μm thick photoresist layer is spun, which is then exposed and developed to leave the desired pattern. Next a wire is attached to the Ni/Cr layer, to form an electrical contact. The gold can then be electroplated directly onto the Ni/Cr layer which is exposed through the gaps in the photoresist. Once the wire and photoresist have been removed, the sample is then ready to be ion-implanted to form channel waveguides. After implantation, the gold and Ni/Cr layers are removed and the crystal end faces polished perpendicular to the channels. The waveguide is now ready for use.

The mask used in this work produced sets of channels with widths of 4, 6, 8, 10, 12, 16 and 20μm. Theoretically the narrowest of these should produce the best laser results but in practice it is often found that the wider channels perform better due to their lower loss. One problem which can occur in the gold plating stage is that the gold layer deposited is not as thick as was hoped for. This leads to a modulated refractive index profile across the channels, rather than one containing only discrete steps. The consequence of this is that the modes which propagate in the waveguides will have a larger than expected spot size parallel to the crystal surface. The laser performance of channels made by this process is described in the remaining sections of this chapter.

Barrier Waveguides

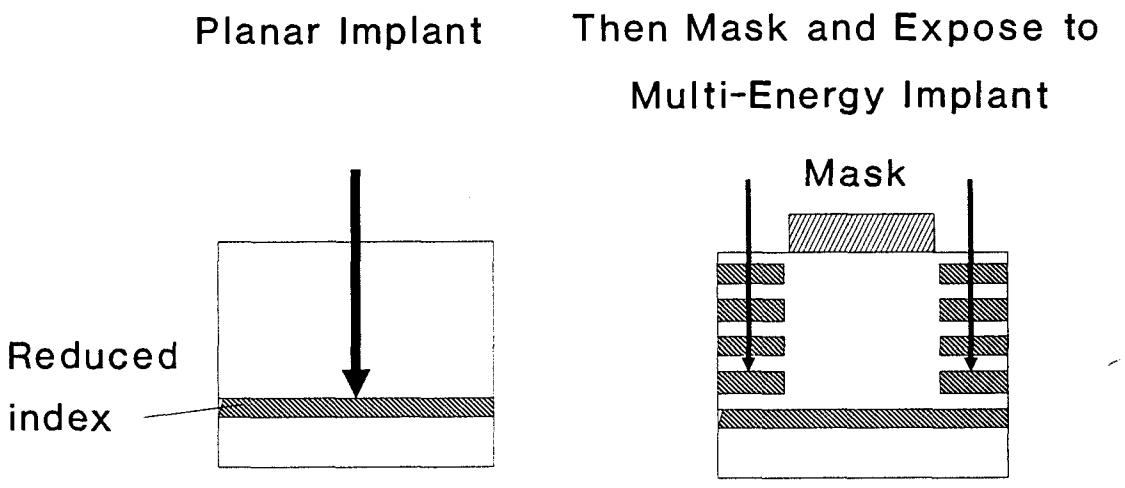

Index Enhancement Waveguides

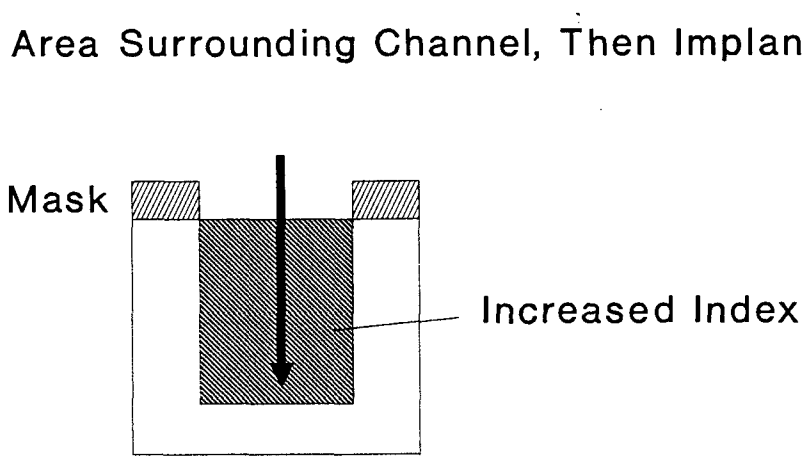

Figure 5.1 - Fabrication of channel waveguides by ion implantation for both barrier and index enhancement type guides.

5.3. Nd:YAG Channel Waveguide Laser.

One obvious candidate for channel waveguide fabrication was the Nd:YAG system which was the first material to work successfully as a planar waveguide [3-5]. Using the procedure described in Appendix B, a gold mask was formed on the crystal surface. As the guide is of the index-enhancement type, the channels were formed by implanting through gaps in the gold mask to give stripes of increased refractive index. The implant consisted of doses of $3x10^{16}$ions/cm^2 at 2.8MeV and $0.75x10^{16}$ions/cm^2 at 1.8, 2.0, 2.2 and 2.4MeV. From the data obtained from planar Nd:YAG guides it was known that the refractive index profile showed a 0.2% index rise in the guiding region. This is shown in figure 5.2. From simple waveguide transmission measurements the waveguide propagation loss was estimated to be 1.5dB/cm for TM modes. This is the same as that found in planar Nd:YAG guides and is an encouraging sign that changing to the channel geometry adds no extra propagation loss to the system. The thickness of the gold mask was about 1.5μm - only half of the desired 3μm depth which would be needed to produce waveguides with well confined modes. Because of the insufficient gold thickness the horizontal spot sizes of the guided modes were larger than expected. These ranged from 6.0-7.3μm at 807nm over the range of channels from 4-20μm in width. As expected the vertical spot size of 2.9μm was the same for all channels.

To test the laser performance the waveguides were cut to a length of 2.5mm and pumped using a 100mW single-stripe laser diode (SDL-5412-H1) which was temperature tuned to 807nm. This pumped Nd^{3+} ions from the ground state to the $^4F_{5/2}$ manifold. A half-wave plate was used to rotate the polarisation of the pump laser to that of a TM mode, as the TE mode in the guide had higher propagation loss. The collimated diode beam was launched into the waveguide using a x10 microscope objective. This gave an input spot which was 2.5 times larger in the horizontal plane than in the vertical - roughly the same ratio of spot sizes as the actual laser mode. Although all channels could support laser action, the best results were obtained for the widest (20μm) channels due to their lower propagation losses. With highly reflecting mirrors attached to the crystal the system lased at 1.064μm with a threshold power of 1.3mW incident on the launch objective [6]. Taking into account the lens and mirror transmissions along with the

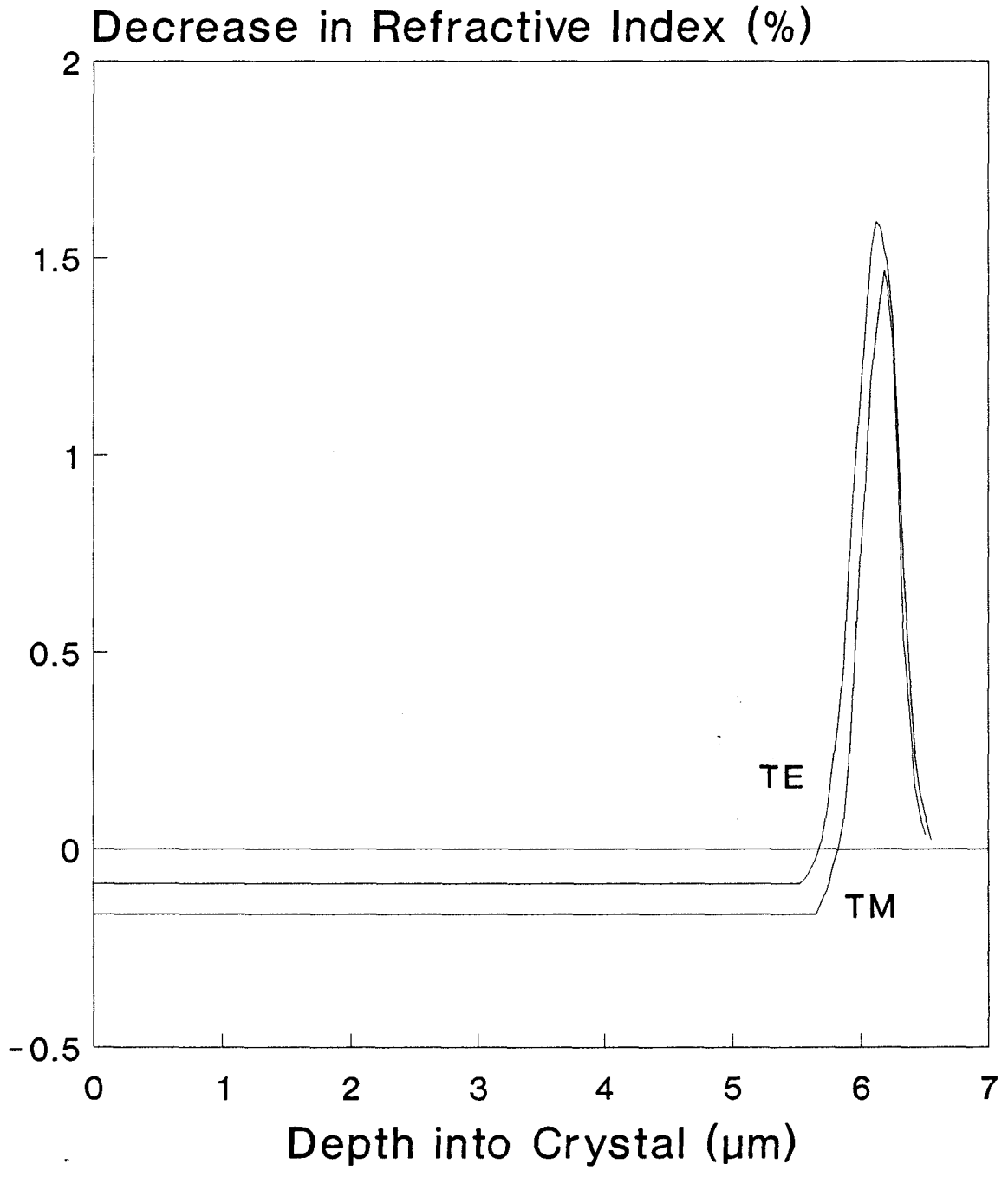

Figure 5.2 - Refractive index against depth into the crystal for a Nd:YAG sample implanted with $3x10^{16}$ions/cm^2 at 2.8MeV and $0.75x10^{16}$ions/cm^2 at 1.8, 2.0, 2.2 and 2.4MeV.

estimated launch efficiency (~70%) and unabsorbed pump power (18%) the figure for absorbed-power threshold was calculated to be 540μW. Repeating the experiment with a 17%-transmitting output coupler, the threshold rose to 1.6mW and the slope efficiency was 29% with respect to absorbed power. A graph of output power against absorbed power for the 17% output coupler is shown in figure 5.3.

This system could be further improved by fabricating a thicker gold mask to produce channels with smaller mode spot sizes and therefore lower laser thresholds. Another improvement would be to coat mirrors directly on to the end faces of the crystal. The mirrors attached by liquid seldom make good contact with more than a few channels whereas directly coated mirrors would give consistency over all the sets. Even with the system in its present state the results are very good. No extra propagation loss is added by the change from a planar geometry to a channel one and the threshold is reduced by a factor of 16 (8mW to 0.5mW) from that of a planar guide.

5.4. Nd:GGG Channel Waveguide Laser.

Another system which we have succeeded in operating as both a channel [7] and a planar [8] waveguide is Nd:GGG. This was fabricated by implanting $2x10^{16}$ions/cm^2 at 2.9MeV producing a refractive index increase of 0.06% in the guiding region. The refractive index profile was measured in a planar guide and is shown in figure 3.3. Due to incomplete Ni/Cr removal, the 4 and 20μm channels in each set were unusable. The other channels, however, all guided with the 16μm channel being the one which gave the best results. The spot sizes in this channel at the pump wavelength of 805nm were 3.7 and 6.4μm in the vertical and horizontal planes respectively. At the laser wavelength of 1.062μm these increased to 4.4 and 7.7μm. The wider than expected horizontal spot sizes were again due to the gold layer being insufficiently thick, at about 1.5μm. The estimated guide losses of ~1dB/cm were the same as in the Nd:GGG planar guides.

To test this system as a laser it was pumped by a 50mW single stripe diode laser, the elliptical output from which gave a good match to the shape of the waveguide modes. The laser threshold for a 2.5mm length of crystal and highly reflecting mirrors attached

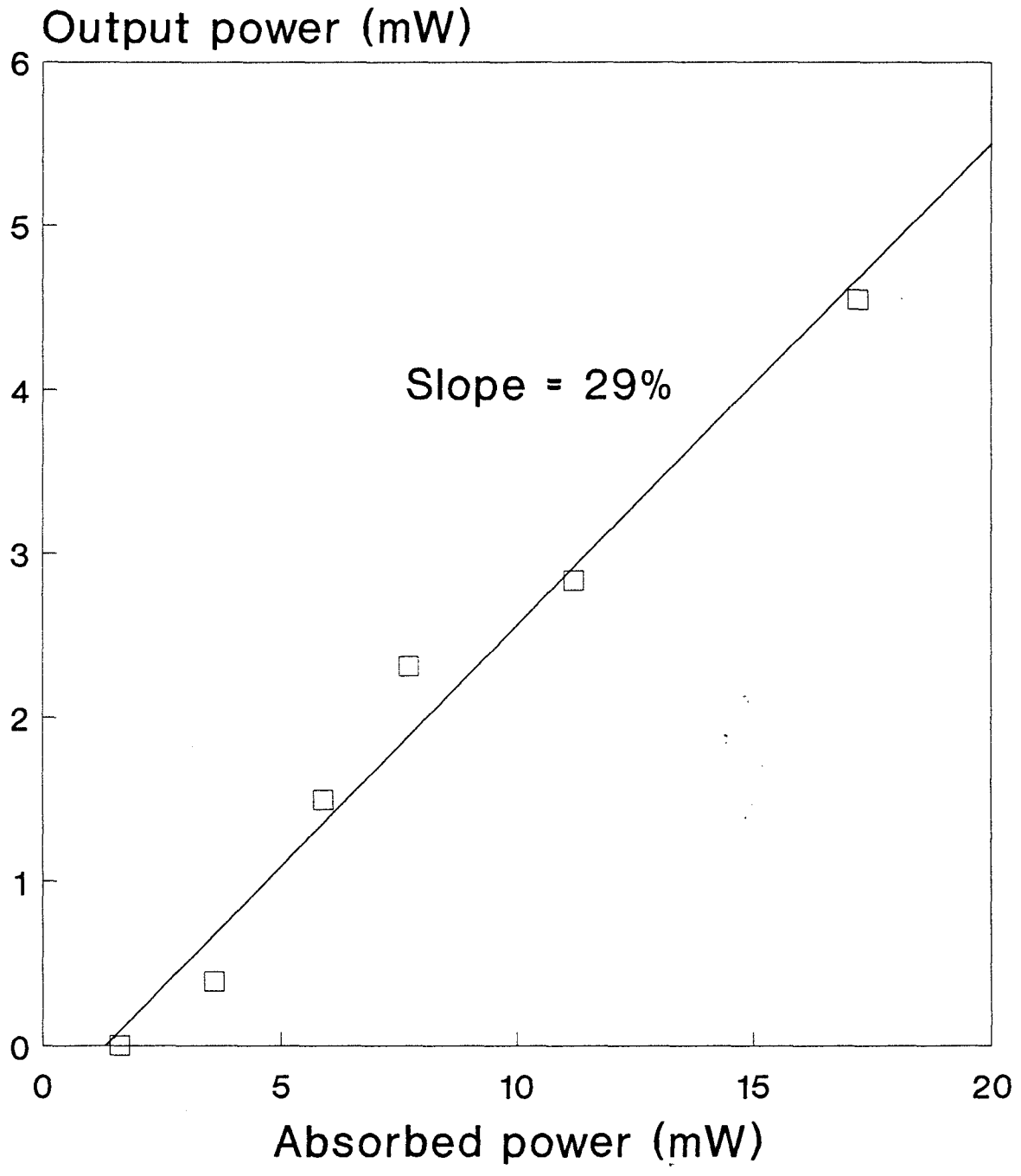

Figure 5.3 - Graph of output power against absorbed pump power for a 20μm wide Nd:YAG channel cut to a length of 2.5mm.

to the crystal was 3.1mW of power incident on the launch objective. Taking into account the objective and mirror transmissions as well as the fact the only 76% of the diode light was absorbed over the length of the crystal, the absorbed power threshold was calculated to be 1.9mW. With a 17% output coupler this absorbed power threshold rose to 6.6mW and a slope efficiency of 27% was obtained. A graph of output power against absorbed pump power is shown in figure 5.4.

A 9mm length of this guide was also operated in an extended cavity configuration, where the output mirror is not attached to the crystal but is some distance away. The light from the guide was collected using a x10 microscope objective and focused onto a highly reflecting mirror 40cm away from the crystal. Even with the added loss from the intracavity objective the absorbed power threshold of the system was only 8mW, compared with 4.3mW for the same waveguide and two directly attached mirrors. This demonstrates the possibility of adding elements into the laser cavity which could be used for tuning, Q switching or mode-locking.

5.5. Nd:MgO:$LiNbO_3$ Channel Waveguide Laser.

Another material which has successfully operated as a planar [9] and channel waveguide laser is Nd:MgO:$LiNbO_3$. There is much interest in $LiNbO_3$ due to is its non-linear and electro-optic properties which lead to the possibilities of Q-switched, mode-locked or self frequency doubled lasers.

The channels were found to lase CW at room temperature with an absorbed power threshold of 22mW. This was in a configuration using one highly reflecting and one 17% transmitting mirror. This contrasts with the planar guide which would only lase in brief flashes at room temperature and had to be heated to 90°C to lessen photorefractive effects in the crystal before CW lasing occurred. When the channels were heated to 90°C the threshold for lasing was found to fall to 17mW of absorbed power. Very low output powers were obtained from this setup with the slope efficiency of the device estimated to be at most 0.5%. The reason for testing the laser with a 17% output coupler was that the threshold was difficult to observe with two highly reflecting mirrors. However a

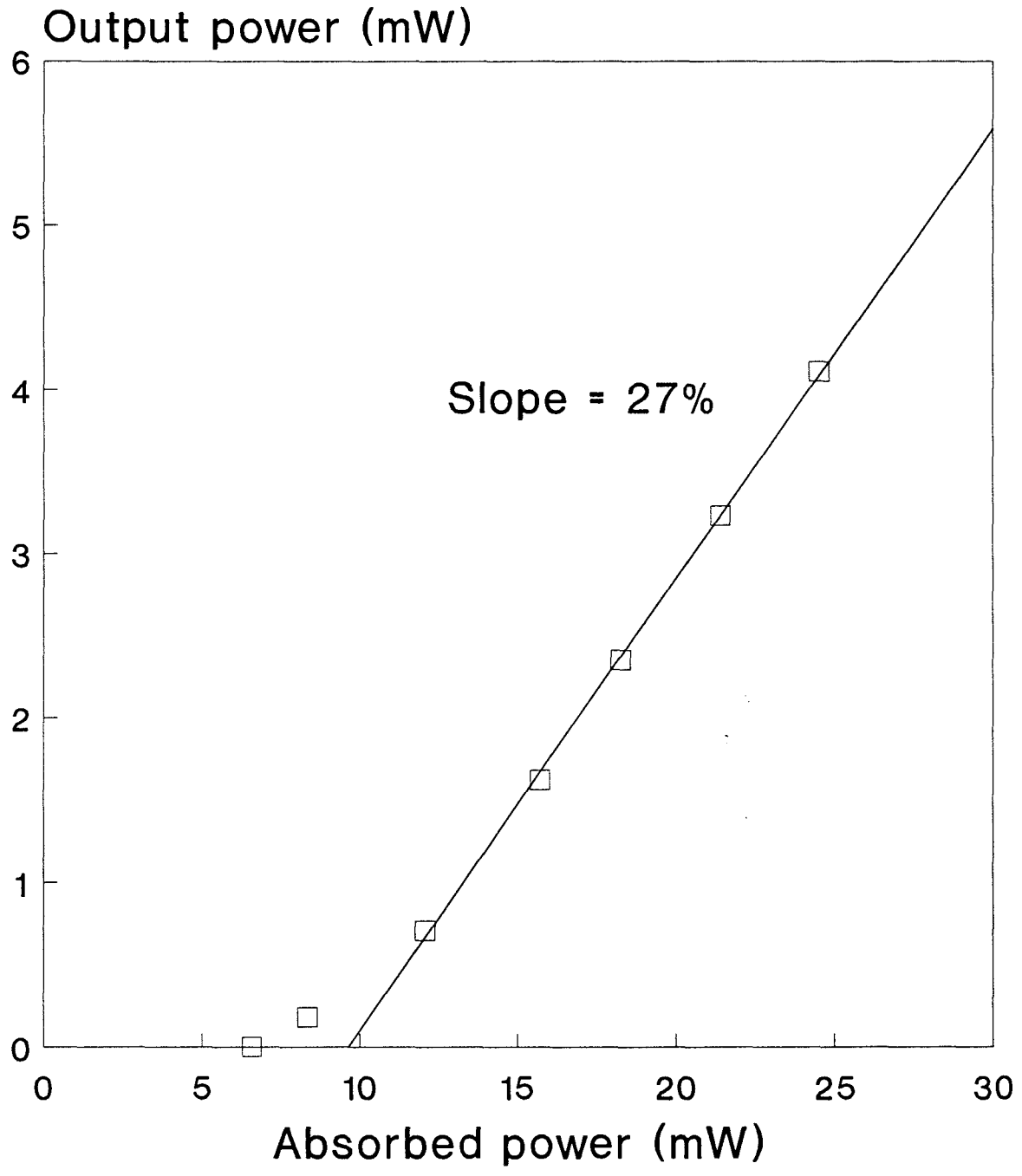

Figure 5.4 - Graph of output power against absorbed power for a 16μm wide Nd:GGG channel waveguide laser cut to a length of 2.5mm.

maximum value of 10mW could be put on this threshold.

Although channel waveguides have been formed in $LiNbO_3$ with propagation losses of ~ 1dB/cm the methods of proton exchange and Ti indiffusion provide methods which can produce lower loss guides in this material. For ion-implantation to become a serious rival technique losses would have to be reduced to 0.2dB/cm.

5.6. Cr:YSAG Channel Waveguides.

The channels described in the three previous sections have all suffered from having too little gold electroplated onto them. Although the electroplating stage remains unreliable, as more experience is gained the chances of success increase. One such successful set of channels was made in Cr:YSAG using a 3.9μm deep gold mask on the crystal surface. This mask was thick enough to shield the regions between the channels from any ion damage and because of this the waveguide modes were tightly confined in the horizontal plane. The transmission was checked off the absorption band with a 810nm laser diode and the guide losses were found to be approximately 3dB/cm (again the same as a planar Cr:YSAG guide). When the channel output was focused onto a camera all the channels were seen to have well confined modes. All channels with widths above 10μm were multimode but all the smaller channels had roughly circular mode shapes. The image of the output from the 4μm channel is shown in figure 5.5. The spot size in this channel was 1.6μm horizontally and 1.4μm vertically. Comparing this with the horizontal spot size achieved in the Nd:YAG channels of 7.3μm shows that a threshold reduction of about 5 times could in principle be achieved in Nd:YAG if more tightly confined channels were produced.

5.7. Tm:MgO:$LiNbO_3$ Channel Waveguides.

Most materials which have been made into channel waveguides show an increase in refractive index when ion-implanted and are therefore fabricated by a one-step implantation process. Some materials, however, form only a low-refractive-index barrier and therefore have to be built up by implanting side walls, removing the gold mask and then implanting a barrier at the bottom of the guide. One such case is that of

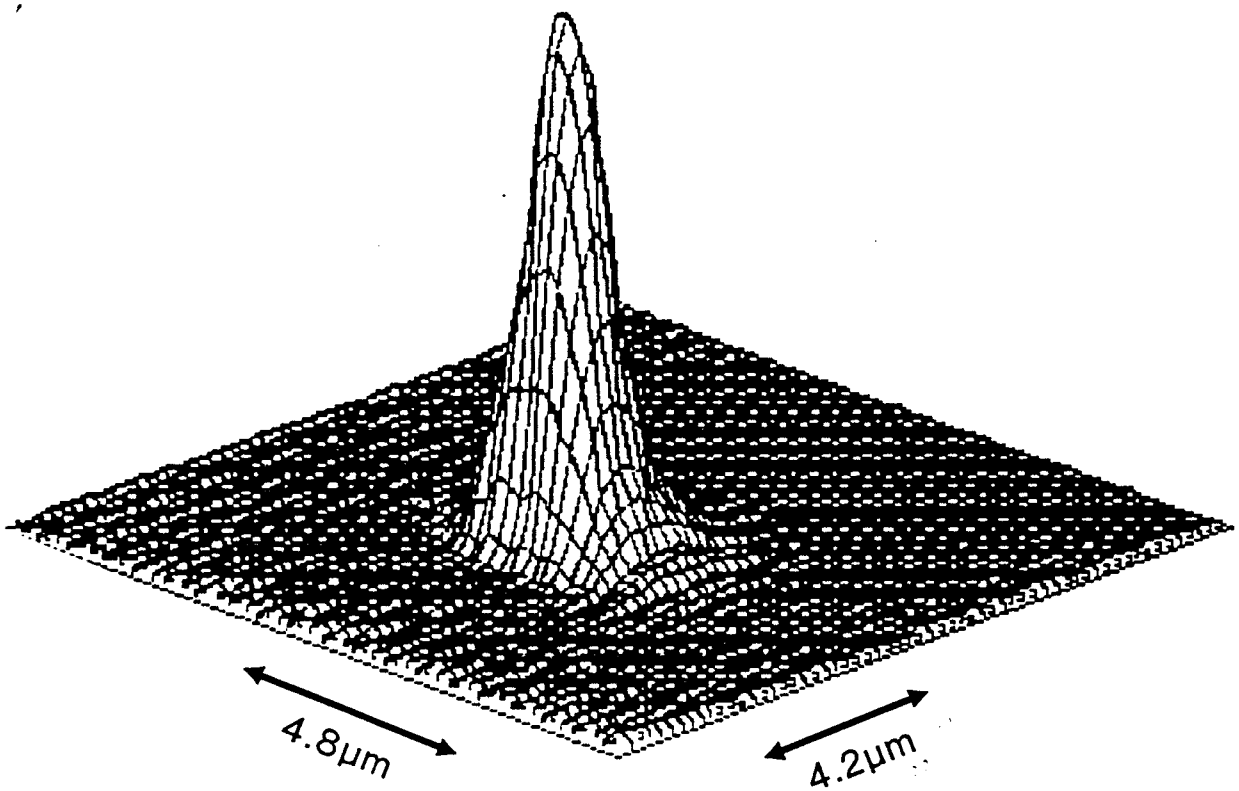

Figure 5.5 - Focused output from a 4μm wide Cr:YSAG channel (1.6 x 1.4μm).

Tm:MgO:$LiNbO_3$, where the emission cross section of the 1.8μm transition is greatest when polarised along n_o. The refractive index profile for n_o is shown in figure 3.2a and consists entirely of an low refractive index barrier.

Channel waveguides were fabricated in Tm:MgO:$LiNbO_3$ by first implanting side walls of $5x10^{15}$ions/cm^2 at 0.9 and 1.8MeV. These relatively low-dose implants were chosen from the evidence of previous experiments on ion-implanted channels in $LiNbO_3$ [10]. Once the gold mask had been removed, a final implant of $3x10^{16}$ions/cm^2 at 2.8MeV was used to define the bottom of the channels. Channels fabricated in this way had the same propagation loss of 1dB/cm as channels formed in Nd:MgO:$LiNbO_3$ by a one step implantation process. This shows that either method of fabrication can be equally successful. The waveguide modes in these channels were well confined within the guiding region with the 10μm channel having a spot size of 4 by 2.5μm at a wavelength of 800nm. Despite the successful formation of channel waveguides in Tm:MgO:$LiNbO_3$ attempts to make them lase on the 1.8μm transition from the $^3H_4$ energy level to the $^3H_6$ ground state proved unsuccessful. The main reason for this is probably the large photorefractive effects which were present in the channels.

5.8. Conclusions.

The fabrication of ion-implanted channel waveguides by the photolithography and gold plating route has proved successful. No extra propagation loss is added to the waveguide by changing from a planar to a channel geometry and because of this threshold reductions of an order of magnitude have been observed. Waveguides with well-confined modes have been produced in samples where a thick enough gold mask was electroplated onto the surface. The main problem with the process is its reliability, especially in the gold-plating stage, where, although a lot has been learnt, the process still appears to be as reliable as the Albion Rovers' defence. Low loss channel waveguides have been produced using tungsten wire to shield the sample [2] and it will surely be this quicker and more reliable method which becomes the standard procedure for channel fabrication.

The losses obtained in ion-implanted guides are generally about 1dB/cm. With

losses at his level some of the advantage of having a channel waveguide geometry is removed from the laser system. It can be seen from the experiments on epitaxially grown waveguides that low loss planar guides can rival even channel guides formed by ion-implantation. This is clearly shown in the case of Nd:YAG where an epitaxially grown planar guide with losses of 0.2dB/cm showed the same laser threshold as the ion-implanted channels described in section 4.3. The results obtained for epitaxially grown guides with Nd:YAG and Yb:YAG active layers are discussed in the next chapter.

5.9. References.

1. G.T.Reed and B.L.Weiss, Nuclear Instruments and Methods in Physics Research, **B19/20**, pp.907-911, 1987.
2. D.Fluck, P.Gunter, M.Fleuster and C.Buchal, Journal of Applied Physics, **70**, pp.1671-1675, 1992.
3. L.Zhang, P.J.Chandler, P.D.Townsend, S.J.Field, D.C.Hanna, D.P.Shepherd and A.C.Tropper, Journal of Applied Physics, **69**, pp.3440-3446, 1991.
4. P.J.Chandler, S.J.Field, D.C.Hanna, D.P.Shepherd, P.D.Townsend, A.C.Tropper and L.Zhang, Electronics Letters, **25**, pp.985-986, 1989.
5. S.J.Field, D.C.Hanna, D.P.Shepherd, A.C.Tropper, P.J.Chandler, P.D.Townsend and L.Zhang, IEEE Journal of Quantum Electronics, **27**, pp.428-433, 1991.
6. S.J.Field, D.C.Hanna, A.C.Large, D.P.Shepherd, A.C.Tropper, P.J.Chandler, P.D.Townsend and L.Zhang, Electronics Letters, **27**, pp.2375-2376, 1991.
7. S.J.Field, D.C.Hanna, A.C.Large, D.P.Shepherd, A.C.Tropper, P.J.Chandler, P.D.Townsend and L.Zhang, Optics Letters, **17**, pp.52-54, 1992.
8. S.J.Field, D.C.Hanna, A.C.Large, D.P.Shepherd, A.C.Tropper, P.J.Chandler, P.D.Townsend and L.Zhang, Optics Communications, **86**, pp.161-166, 1991.
9. S.J.Field, D.C.Hanna, D.P.Shepherd, A.C.Tropper, P.J.Chandler, P.D.Townsend and L.Zhang, Optics Letters, **16**, pp.481-483, 1991.
10. G.T.Reed and B.L.Weiss, Electronics Letters, **23**, pp.792-794, 1987.

Chapter 6 - Epitaxially Grown Waveguide Lasers

6.1. Introduction

One technique which is a very promising method of fabricating planar waveguides is that of epitaxial growth. This technique can be used to grow high quality layers of crystalline material which are suitable for use as planar waveguides. The range of compositions of these materials can be very wide. For example in the doped YAG guides described in this chapter the addition of gallium and lutetium to the melt can be used to alter the lattice parameter and refractive index of the waveguides to obtain the optimum laser performance. Another attractive feature of this technique is that high doping levels can be achieved. In YAG doping levels of up to 15 at.%. of Nd^{3+} can be obtained which is much higher than the doping levels in bulk grown samples. This could improve performance in side pumped systems where the decrease in the absorption length would more than compensate any reduction in lifetime due to concentration quenching. The results in this chapter discuss the end pumped laser performance of epitaxially grown guides in both Nd:YAG and Yb:YAG as well as the side pumped performance of one Nd:YAG guide. For the quasi-three-level Yb:YAG laser the benefits of even a planar waveguide geometry have been seen to give a significant threshold reduction over equivalent bulk lasers.

The guides used in this chapter were all formed by liquid phase epitaxy where an active layer is grown on a substrate by dipping the substrate into a high temperature, saturated solution of the required composition. The atoms in the solution crystallise out onto the substrate and form a layer of different composition. If this layer has a higher refractive index than the substrate then a planar waveguide will be formed.

All the waveguides discussed in this chapter have consisted of a doped YAG layer grown on a pure YAG substrate. The technology for liquid phase epitaxial growth of garnets is well established because of work on magnetic bubble devices [1,2]. The first waveguide laser in an epitaxially grown Nd:YAG waveguide was demonstrated by Van

der Ziel et. al. in 1973 [3] in a flashlamp pumped configuration. In 1975 Grabmaier et. al. [4] demonstrated laser action in a Nd:YAG film grown by the dipping technique (the same method as is used here and one which is about 50 times quicker than the transfer technique used by Van der Ziel). These films lased with a threshold of 700mW when pumped by an argon ion laser at 514nm. This compares with our present result of a 1mW threshold with a dye laser pump at 588nm. The losses in these waveguides are generally about 0.1-0.2dB/cm which is low enough to give the benefits of optical confinement even in a planar waveguide geometry. If channel waveguides could be fabricated without significantly increasing the waveguide losses then further reductions in laser thresholds of an order of magnitude would be expected.

In this chapter I will give a brief outline of liquid phase epitaxial growth as well as a more detailed description of the fabrication process used to form the doped YAG waveguides used in the laser experiments. The waveguides used in the experiments were fabricated by our collaborators at LETI and the experimental work was done jointly in both Grenoble and Southampton. The results for various laser transitions in longitudinally pumped, Nd^{3+} and Yb^{3+} doped guides will be described. Experiments on the Nd:YAG system have also been carried out in a side-pumped regime where the pump and laser emissions propagate perpendicular to each other. Finally, prospects for the fabrication of low loss channel waveguides in epitaxially grown materials will be explored.

6.2. Liquid Phase Epitaxial Growth

Liquid phase epitaxial growth is the process of growing thin films of crystal from a saturated solution. These films are usually grown on a substrate of a different material. The growth can be done by either dipping a substrate into the desired solution or by tipping the solution over the substrate. To start the process of epitaxial growth a saturated solution of the desired material has to be mixed. If this solution is then cooled (supercooling) it becomes supersaturated. If the level of supercooling is high then the solute will spontaneously crystallise out of the solution but if the supercooling is low then the solution will remain stable until some stimulus is added to it. The addition of an appropriate substrate will encourage the crystallisation of the solute onto the surface of

the substrate.

The growth process starts with one molecule adhering to the substrate (an ad atom). When a molecule bonds to the surface it releases energy. The amount of energy released rises as the number of bonds formed with neighbouring molecules rises. Subsequent molecules are therefore most likely to join at a site where the most number of bonds can be formed. The possible bond sites are shown in figure 6.1 [5] where the molecules are represented by cubes which can form up to 6 bonds with their nearest neighbours. Because of this growth process the overall growth happens in a layer by layer fashion. Good quality, thin films can be produced by this method.

6.3. Waveguide Fabrication

The epitaxially grown waveguides used for laser experiments consisted of a doped YAG layer grown on a pure YAG substrate. All the substrates were 2cm in diameter and of [111] orientation. A diagram of the apparatus used to grow the epitaxial waveguides is shown in figure 6.2 [6]. This consists of a furnace inside which a crucible containing the melt is held. The substrate is held horizontally at the bottom of a rod which can be moved into and out of the furnace as well as rotated around its vertical axis. The temperature of the furnace and the position and rotation of the sample are all accurately controlled. The YAG layers are grown from a PbO/B_2O_3 flux with a molar ratio of 12 to 1. For the growth of a pure YAG film the typical melt composition is $PbO/B_2O_3/Y_2O_3/Al_2O_3$ in the proportions of 89.9/7.4/0.4/2.3 mole percent. The melt is made up at 1100°C and stirred for several hours. The actual growth is carried out at 10°C below the saturation temperature which is about 1020°C. At this supersaturation the growth rate is $\sim 1\mu$m/min. Before dipping the sample is held just above the melt to allow its temperature to rise to that of the melt. During the actual growth the substrate is rotated clockwise and anticlockwise at 100rpm for periods of two seconds each way. After growth it is removed from the melt and spun at 800rpm to remove any residual flux.

The layers grown for waveguide laser experiments were doped with either

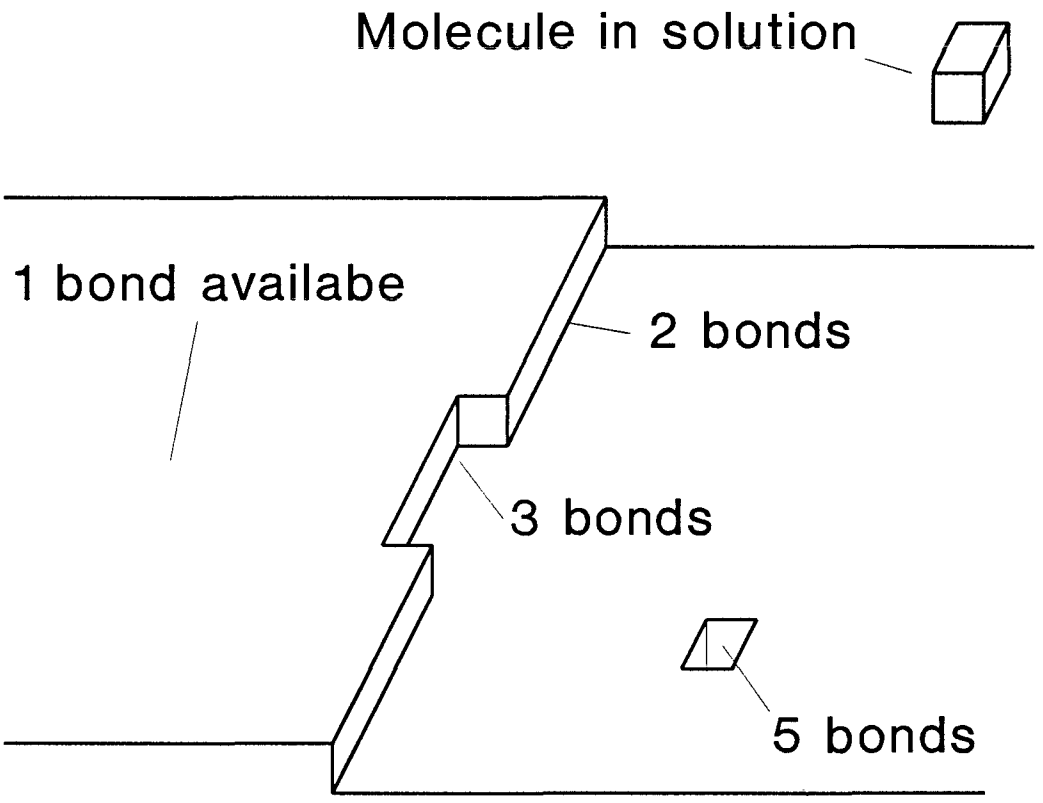

Figure 6.1 - Crystal surface during epitaxial growth showing the number of bonds which can be formed at each available site.

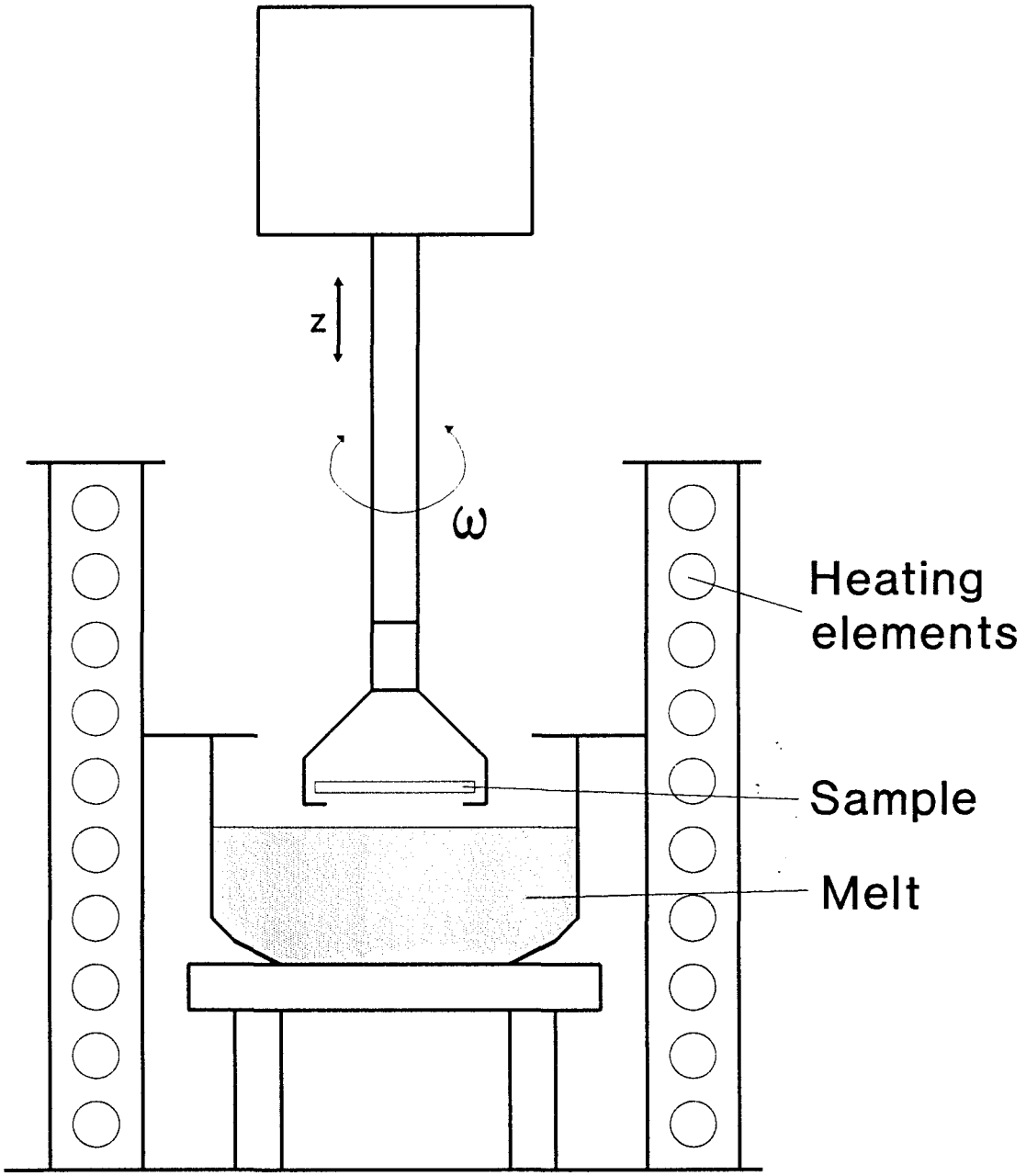

Figure 6.2 - Apparatus used for epitaxial growth. The rotation of the sample (ω) and the position (z) can be accurately controlled.

neodymium or ytterbium. This is achieved by the addition of either Nd_2O_3 or Yb_2O_3 into the melt. Other substitutions which are made to the melt are Ga_2O_3 (gallium) to increase the refractive index of the guiding layer and Lu_2O_3 (lutetium) to compensate for any mismatch in the lattice parameters of the epitaxial layer and the substrate. The substitution of these elements affects both the lattice parameter and refractive index of the grown layers. The effects for the different dopants are summarised in the table below [6]. All values are for 1 at.%. of dopant although values for different doping levels can be easily found as the relationship between Δa or Δn and doping level is linear.

Dopant	Nd	Yb	Ga	Lu
Δn (10^{-3})	0.42	0.2	1.1	0.095
Δa (10^{-3}Å)	-2.1	0.56	-2.3	0.78

Table 6.1 - Change in refractive index and lattice parameter for 1at.% of Nd, Yb, Ga and Lu [6].

Here Δa and Δn are defined as the difference between the substrate and film lattice constants and refractive indices respectively. It is found that the lattice constant for epitaxially grown pure YAG is 12.006Å compared to 12.008Å for the Czochralski grown substrate. This value of $\Delta a = 2 \times 10^{-3}$Å has to be taken into account when estimating the lattice parameters of epitaxially grown layers.

On top of the waveguiding layer is grown a pure YAG cladding layer. This cladding layer has the effect of reducing the scattering loss at the waveguide surface and therefore reducing the propagation loss. Once the waveguides are grown they have to be cut to the desired size and the end faces polished.

6.4. Longitudinally Pumped Nd:YAG Waveguide Lasers

Laser action in epitaxially-grown Nd:YAG waveguides has been demonstrated at 946nm, 1.064μm and 1.32μm. The energy level diagram for Nd:YAG with these laser transitions marked is shown in figure 6.3 [7]. The laser performance for these three transitions in epitaxially grown waveguides will be described in the remainder of this section.

1.064μm operation

The 1.064μm transition in Nd:YAG is a high gain transition which was an obvious choice for the first laser experiments [8]. The guide used consisted of a 38μm deep active layer doped with 1.5at.% of Nd^{3+} ions. This doping level of Nd was sufficient to give an index rise of $\sim 1x10^{-3}$ in the active layer. No Ga or Lu doping was present in the waveguide. With this small index rise the mode spot size in the guided dimension was relatively large (14μm at the laser wavelength). Any reduction in the guide dimensions, however, would produce only a slight reduction in the spot size but would mean that a significant part of the mode was outside the doped region.

In a laser setup using HR mirrors and an R6G-dye laser pump (588nm) the laser threshold was found to be 0.95mW of pump power incident on the launch objective. By taking into account the transmission of the 5cm focal length lens used to launch the pump into the waveguide and the transmission of the mirrors it is calculated that the power entering the waveguide is 0.67mW (assuming a launch efficiency of 100%). Virtually all the pump light which is launched into the guide is absorbed over the 6mm length of waveguide. By using the equation for absorbed power threshold (equation 2.17) a maximum value for the waveguide loss can be calculated. This is calculated to be 0.05dB/cm a value which is only slightly higher than the propagation loss through bulk Nd:YAG samples [9].

When the same setup was pumped with a 100mW single stripe laser diode (807nm) the threshold was found to be 1.3mW. This rise in threshold is unexpected as the pump wavelength for the diode laser is more efficient. The most likely reason for this

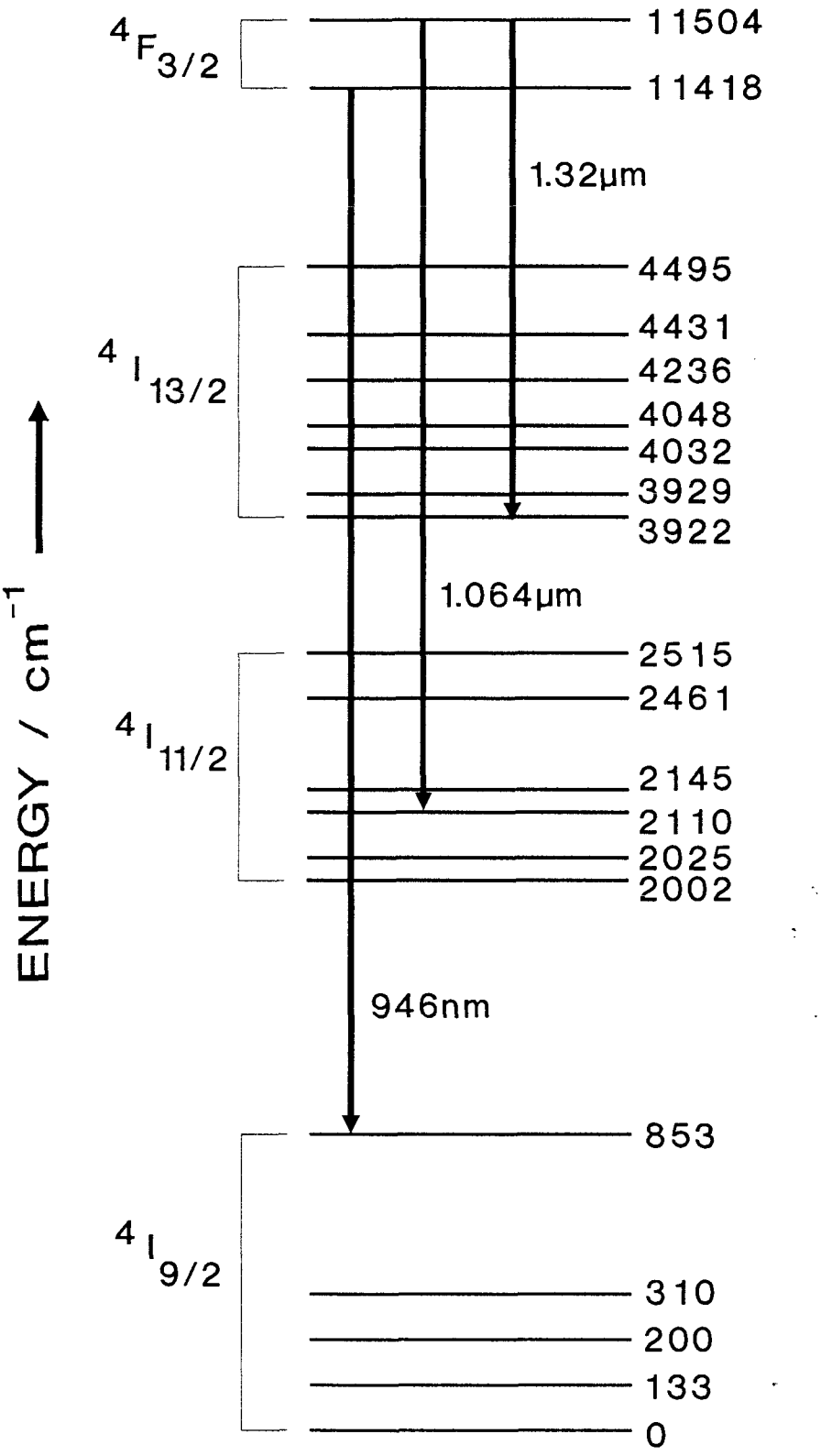

Figure 6.3 - Energy levels and transitions in Nd:YAG.

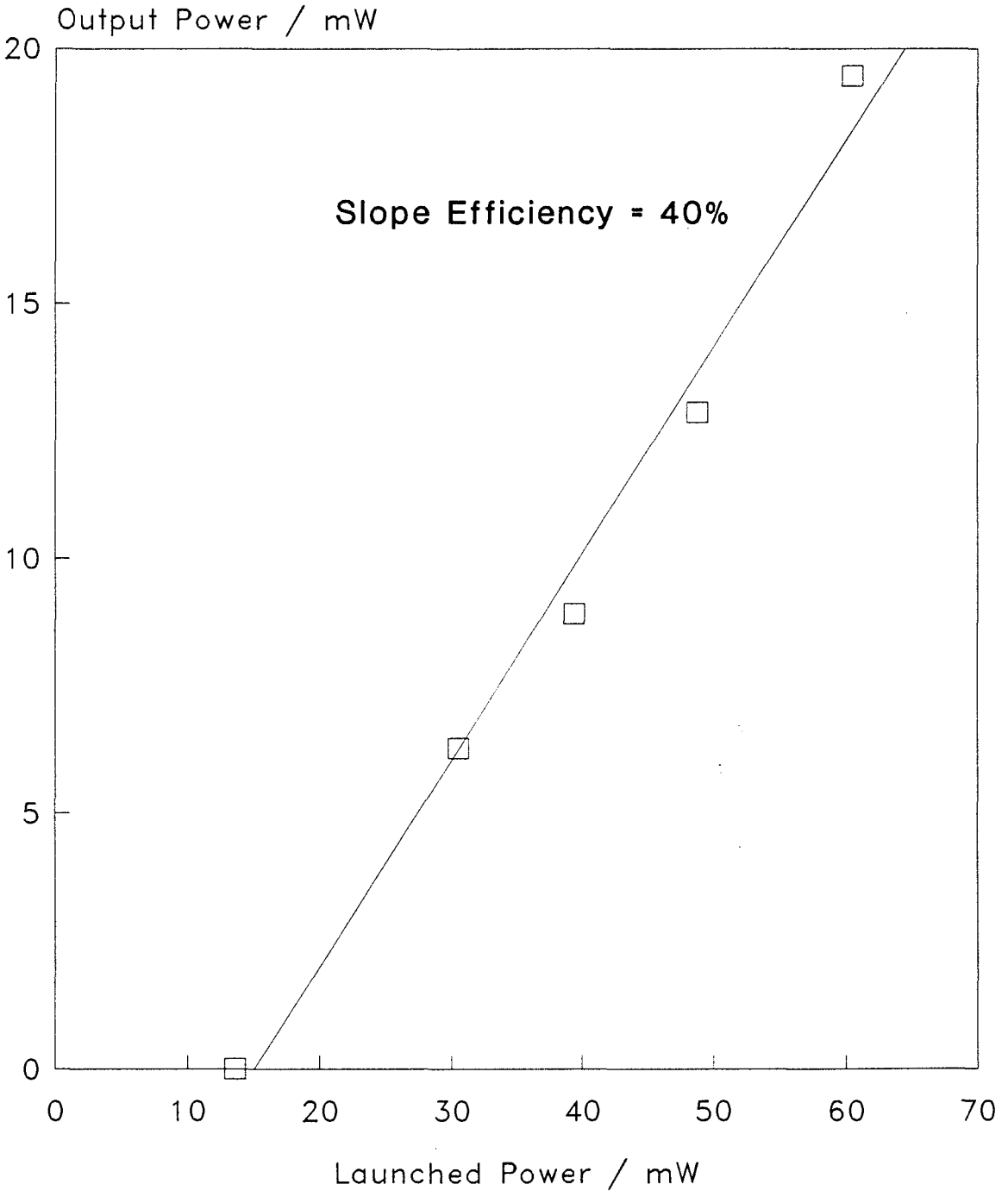

Figure 6.4 - Graph of output power against absorbed power for a diode laser pumped Nd:YAG waveguide laser operating at 1.064μm.

high threshold is that any variations in the quality of the mirror butting will have a large effect on such a low loss waveguide. To overcome this dielectric mirrors could be coated directly to the ends of the waveguide. With an 83% reflecting output coupler replacing one of the HR mirrors the threshold was 14mW and the slope efficiency was 40% as shown in figure 6.4.

1.32μm operation

Another four-level laser transition which has been demonstrated in Nd:YAG waveguides is that from the $^4F_{3/2}$ level to the $^4I_{13/2}$ level. The mirrors used for this had to be highly transmitting (69%) at 1.06μm as well as at the pump wavelength. This suppresses the 1.064μm transition which is the transition which would lase if the mirrors used were highly reflecting at both 1.06μm and 1.32μm. Using the same guide as for the 1.064μm experiments with one highly reflecting and one 98% reflecting mirror the threshold for laser action was 9.1mW of absorbed power and the slope efficiency was 30%.

946nm operation

The $^4F_{3/2}$ to $^4I_{9/2}$ transition in Nd:YAG is a quasi-three-level transition in which the lower laser level is thermally populated. At room temperature 0.7% of the $^4I_{9/2}$ population lies in the lower laser level. The presence of this reabsorption means that the waveguide propagation loss becomes a less significant part of the total loss. For a sample doped with 1at.%. of Nd^{3+} ions the reabsorption loss for the 946nm transition is about 0.17dB/cm. This is similar to the waveguide propagation loss of 0.15dB/cm and is a part of both bulk and waveguide systems.

The waveguide used in this experiment was doped with 12 at.% gallium and 35 at.% lutetium [10]. This was to increase the refractive index in the waveguide allowing the guide to have more tightly confined modes. The addition of these extra dopants has a detrimental effect on the fluorescence spectrum of the Nd^{3+} ions although no change is seen in fluorescence lifetimes. The fluorescence spectra for bulk Nd:YAG, epitaxially grown Nd:YAG and epitaxially grown Nd,Ga,Lu:YAG are shown in figure 6.5. This

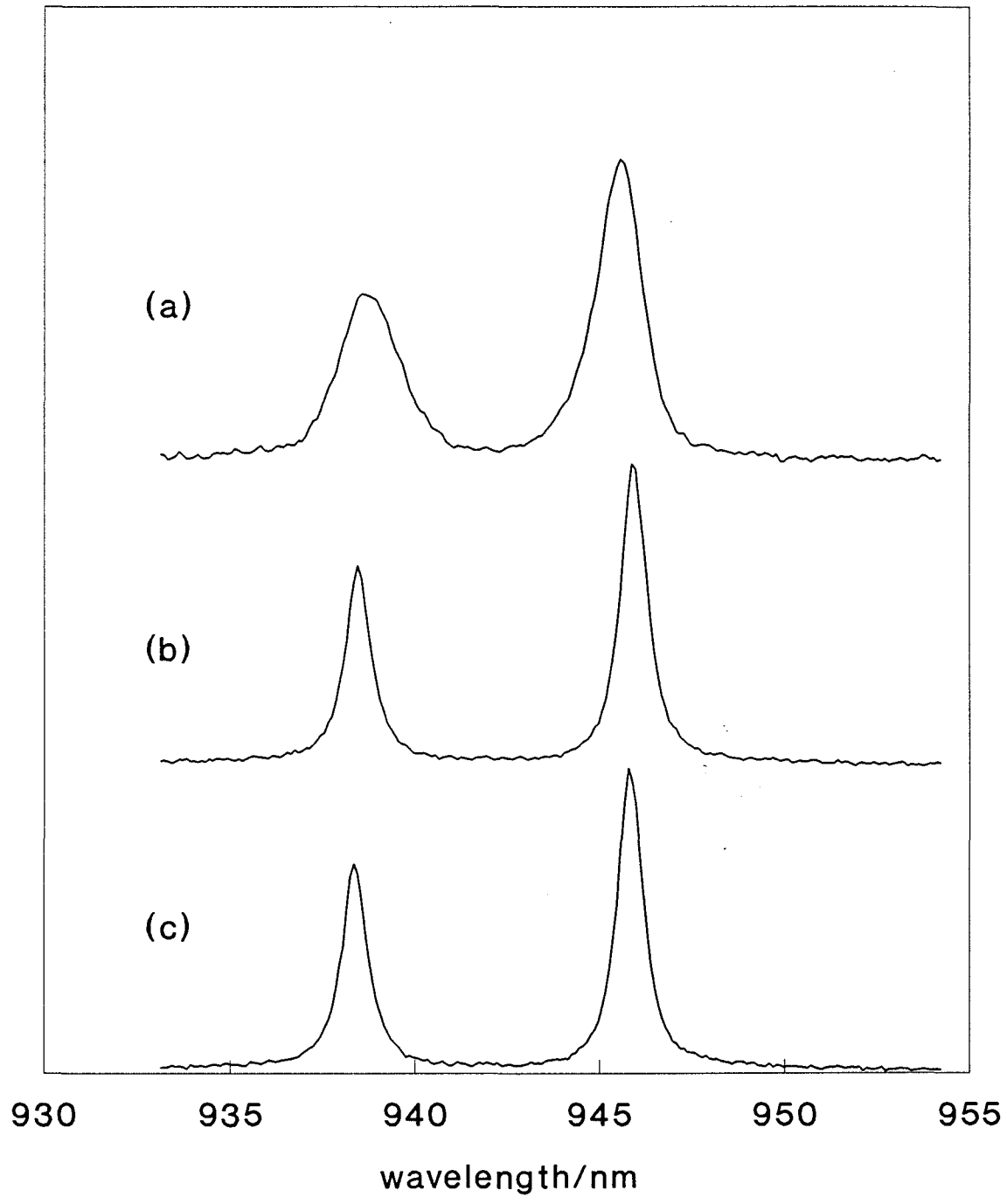

Figure 6.5 - Fluorescence spectra of epitaxially grown Nd,Ga,Lu:YAG (a), epitaxially grown Nd:YAG (b) and bulk Nd:YAG (c).

figure shows that it is the addition of the gallium and lutetium which affects the spectrum and not the growth process. Broadening of the fluorescence spectrum is also seen in bulk Nd,Ga:YAG samples [11]. The effect of the broadening is to reduce the peak emission cross section by a factor of 0.58 from that of pure Nd:YAG giving a revised value of $3.1x10^{-24}m^2$.

Because of gallium doping the refractive index increase in the active layer is relatively high at $1.4x10^{-2}$. With this large increase the guide dimensions could be a lot smaller than in a waveguide which relied purely on the neodymium doping to raise the refractive index. The thickness of the epitaxial layer was only 3.8μm which gave a vertical mode spot size of 2.0μm. To test the waveguide as a laser, mirrors were attached to the ends of a 0.95mm length of guide. These mirrors were highly reflecting at 946nm and 95% transmitting at 1.06μm (to stop 1.064μm lasing). The waveguide was pumped at 588nm by an R6G dye laser. Lasing occurred with a threshold of 4.0mW of pump power incident on the launch objective. Taking into account the launch efficiency and pump absorption this corresponds to an absorbed power of 1.2mW. These results compare well to those obtained in similar bulk systems [12] which found an incident power threshold of 5.7mW. This shows that even in mildly three-level systems (only 0.7% of the Nd^{3+} population in the lower laser level) the advantages of a waveguide geometry can be seen. For quasi-three-level systems where a larger proportion of the population is in the lower laser level, such as Yb:YAG (where 5% of the population is in the lower laser level), further improvements over bulk systems can be seen.

6.5. Longitudinally Pumped Yb:YAG Waveguide Laser.

Yb:YAG is a quasi-three-level laser system which has strong absorption at the laser wavelength. The energy level diagram for Yb:YAG is shown in figure 6.6. This shows the two pump wavelengths of 941 and 968nm used in the experiments as well as the two laser wavelengths of 1.03 and 1.05μm. For the 1.03μm transition 5% of the Yb^{3+} population is in the lower laser level. This corresponds to an absorption loss of about 2.5dB/cm for a 6.2at.% doped sample like the one used here. This absorption loss is far greater than any waveguide propagation loss which is estimated to be less than 0.2dB/cm.

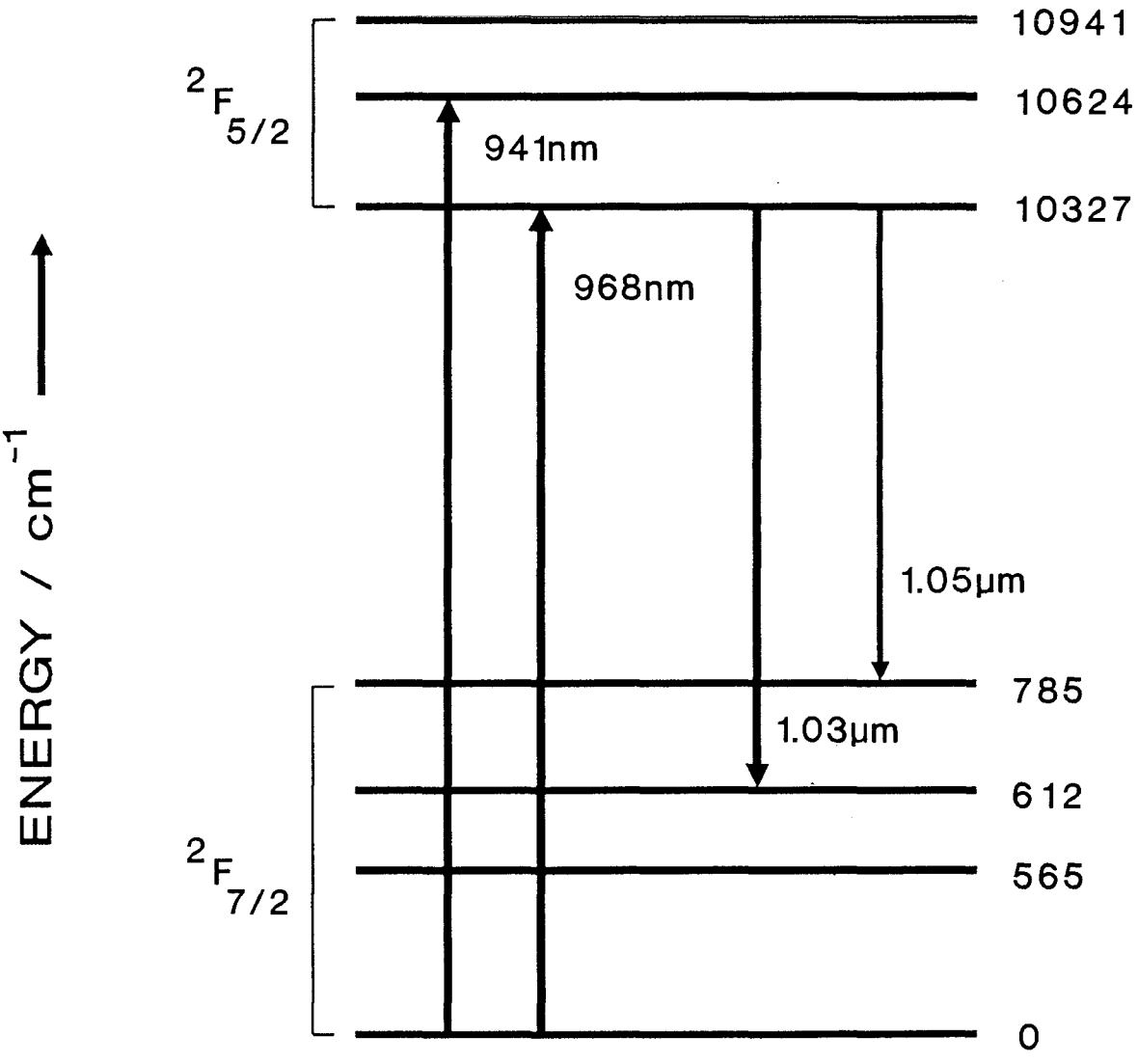

Figure 6.6 - Energy level diagram of Yb:YAG showing pump and laser wavelengths.

Another feature of Yb^{3+} systems is that there is very little excited state absorption or concentration quenching as there is only excited state manifold. It also has the advantage of pump and laser wavelengths which are closer together than in Nd:YAG, meaning that less heat is generated during laser operation, and making it more suitable for high power operation [13].

The waveguide used in these experiments was doped with 6.2at.% Yb^{3+}, 26at.% Lu^{3+} and 11at.% Ga^{3+}. The gallium had to be added to increase the refractive index of the active layer as the increase due to ytterbium alone is very small. The lutetium is added to compensate for the large size of the gallium ions. The waveguide consisted of a 6μm thick active layer on top of which was grown a 19μm cladding layer of pure YAG. The waveguide was cut to a length of 1.6mm (roughly one absorption length) for laser experiments. The fluorescence lifetime of the Yb^{3+} was measured to be 0.8ms which is shorter than that of 0.95ms for bulk Yb:YAG [14]. This reduction is probably due to the addition of Ga and Lu to the active layer.

The pump laser used for the laser experiments was a 1W, InGaAs diode array which emitted at around 968nm. This was collimated using a 6.5mm focal length lens and shaped using an anamorphic prism pair. A x10 microscope objective was used to launch the pump light into the waveguide. To measure the effects of any feedback into the pump laser a beam splitter was inserted into the arrangement before the launch objective and the pump intensity was monitored using a silicon photodiode. A silicon plate was used as a filter to cut out any transmitted pump. By comparing the light transmitted through the bulk YAG substrate to that transmitted through the waveguide the combined figure for launch efficiency times single pass absorption was calculated to be 0.43. If the output mirror was highly transmitting at the pump wavelength this figure would give the proportion of the incident power which is absorbed in the guide. The output mirror, however, reflects 71% of the pump back into the waveguide and because of this the absorbed power cannot be accurately measured. For calculating the absorbed power threshold and slope efficiency it was assumed that the launch efficiency was 100% and the single pass absorption 43%. These figures give an upper limit for the threshold and

a lower limit for slope efficiency.

The mirror reflectivities at 1.05μm were 99.6% and 98.3% for the input and output mirrors respectively. The reflectivities at the other laser wavelength of 1.03μm were only slightly lower than these. When the waveguide was lasing the wavelength of the laser operation could be switched between 1.03 and 1.05μm simply by launching into a different part of the waveguide. The thresholds and output powers for these two wavelengths were, however, very similar and the results given here are for the 1.05μm transition. A plot of output power against absorbed pump power is shown in figure 6.7. The laser threshold was 43mW and the slope efficiency was 77%. It is worth noting that this is an upper limit for the threshold and a lower limit for the slope efficiency as a 100% launch efficiency has been assumed. These results are much better than similar bulk Yb:YAG results [13] which report a threshold of 230mW and a slope efficiency of 31% for diode pumping. Although these bulk slope efficiencies could be optimised it is unlikely that big reductions in the laser threshold could be made. Threshold reductions in the waveguide system would however be possible if channel waveguides could be fabricated in these epitaxial guides without significantly increasing the waveguide propagation loss. The prospects for channel waveguide fabrication are discussed in section 6.7.

6.6. Side Pumped Nd:YAG Waveguide Laser. [15]

All the laser systems discussed so far have been end (longitudinally) pumped where the pump and laser light are parallel to each other. An alternative pumping scheme is that of side (transverse) pumping where the pump light travels perpendicular to the laser light. Because the pump and laser light travel in different directions the ideal geometry for a side pumped laser is that of a planar waveguide. This pumping scheme is particularly suited to diode array pumping as the quality of the pump mode in the horizontal plane is of little importance. Because the power from the pump can be spread out along the length of the waveguide instead of being focused in at one spot, side pumping lends itself to high power operation. A simple model for side pumped laser thresholds and slope efficiencies is given in appendix C.

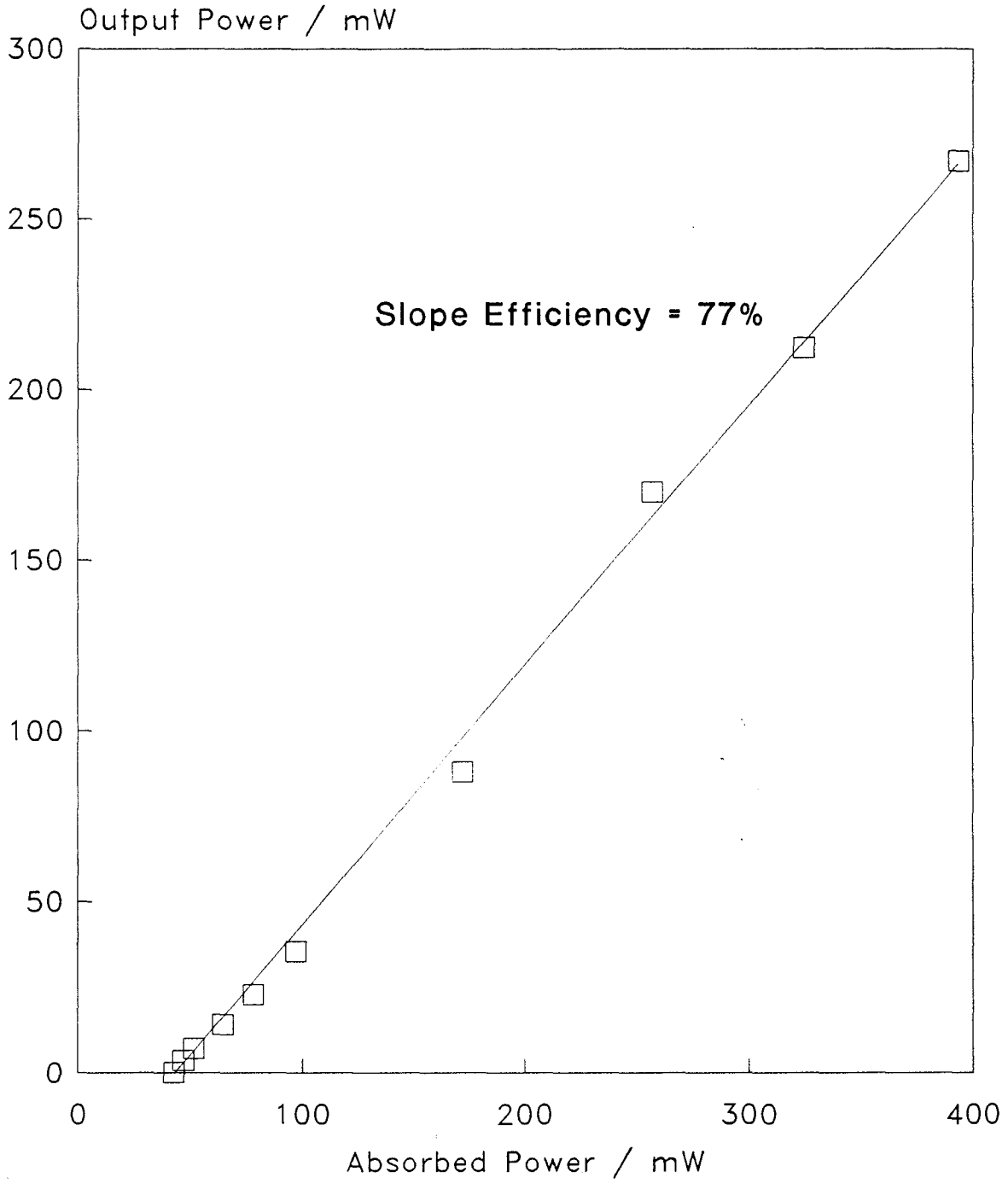

Figure 6.7 - Plot of absorbed pump power against output power for a diode laser pumped Yb:YAG waveguide laser operating at 1.05μm.

The waveguide used in these side pumping experiments was the epitaxially-grown, Nd:YAG guide used in the 1.06μm end pumped experiments described in section 6.4. The experimental arrangement used for side pumping is shown in figure 6.8. A 5cm focal length cylindrical lens was used to focus the pump light along the side of the waveguide. The pump spot at the side of the waveguide measured 7μm by 1.25mm. To form the laser cavity large dielectric mirrors mounted on micropositioners were manually moved up to the ends of the waveguide. This gave a more even reflectivity along the edge of the crystal than the normal method using liquid to attach thin dielectric mirrors.

Pumping with an R6G dye laser at 588nm the threshold for laser operation was found to be 10mW of pump power incident on the cylindrical lens. Taking into account the lens transmission and Fresnel reflection at the crystal surface this corresponds to a launched power of 8mW (assuming 100% launch). The output mode from the laser was observed using a CCD camera. Near threshold this was a fundamental Gaussian mode with spot sizes of 14μm by 140μm as shown in figure 6.9. Above threshold the output spreads out and becomes multimode in the unguided direction. This observed threshold agrees well with the theory which predicts a threshold of 5.8mW for dye laser pumping. When one of the HR mirrors was replaced by a 10% transmitting output coupler then the threshold was 48mW and the slope efficiency was 19%. A prediction for slope efficiency is difficult to make as the theory assumes a lowest order Gaussian mode profile for the laser mode which is not the case when the laser is operating at high power.

The same system was also pumped using a 500mW diode array at a wavelength of 807nm. The threshold with HR mirrors was 19mW and the slope efficiency with the 10% output coupler was only 7%. Figure 6.10 shows a plot of output power against launched pump power for both dye and diode laser pumping. The worse performance obtained when diode pumping is due to the lower absorption coefficient at the diode wavelength (1.4mm^{-1} as opposed to 3.0mm^{-1} at 588nm). To improve the performance of the diode pumped system higher doping levels would have to be achieved in the epitaxially grown films. These higher concentrations would lead to concentration

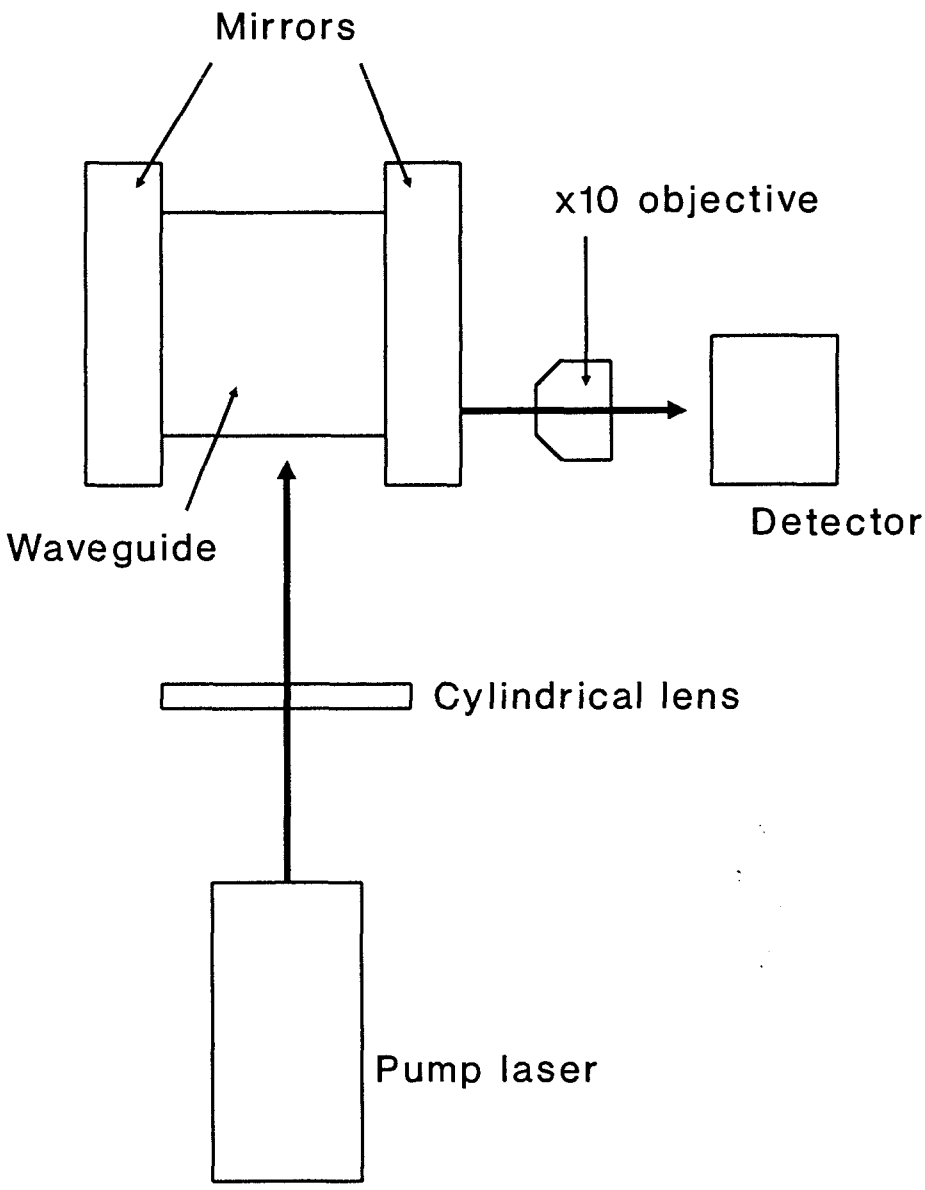

Figure 6.8 - Experimental arrangement for side-pumping experiments.

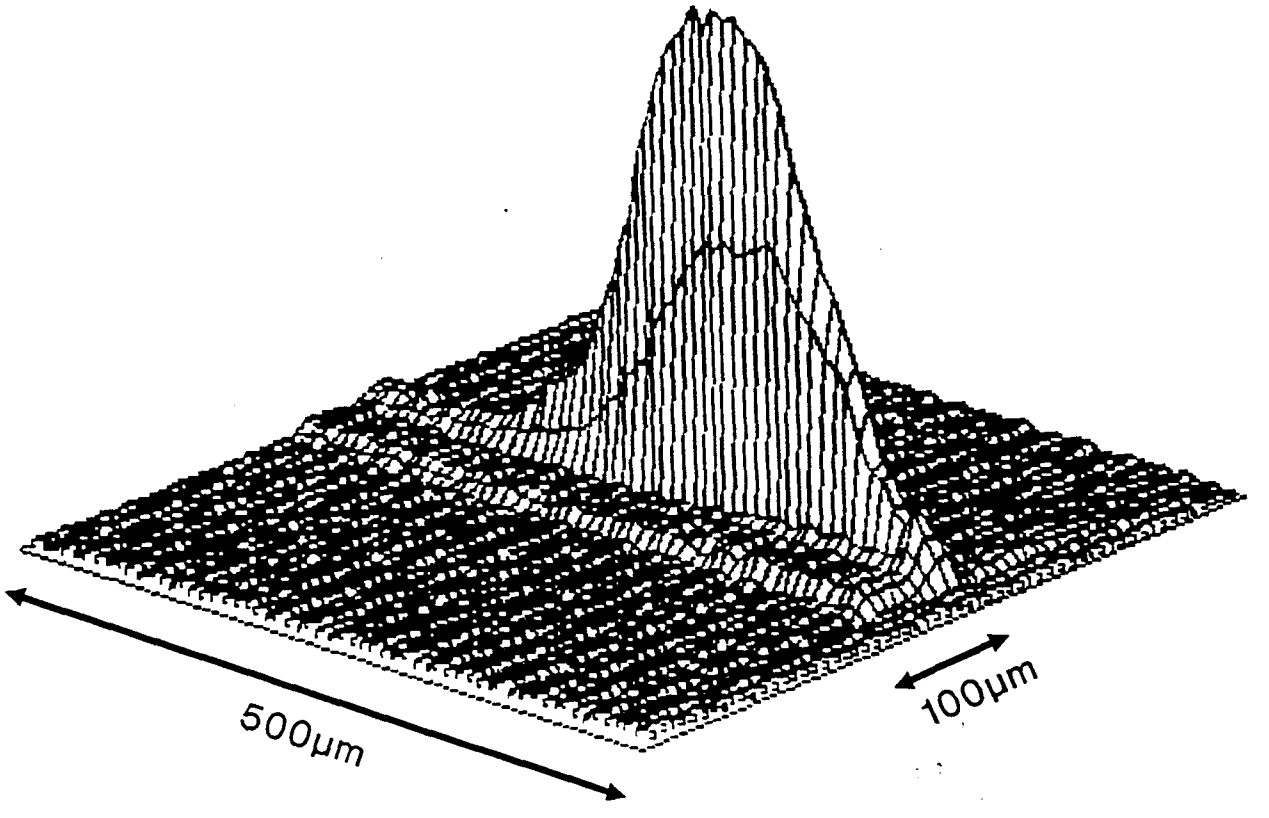

Figure 6.9 - Focused image of the output from a side pumped Nd:YAG waveguide laser taken just above threshold.

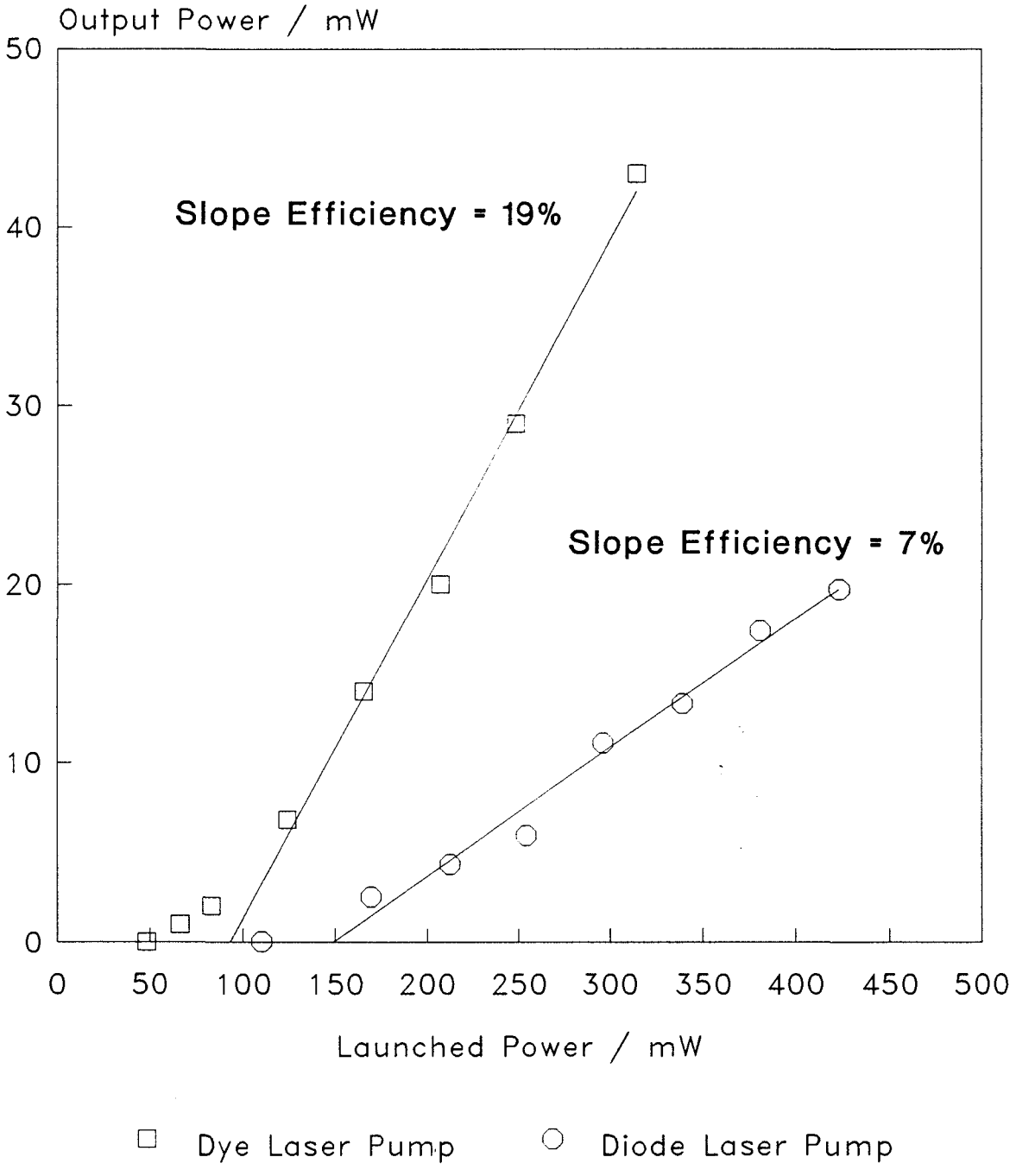

Figure 6.10 - Plot of output power against launched pump power for a dye laser and a diode array side-pumped Nd:YAG waveguide laser.

quenching which would have the effect of raising the laser threshold; but the increase in the absorption coefficient would, however, counteract any threshold increase and would also increase the slope efficiency. The production of highly doped Nd:YAG films can be easily done by liquid phase epitaxial growth.

6.7. Prospects for Channel Waveguide Fabrication.

One method of improving the performance of the longitudinally-pumped waveguide lasers produced by liquid phase epitaxial growth is to fabricate channel waveguides. The growth process by its nature is only suitable for growth over an entire surface. Therefore, to form channels, some method of lowering the refractive index of parts of the epitaxial layer has to be found.

The simplest way of lowering the refractive index of the active layer would be to remove it. This could be done by etching away side walls in the active layer and leaving a raised section of waveguide. After this has been done a cladding layer could be grown on top of this to reduce the waveguides losses. Another method would be to ion-implant side walls into a waveguide with an existing thin cladding layer (1-2μm thick). The fabrication of channels by this method has the advantage that it is done after the entire epitaxial growth stage so it avoids the guides having to be cladded after the formation of side walls. This method of channel fabrication has been seen to work in ion-implanted guides (such as Tm:MgO:$LiNbO_3$) where the guidance relies entirely on a refractive index decrease. Channels fabricated by this method have shown no increase in loss over planar waveguides in the same material. The losses in the ion-implanted guides, however, start at 1dB/cm, and it would be interesting to see if there is any effect on a guide with losses of 0.2dB/cm. The fabrication procedure for this type of waveguide would be similar to the procedure for fabricating channels by ion-implantation alone and tests of this method are currently being done.

A third possible method combines the two possibilities described above. It has been demonstrated that ion-implantation can increase the etch rate of garnets by up to three orders of magnitude [16]. Therefore by implanting side walls and then etching the

material could be removed quickly from the implanted region. The remaining guides could then be cladded to reduce their losses. Whichever method ultimately proves successful the fabrication of channels in epitaxially grown guides will reduce laser thresholds by about a factor of 10.

6.8. Conclusions.

The usefulness of liquid phase epitaxial growth as a fabrication procedure for low loss planar waveguides has been demonstrated. Waveguides have been fabricated with Nd^{3+} and Yb^{3+} doped YAG layers. These have shown low threshold laser action on various different laser transitions and have shown a real advantage over bulk lasers in quasi-three-level systems such as Yb:YAG. The next steps in the development of epitaxially grown guides will be to form low loss channel waveguides and to extend the technique to other materials.

6.9. References.

1. S.L.Blank and J.W.Nielsen, Journal of Crystal Growth, **17**, pp.302-311, 1972.
2. E.A.Giess, J.D.Kuptsis and E.A.D.White, Journal of Crystal Growth, **16**, pp.36-42, 1972.
3. J.P.Van der Ziel, W.A.Bonner, L.Kopf, S.Singh and L.G.Van Uitert, Applied Physics Letters, **22**, pp.656-657, 1973.
4. J.G.Grabmaier, R.D.Plattner, P.Mockel and W.Kruhler, Journal of Crystal Growth, **34**, pp.280-284, 1976.
5. D.Elwell and H.J.Scheel, Crystal Growth from High Temperature Solutions, published by Academic Press, 1975.
6. D.Pelenc, Doctorate Thesis, Universite Joseph Fourier, Grenoble I, France, 1993.
7. S.Singh, R.G.Smith and L.G.Van Uitert, Physical Review B, **10**, pp.2566-2572, 1974.
8. I.Chartier, B.Ferrand, D.Pelenc, S.J.Field, D.C.Hanna, A.C.Large, D.P.Shepherd and A.C.Tropper, Optics Letters, **17**, pp.810-812, 1992.
9. T.Nishimura and T.Omi, Japanese Journal of Applied Physics, **14**, pp.1011-1016, 1975.

10. D.C.Hanna, A.C.Large, D.P.Shepherd, A.C.Tropper, I.Chartier, B.Ferrand and D.Pelenc, Applied Physics Letters, **63**, pp.7-9, 1993.
11. R.K.Watts and W.C.Holton, Journal of Applied Physics, **45**, pp.873-881, 1974.
12. T.Y.Fan and R.L.Byer, Optics Letters, **12**, pp.809-811, 1987.
13. P.Lacovara, H.K.Choi, C.A.Wang, R.L.Aggarwal and T.Y.Fan, Optics Letters, **16**, pp.1089-1091, 1991.
14. D.S.Sumida and T.Y.Fan, Optics Letters, **19**, pp.1343-1345, 1994.
15. D.C.Hanna, A.C.Large, D.P.Shepherd, A.C.Tropper, I.Chartier, B.Ferrand and D.Pelenc, Optics Communications, **91**, pp.229-235, 1992.
16. W.A.Johnson, J.C.North and R.Wolfe, Journal of Applied Physics, **44**, pp.4753-4757, 1973.

Chapter 7 - Conclusion

7.1. Results and Conclusions.

This thesis has reported laser action in waveguides fabricated by both ion-implantation and liquid phase epitaxial growth. A summary of all these waveguide laser results is given in table 7.1.

The most attractive feature of ion-implantation is its versatility. One accelerator is sufficient to implant any material. Because of this, waveguides have been formed in a large range of crystals and glasses. The range of waveguide lasers fabricated covers such materials as Nd:BGO (bismuth germanium oxide), Nd:$LiNbO_3$, Yb:YAG, Nd:YAP and thulium doped lead germanate glass. Another advantage of this method is that channel waveguides can be fabricated. When the current fabrication method using a gold mask to block the ions is replaced by one using tungsten wires then the channel fabrication process will potentially become quicker and more reliable. The main disadvantages of ion-implantation are that the guides formed tend to have losses greater than 1dB/cm and that the spectroscopic properties of the material can be altered (eg. the peak emission cross section is often decreased). The only solution to this is to search for materials which respond well to implantation. Two such materials are lead germanate glass and yttrium ortho-silicate both of which produce guides with losses of less than 0.2dB/cm and can be doped with active ions.

The waveguide fabrication process of liquid phase epitaxial growth tends to succeed where ion-implantation fails. On the evidence of the YAG epitaxial guides described earlier the epitaxial layers are low loss waveguides which have the same spectroscopic properties as bulk grown samples. The method is, however, not as versatile as ion-implantation and a change in material could only be done by either using a new furnace or thoroughly cleaning out an existing one. This should not be too much of a problem, though, as the cost of a furnace is not prohibitive and there is no reason why several materials could not be worked on simultaneously. Unlike YAG and other garnets

Table 7.1 - Summary of waveguide laser results reported in this thesis.

Fabrication method	Material	Geometry	Laser wavelength	Pump wavelength	Minimum Threshold	Maximum Slope efficiency
ion-implantation	Nd:GGG	planar	1.06μm	805nm	8mW	30%
ion-implantation	Yb:YAG	planar	1.03μm	941nm	30mW	19%
ion-implantation	Nd:YAG	channel	1.06μm	807nm	0.54mW	29%
ion-implantation	Nd:GGG	channel	1.06μm	805nm	1.9mW	27%
ion-implantation	Nd:MgO:$LiNbO_3$	channel	1.09μm	814nm	< 10mW	-
epitaxial growth	Nd:YAG	planar	946nm	807nm	1.2mW	-
epitaxial growth	Nd:YAG	planar	1.06μm	807nm 588nm	1.3mW 0.67mW	40% -
epitaxial growth	Nd:YAG	planar	1.32μm	588nm	9.1mW	30%
epitaxial growth	Yb:YAG	planar	1.03μm and 1.05μm	968nm	43mW	77%
epitaxial growth	Nd:YAG	side pumped	1.06μm	588nm	8mW	19%

any new materials will probably be more difficult to produce waveguides in as little will be known about their suitability for epitaxial growth, or how to alter their refractive indices to produce waveguides. The fact that different materials can be tested is certainly an advantage over fabrication methods such as proton exchange or titanium indiffusion which are specific to a very limited range of materials. The one remaining problem which has still to be solved for epitaxially grown guides is the fabrication of channels. Several plans for fabricating channels already exist and it should not be long before this problem is ironed out.

The laser performance of the epitaxially grown waveguides has shown the advantages that waveguides can offer over bulk systems. The laser thresholds for the 946nm transition in Nd:YAG and the 1.03 and 1.05μm transitions in Yb:YAG are already better than in equivalent bulk systems. Although the quasi-three-level nature of these transitions makes it easier for the waveguides to surpass bulk results it must be remembered that these results were obtained in the far from ideal case of a planar waveguide. When the fabrication of low loss channel waveguide is a reality then waveguides should produce lower thresholds than bulk lasers in a wide range of four-level and quasi-three-level laser transitions.

7.2. Future Work.

There are two main areas of future work that exist for ion-implanted waveguides. One is to find a quick and reliable method of producing channel guides. The most probable way of doing this is by using a grid of tungsten wires to block the ions in the desired areas. The other area is to continue the search for materials which react well to implantation. As more laser materials become available the chances of finding one which form low loss guides must increase. Two materials which seem very promising at the moment are lead germanate glass and yttrium ortho-silicate both of which produce guides with losses of less than 0.2dB/cm. In fact thulium doped lead germanate glass has already operated as a planar waveguide laser.

The fabrication of low loss channels is also a priority for epitaxially grown

waveguides. Another area for work which is currently underway at LETI is to extend the range of materials and dopants. With new materials available new laser transitions (including upconversion transitions) can be tested. At present YAG layers are being grown with erbium and thulium doping. For Er:YAG the available laser transitions are at 560nm, 1.6μm, and 2.94μm [1-3] and for Tm:YAG the laser transitions occur at 486nm and 2.1μm [4,5]. For the upconversion transitions to work in these materials the samples may have to be cooled considerably. This poses a new set of experimental problems which will have to be overcome.

Another advantage of the waveguide geometry is that it is highly suited to non-linear processes such as second harmonic generation and parametric oscillation. Some of these non-linear properties could be incorporated into laser devices perhaps in the form of a self frequency doubled laser. The potential result of this could be a range of diode pumped, miniature lasers emitting from visible wavelengths out into the infra-red.

7.3. References.

1. R.Brede, E.Heumann, J.Koetke, T.Danger and G.Huber, Applied Physics Letters, **21**, pp.2030-2032, 1993.
2. G.Huber, E.W.Duczynski and K.Petermann, IEEE Journal of Quantum Electronics, **QE-24**, pp.920-923, 1988.
3. E.V.Zharikov, V.I.Zhekov, L.A.Kulevskii, T.M.Murina, V.V.Osiko, A.M.Prokhorov, A.D.Savel'ev, V.V.Smirnov, B.P.Starikov and M.I.Timoshechkin, Soviet Journal of Quantum Electronics, **4**, pp.1039-1040, 1975.
4. B.P.Scott, F.Zhao, R.S.F.Chang and N.Djeu, Optics Letters, **18**, pp.113-115, 1993.
5. R.C.Stoneman and L.Esterowitz, Optics Letters, **15**, pp.486-488, 1990.

Appendix A - Numerical Solution to the Waveguide Equation

The solution to the problem of the asymmetric slab waveguide can be found by solving equations (2.13) and (2.14). This can be done by first simplifying the equations by making the substitutions

$$v = k_0 d\sqrt{n_2^2 - n_3^2} \tag{A.1}$$

$$b = \frac{n_e^2 - n_3^2}{n_2^2 - n_3^2} \tag{A.2}$$

$$a = \frac{n_3^2 - n_1^2}{n_2^2 - n_3^2} \tag{A.3}$$

The equation which has to be solved then becomes

$$v\sqrt{1-b} = \tan^{-1}\left(TM1\sqrt{\frac{b}{1-b}}\right) + \tan^{-1}\left(TM2\sqrt{\frac{b+a}{1-b}}\right) + p\pi \tag{A.4}$$

where TM1 and TM2 are scaling factors for TM modes and are given by

$$TM1 = \frac{n_2^2}{n_3^2} \qquad TM2 = \frac{n_2^2}{n_1^2} \tag{A.5}$$

The value of b can vary from 0 to 1 as the effective refractive index goes from n_2 to n_3. Equation (A.4) can be solved by bisection. This means that an initial guess has to be made for b and then the difference between the left and right hand sides of equation (A.4) calculated. Depending on whether this difference is positive or negative a new guess can be made. This procedure will quickly converge to the solution. By taking this value of b and working backwards the shape of the modes can be calculated from equations (2.8) and (2.11). To do this a computer program was written which could calculate the

effective indices of the waveguide modes and calculate their shape and spot sizes (taken to be the distance between the 1/e points in the wings of the mode).

Appendix B - Ion-Implanted Channel Waveguide Fabrication

The exact process used to form channel waveguides by ion-implantation is discussed in this appendix. This involves many steps which are described below.

Resin encapsulation

The first step in producing channel guides is to cut the crystal to the desired size using a circular saw. This has to be less than 3mm thick to allow it to fit under the mask aligner in later stages. Then one of its side faces (one which will run parallel to the final channels) is polished to give a reference face for mask alignment and later polishing. After this the sample is set in resin. The resin used was Acyfix a relatively low cost product with a quick setting time (7-8min). Once the resin has set it is cut to less than 3mm in thickness and polished so that the crystal surface is exposed. The purpose of the resin is to reduce photoresist build up at the edges of the crystal and make the surface larger and therefore easier to attach electrodes to.

Ni/Cr evaporation

The next three steps in the process are performed in a clean room to give a high quality surface finish before the gold plating stage. Cleaning of the sample is the first important step in the clean room stage. This is done in a solution of microclean until the surface looks free of dust under microscopic examination. A 100nm layer of 80% nickel, 20% chromium is then evaporated onto the sample in an Edwards coater to act as an electrode for the later gold plating stage.

Photoresist spinning

Onto the Ni/Cr is then spun a 4μm thick layer of photoresist. This is done using Microposit S1400-37 a relatively thick resist which has to be spun for 40s at 3000rpm to give the desired thickness. After softbaking for 30min at 90°C this is then ready to be masked and developed.

Masking and developing

The mask used to cover the sample was chromium on glass made by electron beam lithography at R.A.L. and consisted of different sets of stripes ranging from 4-20μm. Two masks were made - one with chromium stripes and one in the opposite sense to this with long holes in the chromium layer. These stripes could be accurately aligned with the polished side face of the crystal using a Karl Suss MA6 mask aligner, which enables the mask and sample to be brought together and viewed under a microscope. The edge of the sample can then be aligned parallel with the stripes on the mask to within a fraction of the width of the smallest stripe (usually 4μm) over the length of the sample (typically 1cm). Assuming that the end faces are polished accurately perpendicular to the side face, then the difference in angle between the channels and the normal to the end face should be no more than 0.02°. Once the mask is aligned, it is exposed for 25s under UV light, then developed for 1min to remove all the exposed photoresist.

Electrode attachment

For the sample to be successfully gold plated the Ni/Cr layer has to be electrically connected to the outside world. This is done by attaching a piece of wire to the Ni/Cr layer; any photoresist has to be removed from where the wire is joined. The wire is connected using a silver-loaded epoxy. After setting, the exposed areas of epoxy are given a coat of paint to prevent the gold from plating preferentially on to them. Figure B.1 shows how the sample looks at this point in the processing.

Gold plating

Trials carried out at R.A.L. of the evaporation of gold onto the samples found that layers thicker than 1μm could not be grown. The thickness of gold (in microns) required to stop $^4He^+$ ions of a given energy is closely approximated by multiplying the energy (in MeV) by 1.5. Figure B.2 shows a graph of the amount of gold required to stop the He ions against the energy of the ions. The line represents the simple "multiply by 1.5" rule. To stop 3MeV He ions the gold mask would therefore have to be 4.5μm thick. A 3μm layer of gold would, however, be enough to give well-confined channel waveguides. To get these layers sufficiently thick the gold had to be electroplated into the gaps in the

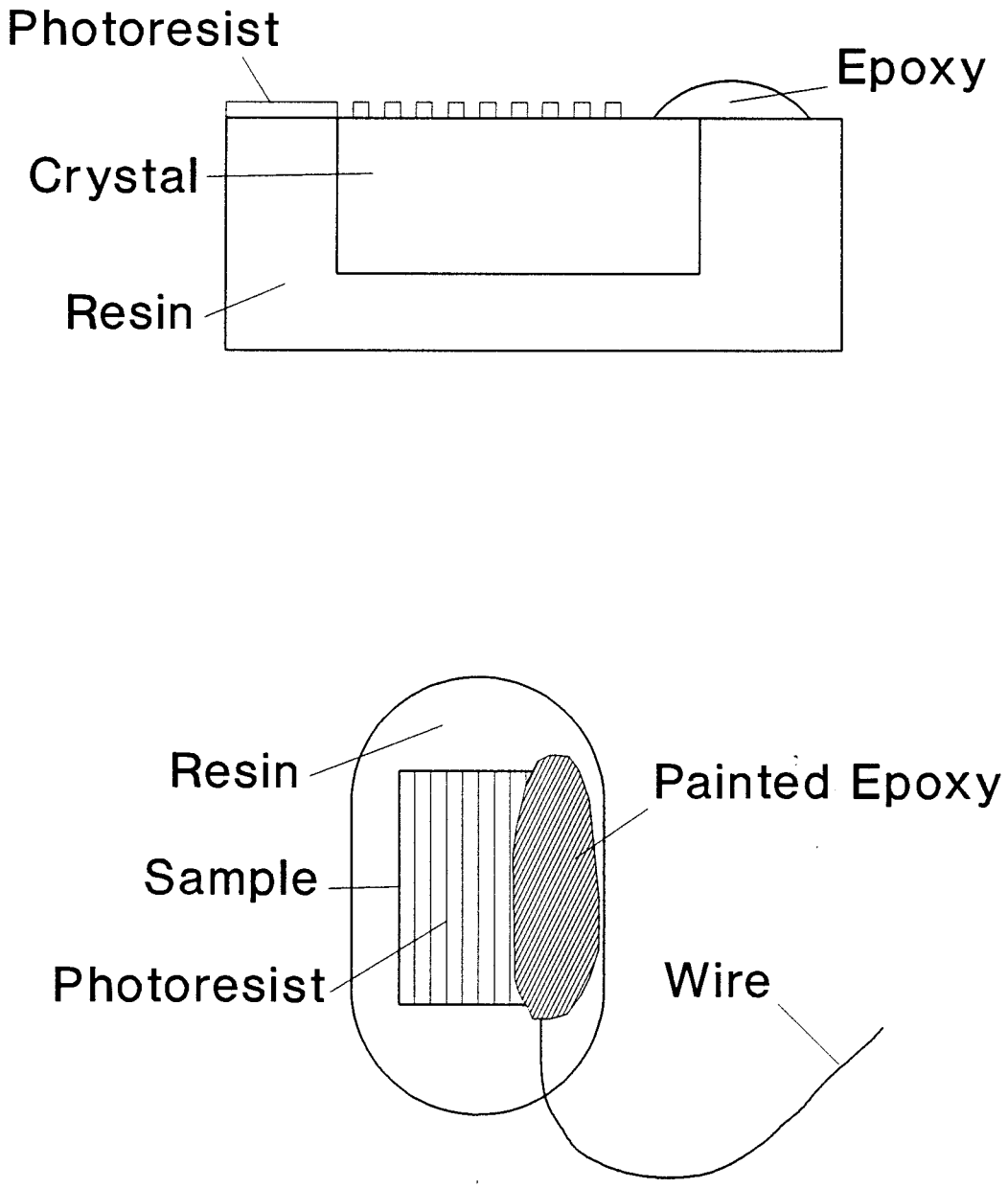

Figure B.1 - Diagram of the sample before the gold plating stage.

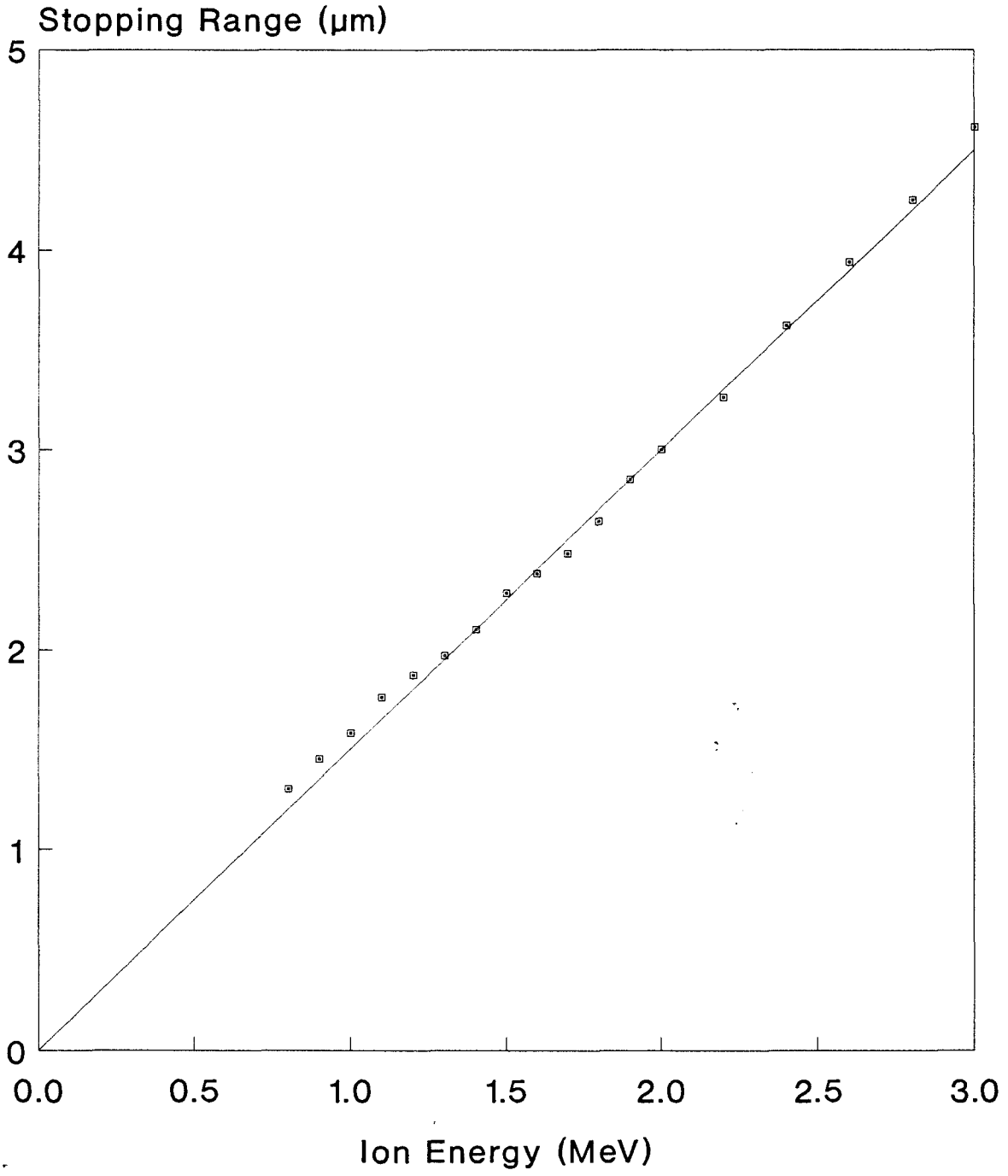

Figure B.2 - Graph of the thickness of gold required to stop $^4He^+$ ions against the energy of the ions. The solid line represents the ion energy (in MeV) multiplied by 1.5.

photoresist. Attempts at in-house gold plating proved unsuccessful, and for this reason all the gold plating was done by P.D.S. - a commercial gold-plating company. After pretreating the surface of the sample to increase the adhesion of the gold it is placed in a solution of potassium cyano-aurate ($AuK(CN)_2$) in distilled water. The sample then acts as the cathode in the electroplating stage. A constant current is used during the electroplating so that the number of gold ions and therefore the gold thickness can be calculated simply from the area of exposed Ni/Cr.

Ion-implantation

When the sample is received back from gold plating, the photoresist is removed from between the gold stripes using acetone. The wire and epoxy are also detached before the sample is sent to Sussex University to be ion-implanted. The implant performed will either form high refractive index guiding regions or low refractive index side walls, depending on the response of the material to ion-implantation.

Gold removal

After the initial implant the gold and Ni/Cr layers have to be removed. This is done in aqua regia (4 parts hydrochloric acid and 1 part nitric acid) a solution which effectively removes the gold but not usually the Ni/Cr. Complete removal of the Ni/Cr is done by lightly polishing the surface for as short a time as is required (generally a few minutes). If the sample is a barrier type guide it is then sent back to Sussex for a final implant, if not it is ready to be end polished for laser trials.

End polishing

The final stage in the preparation of the channel waveguides is to make sure that the end faces are polished accurately perpendicular to the channels. The sample is mounted on a polishing jig in such a way that the light from a He-Ne laser is reflected from the polished side face. Earlier in the setup a note is taken of the point that the reflected He-Ne beam would hit if the base of the polishing jig an the side face of the sample were perpendicular. This is done using a right angled prism and an autocollimator. The polishing jig can then be adjusted so that the reflection from the side

face is aligned with the reference point.

Appendix C - Side Pumped Waveguide Laser Theory.

The threshold pump power (P_{th}) and slope efficiency (η) of a laser-pumped four-level laser are given by [1]

$$P_{th} = \frac{h\nu_p L}{\eta_q W \sigma \tau_f [1-\exp(-\alpha_p l)]} \left(\int_{cavity} r_o(x,y,z) s_o(x,y,z) dV \right)^{-1} \qquad \text{(C.1)}$$

and

$$\eta = \frac{T\nu_l}{2L\nu_p} [1-\exp(-\alpha_p l)] \eta_q \eta_{pl} \qquad \text{(C.2)}$$

where ν_p is the pump frequency, ν_l is the laser frequency, L is the single pass loss, σ is the emission cross section, τ_f is the fluorescence lifetime, η_q is the pumping efficiency, W is the length of the crystal in the lasing direction, l is the length of the crystal in the pumping direction, α_p is the pump absorption coefficient and T is the output mirror transmission. The factor η_{pl} modifies the plane wave expression for η. For low power operation this is given by

$$\eta_{pl} = \frac{\left(\int_{cavity} r_o(x,y,z) s_o(x,y,z) dV \right)^2}{\left(\int_{cavity} r_o(x,y,z) s_o^2(x,y,z) dV \right)} \qquad \text{(C.3)}$$

The normalised pump rate per unit volume, r_o, which is the rate of pumping to the upper laser level over the doped region and the photon density, s_o, which is the density of laser photons are normalised by the equations

$$\int_{cavity} r_o(x,y,z)dV = \int_{cavity} s_o(x,y,z)dV = 1 \qquad \textbf{(C.4)}$$

Figure C.1 shows the layout of the side pumped waveguide laser. The doped region is defined by the limits $0<x<l$, $-d<y<d$ and $0<z<W$. These also define the boundary outwith which $r_o=0$. The limits outwith which $s_o=0$ are the same except in the y direction where the limits are taken to be $\pm\infty$ as the laser mode can extend significantly into the cladding. To calculate the functions for r_o and s_o their shape has to be assumed. The pump photon density is assumed to decay exponentially in the x direction with the pump absorption and to have a fundamental mode Gaussian profile in the other direction. The laser photon density is assumed to have fundamental Gaussian modes in the x and y directions and an unvarying spot size along z. The normalised expressions for r_o and s_o are therefore given by

$$r_o = \frac{\dfrac{4\alpha_p}{\pi W_{pz} W_{py}[1-\exp(-\alpha_p l)]} \exp\left[-\left(\dfrac{2y^2}{W_{py}^2}+\dfrac{2z^2}{W_{pz}^2}+\alpha_p x\right)\right]}{\left[\operatorname{erf}\left(\dfrac{\sqrt{2}d}{W_{py}}\right)\operatorname{erf}\left(\dfrac{\sqrt{2}W}{W_{pz}}\right)\right]} \quad \text{for } \begin{matrix}0<x<1\\ -d<y<d\\ 0<z<W\end{matrix} \qquad \textbf{(C.5)}$$

$$r_o = 0 \quad \text{elsewhere}$$

and

$$s_o = \frac{\dfrac{4}{\pi W_{ly} W_{lx} W} \exp\left[-\left(\dfrac{2(x-a)^2}{W_{lx}^2}+\dfrac{2y^2}{W_{ly}^2}\right)\right]}{\left[\operatorname{erf}\left(\dfrac{\sqrt{2}l}{W_{lx}}-\dfrac{\sqrt{2}a}{W_{lx}}\right)+\operatorname{erf}\left(\dfrac{\sqrt{2}a}{W_{lx}}\right)\right]} \quad \text{for } \begin{matrix}0<x<1\\ -\infty<y<\infty\\ 0<z<W\end{matrix} \qquad \textbf{(C.6)}$$

$$s_o = 0 \quad \text{elsewhere}$$

where a is the distance from the edge of the crystal to the centre of the laser mode. The

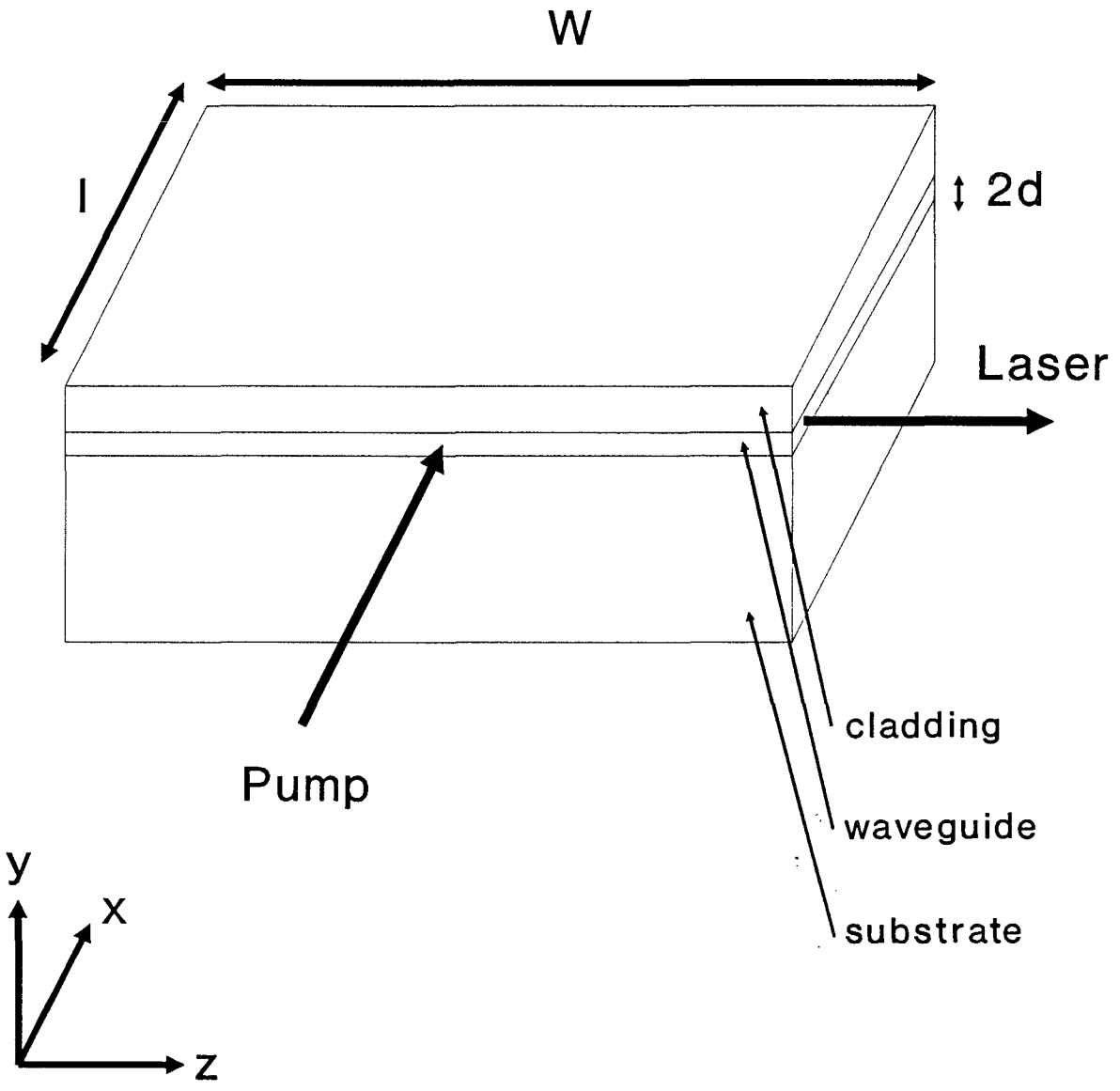

Figure C.1 - Layout of side-pumped waveguide laser.

error functions in these equations arise from the choice of the function for r_o and s_o. In most cases where $W_{lx}<a<l$, $W_{py}<d$ and $W_{pz}<W$ these error functions are approximately equal to 1. Substituting these expressions into equations (C.1), (C.2) and (C.3) gives equations for threshold and slope efficiency as

$$P_{th} = \frac{k\sqrt{\pi}h\nu_p L}{\sqrt{2}\sigma\tau_f\eta_q\alpha_p}(W_{lx}^2+W_{py}^2)^{1/2}\exp\left(a\alpha_p-\frac{W_{lx}^2\alpha_p^2}{8}\right) \qquad \textbf{(C.7)}$$

and

$$\eta = \frac{k'\sqrt{\pi}T\nu_l\eta_q}{2L\nu_p}\frac{\alpha_p W_{lx}W_{ly}(W_{ly}^2+2W_{py}^2)^{1/2}}{W_{ly}^2+W_{py}^2}\exp\left(\frac{3W_{lx}^2\alpha_p^2}{16}-a\alpha_p\right) \qquad \textbf{(C.8)}$$

The factors k and k' in these equations contain the error functions arising from the integration. These are given by the equations

$$k = \frac{\operatorname{erf}\left(\frac{\sqrt{2}d}{W_{py}}\right)\left[\operatorname{erf}\left(\frac{\sqrt{2}l}{W_{lx}}-\frac{\sqrt{2}a}{W_{lx}}\right)+\operatorname{erf}\left(\frac{\sqrt{2}a}{W_{lx}}\right)\right]}{\operatorname{erf}\left[\sqrt{2}d\left(\frac{1}{W_{py}^2}+\frac{1}{W_{ly}^2}\right)^{1/2}\right]\left[\operatorname{erf}\left(\frac{\sqrt{2}l}{W_{lx}}-\frac{\sqrt{2}a}{W_{lx}}+\frac{\alpha_p W_{lx}}{\sqrt{8}}\right)+\operatorname{erf}\left(\frac{\sqrt{2}a}{W_{lx}}-\frac{\alpha_p W_{lx}}{\sqrt{8}}\right)\right]} \qquad \textbf{(C.9)}$$

and

$$k' = \frac{\left[\operatorname{erf}\left[\sqrt{2}d\left(\frac{1}{W_{py}^2}+\frac{1}{W_{ly}^2}\right)^{1/2}\right]\right]^2\left[\operatorname{erf}\left(\frac{\alpha_p W_{lx}}{\sqrt{8}}+\frac{\sqrt{2}l}{W_{lx}}-\frac{\sqrt{2}a}{W_{lx}}\right)-\operatorname{erf}\left(\frac{\alpha_p W_{lx}}{\sqrt{8}}-\frac{\sqrt{2}a}{W_{lx}}\right)\right]^2}{2\operatorname{erf}\left(\frac{\sqrt{2}d}{W_{py}}\right)\operatorname{erf}\left[\sqrt{2}d\left(\frac{1}{W_{py}^2}+\frac{1}{W_{ly}^2}\right)^{1/2}\right]\left[\operatorname{erf}\left(\frac{\alpha_p W_{lx}}{4}+\frac{2l}{W_{lx}}-\frac{2a}{W_{lx}}\right)-\operatorname{erf}\left(\frac{\alpha_p W_{lx}}{4}-\frac{2a}{W_{lx}}\right)\right]} \qquad \textbf{(C.10)}$$

Although in most cases these constants are close to unity they do give information about the threshold and slope efficiency as W_{lx} becomes large.

Reference

1. W.A.Clarkson and D.C.Hanna, Journal of Modern Optics, **36**, pp.483-498, 1989.

Appendix D - Publications and Conference Papers

Publications

1. S.J.Field, D.C.Hanna, A.C.Large, D.P.Shepherd, A.C.Tropper, P.J.Chandler, P.D.Townsend and L.Zhang, "Ion-Implanted Crystal Waveguide Lasers," in *OSA Proceedings on Advanced Solid State- Lasers*, G.Dubé and L.Chase, eds. (Optical Society of America, Washington, D.C., 1991), vol.10, pp.353-357.
2. S.J.Field, D.C.Hanna, A.C.Large, D.P.Shepherd, A.C.Tropper, P.J.Chandler, P.D.Townsend and L.Zhang, "An Efficient, Diode-Pumped, Ion-Implanted Nd:GGG Planar Waveguide Laser," Opt. Comm., vol.86, pp.161-166, 1991.
3. S.J.Field, D.C.Hanna, A.C.Large, D.P.Shepherd, A.C.Tropper, P.J.Chandler, P.D.Townsend and L.Zhang, "Low Threshold, Ion-Implanted Nd:YAG Channel Waveguide Laser," Electr. Lett., vol.27, pp.2375-2376, 1991.
4. J.O.Tocho, L.Nunez, J.A.Sanz-Garcia, F.Cusso, D.C.Hanna, A.C.Tropper, S.J.Field, D.P.Shepherd and A.C.Large, "Optical Properties of Tm Doped $LiNbO_3$ and $LiNbO_3$(MgO)," J. de Physique JP IV, vol.1, pp.293-296, 1991.
5. S.J.Field, D.C.Hanna, A.C.Large, D.P.Shepherd, A.C.Tropper, P.J.Chandler, P.D.Townsend and L.Zhang, "Ion-Implanted Nd:GGG Channel Waveguide Laser," Opt. Lett., vol.17, pp.52-54, 1992.
6. I.Chartier, B.Ferrand, D.Pelenc, S.J.Field, D.C.Hanna, A.C.Large, D.P.Shepherd, and A.C.Tropper, "Growth and Low Threshold Laser Oscillation of an Epitaxially Grown Nd:YAG Waveguide," Opt. Lett., vol.17, pp.810-812, 1992.
7. D.C.Hanna, A.C.Large, D.P.Shepherd, A.C.Tropper, I.Chartier, B.Ferrand and D.Pelenc, "A Side-Pumped Nd:YAG Epitaxial Waveguide Laser," Opt. Comm, vol.91, pp.229-235, 1992.
8. W.S.Brocklesby, S.J.Field, D.C.Hanna, A.C.Large, J.R.Lincoln, D.P.Shepherd, A.C.Tropper, P.J.Chandler, P.D.Townsend, L.Zhang, X.Q.Feng and Q.Hu, "Optically Written Waveguides in Ion-Implanted $Bi_4Ge_3O_{12}$," Opt. Mat., vol.1, pp.177-183, 1992.

9. S.J.Field, D.C.Hanna, A.C.Large, D.P.Shepherd, A.C.Tropper, P.J.Chandler, P.D.Townsend and L.Zhang, "Efficient, Low Threshold Ion Implanted Channel Waveguide Lasers," in *OSA Proceedings on Advanced Solid-State Lasers*, L.Chase and A.Pinto, eds. (Optical Society of America, Washington, D.C., 1992), vol.11.

10. D.C.Hanna, A.C.Large, D.P.Shepherd, A.C.Tropper, I.Chartier, B.Ferrand and D.Pelenc, "Low Threshold Quasi-Three-Level 946nm Laser Operation of an Epitaxially Grown Nd:YAG Waveguide," Appl. Phys. Lett., vol.63, pp.7-9, 1992.

11. D.C.Hanna, J.K.Jones, A.C.Large, D.P.Shepherd, A.C.Tropper, P.J.Chandler, P.D.Townsend and L.Zhang, "Quasi-Three-Level 1.03μm Laser Operation of a Planar Ion Implanted Yb:YAG Waveguide," Opt. Comm., vol.99, pp.211-215, 1993.

12. L.Nunez, J.O.Tocho, J.A.Sanz-Garcia, E.Rodriguez, F.Cusso, D.C.Hanna, A.C.Tropper and A.C.Large, "Optical Absorption and Luminescence of Tm^{3+}-Doped $LiNbO_3$ and $LiNbO_3$ (MgO) Crystals," Journal of Luminescence, vol.55, pp.253-263, 1993.

13. A.C.Large, D.C.Hanna, D.P.Shepherd, A.C.Tropper, I.Chartier, B.Ferrand and D.Pelenc, "Low Threshold Quasi-Three-Level 946nm Laser Operation of an Epitaxially Grown Nd:YAG Waveguide," in *OSA Proceeding on Advanced Solid-State Lasers*, A.Pinto and T.Y.Fan, eds. (Optical Society of America, Washington, D.C., 1993), vol.12.

Conference Papers

1. S.J.Field, D.C.Hanna, A.C.Large, D.P.Shepherd, A.C.Tropper, P.J.Chandler, P.D.Townsend and L.Zhang, "Ion-Implanted Crystal Waveguide Lasers," Advanced Solid State Lasers Topical Meeting, Hilton Head, South Carolina, 1991, paper WF3.
2. S.J.Field, D.C.Hanna, A.C.Large, D.P.Shepherd, A.C.Tropper, P.J.Chandler, P.D.Townsend and L.Zhang, "Ion-Implanted Crystal Waveguide Lasers," Conference on Lasers and Electro-Optics, Baltimore, 1991, paper CThL1.
3. J.O.Tocho, L.Nunez, J.A.Sanz-Garcia, F.Cusso, D.C.Hanna, A.C.Tropper, S.J.Field, D.P.Shepherd and A.C.Large, "Optical Properties of Tm Doped $LiNbO_3$ and $LiNbO_3$(MgO)," Laser M2P, Grenoble, 1991, paper L18.
4. S.J.Field, D.C.Hanna, A.C.Large, D.P.Shepherd, A.C.Tropper, P.J.Chandler, P.D.Townsend and L.Zhang, "Ion-Implanted Crystal Waveguide Lasers," The Tenth National Quantum Electronics Conference, Edinburgh, 1991, paper PLTu11.
5. S.J.Field, D.C.Hanna, A.C.Large, D.P.Shepherd, A.C.Tropper, P.J.Chandler, P.D.Townsend and L.Zhang, "Efficient, Low Threshold, Ion-Implanted, Channel Waveguide Lasers," Advanced Solid State Lasers, Santa Fe, New Mexico, 1992, paper TuA2.
6. A.C.Large, S.J.Field, D.C.Hanna, D.P.Shepherd, A.C.Tropper, P.J.Chandler, P.D.Townsend and L.Zhang, "Diode Pumped Garnet Channel Waveguide Lasers," Integrated Photonics Research Topical Meeting, New Orleans, Louisiana, 1992, paper WF6.
7. A.C.Large, S.J.Field, D.C.Hanna, D.P.Shepherd, A.C.Tropper, P.J.Chandler, P.D.Townsend and L.Zhang, "Ion-Implanted Channel Waveguide Lasers," Conference on Lasers and Electro-Optics, Anaheim, California, 1992, paper CWE1.
8. D.P.Shepherd, S.J.Field, D.C.Hanna, A.C.Large, A.C.Tropper, I.Chartier, B.Ferrand and D.Pelenc, "Very Low Threshold Laser Operation of an Epitaxially Grown Nd:YAG Waveguide," Conference on Lasers and Electro-Optics, Anaheim, California, 1992, paper CWE7.

9. D.C.Hanna, A.C.Large, D.P.Shepherd, A.C.Tropper, I.Chartier, B.Ferrand and D.Pelenc, "A Low Threshold Quasi-Three-Level 946nm Nd:YAG Epitaxial Waveguide Laser," Advanced Solid State Lasers, New Orleans, Louisiana, 1993, paper JWD4.

10. A.C.Large, D.C.Hanna, D.P.Shepherd, A.C.Tropper, I.Chartier, B.Ferrand and D.Pelenc, "A Low Threshold Epitaxially Grown Nd:YAG Waveguide Laser Operating at 946nm," Conference on Lasers and Electro-Optics, Baltimore, 1993, paper CFJ1.

11. D.P.Shepherd, D.C.Hanna, J.K.Jones, A.C.Large, A.C.Tropper, P.J.Chandler, P.D.Townsend and L.Zhang, "Ion Implanted Quasi-Three-Level Yb:YAG Waveguide Lasers," Conference on Lasers and Electro-Optics, Baltimore, 1993, paper CFJ7.

12. D.Pelenc, B.Chambaz, I.Chartier, B.Ferrand, D.C.Hanna, A.C.Large, D.P.Shepherd and A.C.Tropper, "First Laser Operation at 1.03μm of an Epitaxially Grown Yb:YAG Waveguide," ECIO, Neuchatel, 1993.

13. A.C.Large, D.C.Hanna, J.K.Jones, D.P.Shepherd, A.C.Tropper, P.J.Chandler, P.D.Townsend L.Zhang, I.Chartier, B.Ferrand and D.Pelenc, "Quasi-Three-Level Laser Operation of Yb:YAG Waveguides," The Eleventh National Quantum Electronics Conference, Belfast, 1993, paper 1052.